Determination of the chemical structures of atmospheric organic aerosols and their light-absorption and fluorescence properties based on solvent extraction

（溶媒抽出に基づく大気有機エアロゾルの化学構造及び光吸収・蛍光特性の決定）

CHEN, Qingcai

（陳　慶彩）

A dissertation for the degree of Doctor of Science

Department of Earth and Environmental Sciences,

Graduate School of Environmental Studies, Nagoya University

（名古屋大学大学院環境学研究科地球環境科学専攻学位論文　博士（理学））

2016

Note

(1) Qingcai Chen, Fumikazu Ikemori, Hayato Higo, Daichi Asakawa, Michihiro Mochida*. Chemical structural characteristics of HULIS and other fractionated organic matter in urban aerosols: Results from mass spectral and FT-IR analysis. Environ. Sci. Technol. 2016a, 50 (4), pp1721−1730.

(2) Qingcai Chen, Yuzo Miyazaki, Kimitaka Kawamura, Kiyoshi Matsumoto, Sean Coburn, Rainer Volkamer, Yoko Iwamoto, Sara Kagami, Yange Deng, Shuhei Ogawa, Sathiyamurthi Ramasamy, Shungo Kato, Akira Ida, Yoshizumi Kajii, and Michihiro Mochida*. Characterization of chromophoric water-soluble organics in an urban, a forest, and the eastern equatorial Pacific aerosols using EEM and HR-ToF-AMS spectroscopy. Environ. Sci. Technol., 2016b, 50 (19), pp 10351−10360.

(3) Qingcai Chen, Fumikazu Ikemori, Michihiro Mochida*. Light absorption and excitation-emission fluorescence of urban organic aerosol components and their connection to the chemical structures. Environ. Sci. Technol., 2016c, 50 (20), pp 10859−10868.

(4) Qingcai Chen, Fumikazu Ikemori, Yuua Nakamura, Petr Vodicka, Kimitaka Kawamura, and Michihiro Mochida*. Structural and Light-Absorption Characteristics of Complex Water-Insoluble Organic Mixtures in Urban Submicrometer Aerosols. Environ. Sci. Technol. 2017, 51(15), pp 8293−8303.

Abstract

Organic compounds constitute a large fraction of aerosols in the atmosphere. Their presence influences on the properties of the aerosols, thereby affects the role of aerosols in climate and human health. Characterization of the chemical structures of organics is important for understanding their sources and properties. However, the entire structural characteristics of the organic aerosol components remains poorly characterized to date because they are comprised of a wide variety of compounds. Brown carbon in organic aerosols has an ability to absorb light at visible and near-ultraviolet (UV) wavelengths. Brown carbon therefore potentially plays important roles in photo-initiated reactions of organic aerosols and thus in the macroscopic-scale radiative balance of the Earth. Characterization of brown carbon is important to gain insight into their source and formation processes, and to examine the estimates of the direct radiative effect by brown carbon in model simulations.

This study applied fractionation methods for organic aerosol components according to their solubility and polarity using solvent extraction and solid phase extraction (SPE) methods, in order to understand the chemical-structural characteristics and optical properties of complex organic aerosol mixtures. This approach makes it possible to characterize different organic components with multiple analytical techniques and thus to understand the relationship between the chemical-structural characteristics of organic aerosols and their properties. Based on this method, this study aimed at revealing the followings: (1) the chemical structures of total organic matter in total suspended particulates (TSP) collected in the city of Nagoya in summer/early autumn and winter; (2) the light-absorption and fluorescence properties of total organic matter in the TSP samples; (3) the chemical structures and light-absorption of water-insoluble organic mixtures (WISOM) in the submicron aerosols ($PM_{0.95}$) collected in Nagoya; and (4) the light-absorption and fluorescence properties of water-soluble organic matter (WSOM) in $PM_{0.95}$

collected in urban, forest and marine environments (Nagoya, Kii Peninsula, and the tropical Eastern Pacific).

For the first and second objectives, a combination of solvent extraction and reverse-phase SPE was used to extract and fractionate organic compounds with different polarities in the TSP samples (WSOM, WISOM, two fractions of humic-like substances, showing neutral and acidic behavior (HULIS-n and HULIS-a, respectively), and the remaining highly-polar part of WSOM). Their chemical structures and optical properties were obtained from the high-resolution aerosol mass spectra (HR-AMS spectra), soft ionization mass spectra, Fourier transform infrared (FT-IR) spectra, UV-visible absorption spectra and the excitation-emission matrices (EEMs). Nearly total aerosol organics were collected from the urban TSP filter samples using multiple solvent extractions (water, methanol and a mixture of methanol and dichloromethane) and separation using an Oasis HLB column. Then the mass fractions, elemental composition, average molecular weights, mass fractions of chemical functional groups, and the optical characteristics (i.e., MAE, *Å*, fluorescence efficiency and relative contribution of the fluorescence components) of the organic components respective fractions were determined. The WISOM and HULIS-n, the less polar fractions of the organics, accounted for large fractions both of the masses (mean; 70%) and the total light-absorption (mean: 84% at 400 nm) of the total organics in the urban TSP. Correlation analyses between their optical characteristics and chemical structures indicate that organic compounds with oxygen and nitrogen atoms may contribute largely to the total light absorption and fluorescence of the organic aerosol components.

For the third objective, the WISOM in the urban $PM_{0.95}$ were fractionated to six sub-fractions using solvent extraction and normal-phase SPE. The structural and light-absorption characteristics of these sub-fractions were then determined using multiple analytical techniques including HR-AMS and FT-IR analyses. The characteristic compounds in the six sub-fractions of

WISOM in the $PM_{0.95}$ samples were aliphatic hydrocarbons, phthalic acid esters, aliphatic nitrates and esters, esters, alcohols, ethers and ketones, phenols and quinones, and carboxylic acids and carboxylate esters. The MAEs of relatively more polar organic fractions were much higher than those of relatively low and non-polar organic fractions. The high MAE values of organics may associate with compounds containing aromatic structures and heteroatomic functional groups (containing oxygen and/or nitrogen atoms) and compounds with high molecular weights.

For the fourth objective, chemical-structural and optical characteristics of WSOM in urban, forest and marine $PM_{0.95}$ samples were investigated based on EEMs and HR-AMS spectra. The origins of water-soluble brown carbon were inferred from the signatures in the HR-AMS spectra and EEMs, and from hierarchical cluster analysis and backward air mass trajectory analysis. The results show that fluorescence components in the HULIS and protein-like organic matter are ubiquitous classes of water-soluble chromophores in different types of aerosols, and their relative abundances are highly variable depending on locations and time periods. The results indicate the differences of their origins and formation processes. The EEM components of HULIS-1 and HULIS-2 were associated with highly and less-oxygenated structures, respectively. Whereas HULIS-1 was ubiquitous in water-soluble chromophores in different environments, HULIS-2 was abundant only in terrestrial aerosols.

The analytical methods used in this study provided quantitative information on the chemical-structural and optical characteristics of atmospheric organic aerosol components from low- to high-polar compounds, which comprised the total organic matter. Application of this approach to the characterization of other types of aerosols in different environments may provide further insights into the concentrations, structural characteristics, sources and formation processes. The obtained values of MAE and $\mathring{A}$ can be used as inputs for atmospheric radiative models and can

be used to examine the estimates of the direct radiative effect by brown carbon in model simulations. The results from the correlation analysis of the light-absorption and fluorescence properties of organic matters against their chemical structural characteristics are useful for understanding the reaction pathways that lead to the formation/loss of chromophores and for further classification and source identification of brown carbon.

Table of Contents

1 Introduction

1.1 The complexity of organic aerosol composition

Atmospheric aerosols play important roles on global climate and material cycles, and bring negative effects to air quality and public health [*Pöschl,* 2005]. The major aerosol components in urban areas include sulfate, nitrate, ammonia, element carbon (EC)/black carbon (BC), organic compounds and others [*Pöschl,* 2005]. Among those components, organic compounds constitute a large fraction of the aerosol particles in the atmosphere (20–90%) [*Zhang et al*., 2007; *Jimenez et al*., 2009]. Their presence influences the properties of aerosols (e.g., light-absorptivity and toxicity) thereby affects the role of aerosols in climate and human health. Characterization of the chemical structures of organic mixtures is important for understanding the sources of these organics and their contribution to aerosol properties. However, these organics remain poorly characterized because of their highly complex composition.

As presented in Figure 1.1, organic aerosols may comprise a wide variety of organic compounds with different physicochemical properties [*Kroll et al*., 2011]. Some studies have suggested the complexity of the organic composition of ambient aerosols in molecular level. *Lin et al*. [2012] reported that the humic-like substances (HULIS) separated from atmospheric aerosols in the rural location of the Pearl River Delta Region, China, contained more than 1269 and 1679 organic species, based on the detection and identification using an ultrahigh resolution mass spectrometer (UHRMS) in positive and negative electrospray ionization (ESI) modes, respectively. The molecular formulas of organic compounds in aerosol HULIS fractions (with elements among C, H, O, N and S) were determined on the basis of the accurate mass measurement of molecule ions [*Lin et al*., 2012]. *Wozniak et al*. [2008] analyzed the chemical composition of water-soluble organic matter (WSOM) in aerosols at rural sites in Virginia and

New York, USA. The aerosol-derived WSOM was highly complex, and more than 3000 peaks were detected by ESI-UHRMS analysis. To understand the highly complexity of organic aerosol composition, it is important to study not only WSOM, but also water-insoluble organic matter (WIOSM) in atmospheric aerosols. *Willoughby et al*. [2014] analyzed WISOM in aerosols using ESI-UHRMS and nuclear magnetic resonance (NMR) spectroscopy. Their results show that at least 5106 organic species were present in the fractionated organics extracted with solvents (pyridine and acetonitrile) from urban aerosols in Gloucester Point, VA. Molecular level analysis of the aromatic fraction isolated from aerosol samples in Beijing was performed using atmospheric pressure photoionization (APPI)-UHRMS by *Jang et al*. [2014]. The results show that the aromatic fractions contain not only polycyclic aromatic hydrocarbons (PAHs), but also molecules with PAH structures and O, N and S containing functional groups. To date, many compounds detected in the molecular level analysis as explained above are also not identified. Qualitative and quantitative analysis of the chemical structural characteristics of the highly complex organic matter in aerosols is a challenging topic in the atmospheric community.

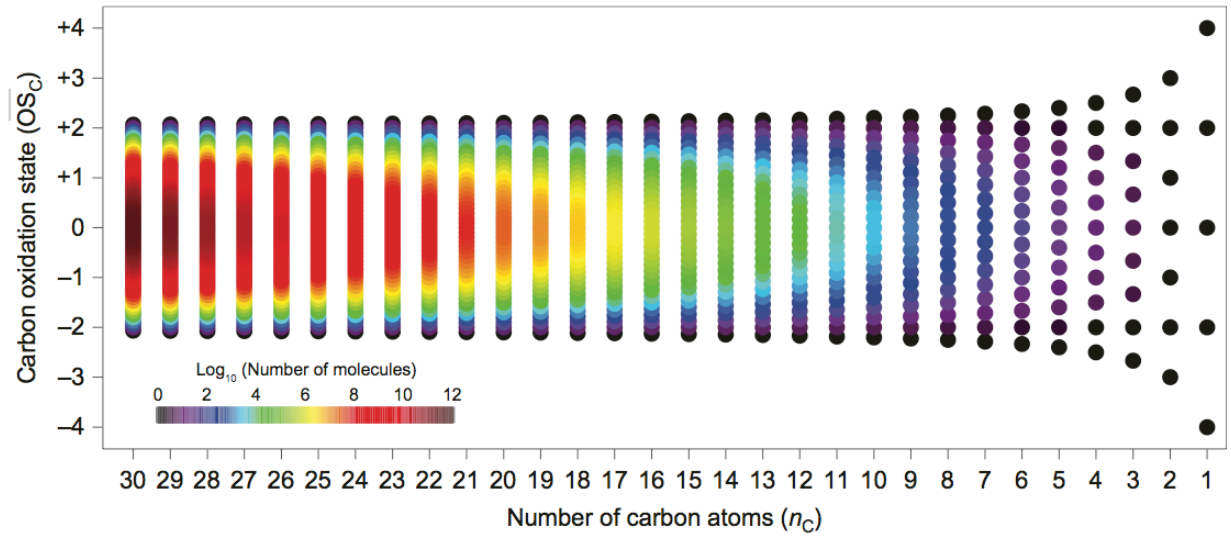

Figure 1.1. Plots representing the chemical complexity of organics (number of molecules) as a function of oxidation state and carbon number with assumptions of an unbranched, acyclic carbon skeleton, and additions of only carbonyl, alcohol and acid groups. Adopted from *Kroll et al*. [2011].

1.2 Atmospheric brown carbon (BrC)

Atmospheric aerosols scatter and absorb solar radiation and thereby play an important role in Earth's radiative balance [*Stocker et al*., 2013]. Whereas the light absorption of atmospheric aerosols is dominated by the absorption by BC [*Andreae and Gelencsér*, 2006; *Stocker et al*., 2013; *Feng et al*., 2013; *Moise et al*., 2015], recent studies have revealed that optical absorption by organics also occurs, suggesting that the presence of light absorptive organics should be explicitly considered in radiative forcing models [*Alexander et al*., 2008; *Feng et al*., 2013]. Brown carbon (BrC) is a component of aerosol organic mixtures that has an ability to absorb sunlight at visible and near-ultraviolet (UV) wavelengths and takes part in photo-initiated reactions. BrC therefore potentially plays important roles in microscopic-scale aqueous phase reactions of organics in aerosols and thus in the macroscopic-scale radiative balance of the Earth.

Based on a model simulation, Feng et al. showed that atmospheric BrC is responsible for 7%~19% of the total (global average) aerosol absorption [*Feng et al*., 2013]. *Jo et al*. [2015] showed that the direct radiative cooling and warming effects of BrC are approximately equal at the top of the atmosphere, thus the global direct radiative effect by BrC is nearly zero and decreases the direct radiative cooling effect by organic aerosols by 17%. Because the light absorption by BrC increases dramatically as the wavelength decreases, the light absorption by BrC can affect atmospheric photochemistry. *Jo et al*. [2015] suggested that light absorption by BrC in near-UV wavelength ranges can decrease surface ozone concentrations and NO_2 photolysis rate observably in a model simulation (Figure 1.2).

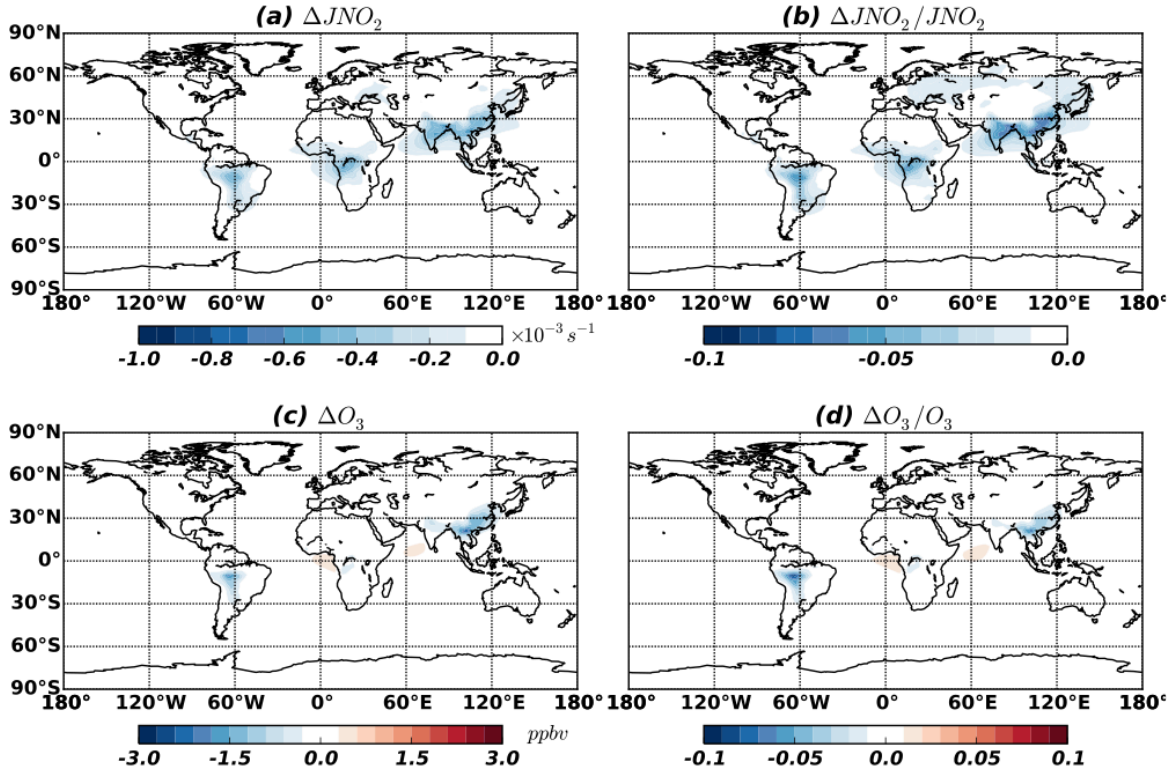

Figure 1.2. Changes in annual NO_2 photolysis rate (a, b) and O_3 concentration (c, d) at the surface due to BrC absorption in a model simulation. Adopted from *Jo et al*. [2015]

Mass absorption efficiency (MAE) as a function of the UV-Vis wavelength and the wavelength dependence, as represented by the Ångström exponent (*Å*) according to a power raw fit, are used to characterize aerosol optical properties. The MAEs of atmospheric aerosols in the visible and UV regions increase strongly as the wavelength decreases. Whereas the MAEs of urban and rural aerosols and isolated HULIS from biomass burning organic aerosol (BBOA) are below 0.1 m^2g^{-1} [OC] at >500 nm [*Hoffer et al*., 2006; *Zhang et al*., 2011; *Utry et al*., 2013; *Liu et al*., 2014], the MAEs at 350–500 nm are as high as 1~3 m^2 g^{-1} [OC] [*Hoffer et al*., 2006; *Chen and Bond*, 2010; *Yang et al*., 2009; *Cheng et al*., 2011; *Zhang et al*., 2013]. Results from multiple studies showed that the *Å* values varied in the range of 2–14, depending on the types and origins of the aerosols [*Hoffer et al*., 2006; *Chen and Bond*, 2010; *Yang et al*., 2009; *Cheng et al*., 2011; *Zhang et al*., 2011 and 2013; *Utry et al*., 2013; *Liu et al*., 2014]. The dependence of *Å* on both the aerosol types and the wavelength suggests that using a single *Å* value may not be sufficient to represent the MAEs of BrC and that an extensive and thorough investigation on the variability of *Å* for BrC is necessary. Investigation of the amounts of BrC and their light-absorption properties, e.g., their MAE and *Å*, are necessary to use them as inputs of atmospheric radiative models and to examine the direct radiative effect by BrC.

The relationship between the optical properties of organic aerosols and their chemical structures has been investigated in several recent studies [*Laskin et al*., 2015]. The MAE values of organics relate to the degree of conjugation and the amount of electron delocalization in molecules. Whereas the MAE of secondary organic aerosol (SOA) from the oxidation of biogenic and anthropogenic volatile organic compounds with hydroxyl radical at 405 nm increases with the O/C ratio [*Lambe et al*., 2013], the absorptivity of model organics generated via the photolysis of pyruvic acid solutions does not increase monotonically with the oxidation level [*Kameel et al*., 2014]. The contributions of some individual organic compounds in the

atmosphere to light absorption and the dependence of absorption on chemical structure have also been investigated. For instance, *Desyaterik et al*. [2013] reported that approximately half of the measured sample absorption in the region of 300–400 nm are attributable to 16 major light-absorbing compounds, which are considered to be nitrophenols and aromatic carbonyls, in BBOA-dominated fog water. *Zhang et al*. [2013] showed that the ambient concentrations of eight nitro-aromatic compounds correlate with the light absorption by water-soluble BrC at 365 nm, although these compounds accounted for only 4% of the overall water-soluble BrC absorption. Recent studies also suggested that the light absorption by aerosol WSOM may also be caused by charge transfer interactions [*Phillips and Smith*, 2014 and 2015]. *Phillips and Smith* [2014] inferred that the charge transfer complexes were responsible for approximately 50% of the observed absorption by the water-soluble fraction of particulate matter collected in Athens, GA. However, their overall chemical structural characteristics remain poorly understood.

Characterization of BrC is important to obtain insight into their sources and formation processes in the atmosphere. BrC in aerosols is emitted into the atmosphere by biomass burning [*Hoffer et al*., 2006; *Yan et al*., 2015], and forms from secondary sources [*Barnard et al*., 2008]. SOA chromophores can be formed via a variety of reaction pathways. Nitrophenols are major chromophores in chamber generated SOA from toluene photo-oxidation in the presence of NOx [*Lin et al*., 2015a]. Nitrogen-containing chromophoric organics are formed by the reactions of carbonyl compounds with amines and ammonia [*Lin et al*., 2015b; *Nozière et al*., 2009; *Galloway et al*., 2009; *Shapiro et al*., 2009; *Kampf et al*., 2012; *Powelson et al*., 2013]. An important characteristic of BrC in view of their role in the atmosphere is their sensitivity to light. Photo-initiated reactions with BrC include both degradation and polymerization [*Kieber et al*., 2012; *De Laurentiis et al*., 2013; *Lee et al*., 2014]. Significant photodegradation of BrC in rainwater and laboratory-generated solutions containing BrC occurs when exposed to simulated

sunlight [*Kieber et al*., 2007 and 2012; *Zhao et al*., 2015]. BrC has potential to have triplet excited states, i.e., $^3C^*$, through the capture of the excitation energy from photons, and thus plays a significant role in aqueous-phase oxidations of organics [*Smith et al*., 2014; *Richards-Henderso et al*., 2015]. 1-Nitronaphthalene in the triplet state reacts with phenol to form humic-like substances (HULIS) [*De Laurentiis et al*., 2013]. Water-insoluble BrC has not received much attention to date. *Zhang et al*. [2013] showed that WISOM has a significant light absorptivity that is stronger than that of WSOM. Light absorption by methanol-extracted matter from ambient aerosols in Los Angeles was ~3 (365 nm) and 21 (532 nm) times higher than that extracted by water. Among the organic compounds in WISOM, unsaturated compounds such as PAHs and oxygenated and nitrated PAHs have electron-conjugated systems and absorb light at near-ultraviolet and -visible wavelengths [*Nocun and Schantz*, 2013]. However, it is not clear what classes or structures of organic compounds in WISOM actually contribute to light absorption. The BrC in different types of aerosols (e.g., urban, forest and ocean aerosols) may also be different, which must result in differences in the optical properties and the photochemical reactivity of the organic components. Investigation of the relationships between the optical properties and structural characteristics of BrC in different types of aerosols is also important to better understand the structures, sources and chemistry of BrC in atmospheric aerosols.

1.3 Solvent extraction and solid phase extraction for aerosol study

Chemical characterization of the highly complex organic matter in aerosols is a challenging subject in the atmospheric community. Although previous studies have made a lot of effort on this topic, quantitative information on the overall chemical structural characteristics of organic complex matter are not understand [*Simoneit et al*., 2004]. The view of the study of chemical compositions of aerosol organics are significantly changed by *Andreae* [2009]; he proposed that

the identification of individual organic species in the complex organic matter are not so important for understanding the role of organic aerosols in climate and atmospheric chemistry, because the key variables of organic aerosols related to their ability to influence climate can be derived from their properties that can be measured relatively easily. Instead, information on properties of organic matter in a number of categories (e.g., positive matrix factorization (PMF) derived factors) is necessary [*Jimenez et al*., 2009]. Overall chemical properties such as elemental composition, relative abundance of functional groups and a variety of molecular fragments of organic matter in aerosol are obtained by high-resolution aerosol mass spectrometers (HR-AMS) and Fourier transform infrared (FTIR) spectroscopy. These characteristics relate to their origins, aging process of organic aerosols [*Andreae,* 2009].

An effective means of understanding the chemical structures of highly complex organic compounds is fractionation of organic aerosol components according to their physicochemical characteristics (e.g., volatility, solubility and polarity) [*Varga et al*., 2001; *Polidori et al*., 2008; *Mihara and Mochida*, 2011; *Psichoudaki and Pandis*, 2013; *Willoughby et al*., 2014; *Jiang et al*., 2014; *Matsumoto et al*., 2014]. Solvent extraction and solid-phase extraction (SPE) are methods to extract the organic component of aerosols. Among the solvent-based methods to fractionate organics, methods based on differences in water solubility have been widely utilized to fractionate WSOM [*Kondo et al*., 2007; *Sun et al*., 2011; *Zhang et al*., 2012; *Wozniak et al*., 2012; *Verma et al*., 2012 and 2013; *Psichoudaki and Pandis*, 2013; *Zhang et al*., 2013; *Park et al*., 2013]. A theoretical analysis for the separation of WSOM from WISOM by the extraction of aerosol samples with water was performed by *Psichoudaki and Pandis*, [2013]. As shown in Figure 1.3, they proposed a value of 0.1 cm^3 m^{-3} (the ratio of water used per volume of air sampled on the analyzed filter) for the extraction of WSOM for typical organic aerosol concentrations of 1–10 μg m^{-3}. For solvent extraction of more organic components from aerosol

samples, various organic solvents (i.e., acetone, methanol, ethyl acetate, dichloromethane, and *n*-hexane) have been used in the extraction of organic organics. *Willoughby et al*., [2014] determined that 31%–59% of the total aerosol organics is extractable with pyridine from total suspended particulate (TSP) samples in Gloucester Point, VA. Their result showed that the organics in the pyridine-extractable fraction is less polar and more aliphatic than those in the water-extractable fraction. *Mihara and Mochida*, [2011] showed that most organics can be extracted with methanol from submicron particles in Nagoya, Japan, and that the elemental ratios of O/C in organics tend to increase with the polarity of corresponding solvent for extraction, in the order of ethyl acetate, methanol and water. Nearly total organic carbon was extracted successively with solvents of dichloromethane (64% of the extractable OC), acetone (21%) and water (15%) in $PM_{2.5}$ aerosols collected from five US national parks for the determination of the ratio of organic aerosol mass to organic carbon [*El-Zanan et al*., 2005]. Cheng et al., [2012] showed that about 55% of the total organic carbon in $PM_{2.5}$ aerosols in Beijing can be extracted with a mixture of *n*-hexane, dichloromethane and acetone. The above studies demonstrated that the solvent extraction method is an effective means to separate the complex organic matter into distinct fractions. However, the technical aspects listed below have not been addressed.

(1) Because organic solvents are used for extraction of aerosol organics, studies on the quantification of the organic masses in the extracts are relatively few [*Mihara and Mochida*, 2011].

(2) Although the different aerosol fractions have been extracted by different solvents in several recent studies [*Mihara and Mochida*, 2011], overlap in organic mass between different extracted fractions may exist. A sequential extraction of the same filter sample with different solvents is limited [*El-Zanan et al*., 2005].

(3) The chemical characterization of organics in extracts is often influenced by inorganic salts. Isolation of organics from most inorganic salts in aerosol extracts is required.

(4) Extraction of many fractions from aerosols by solvent extraction is difficult.

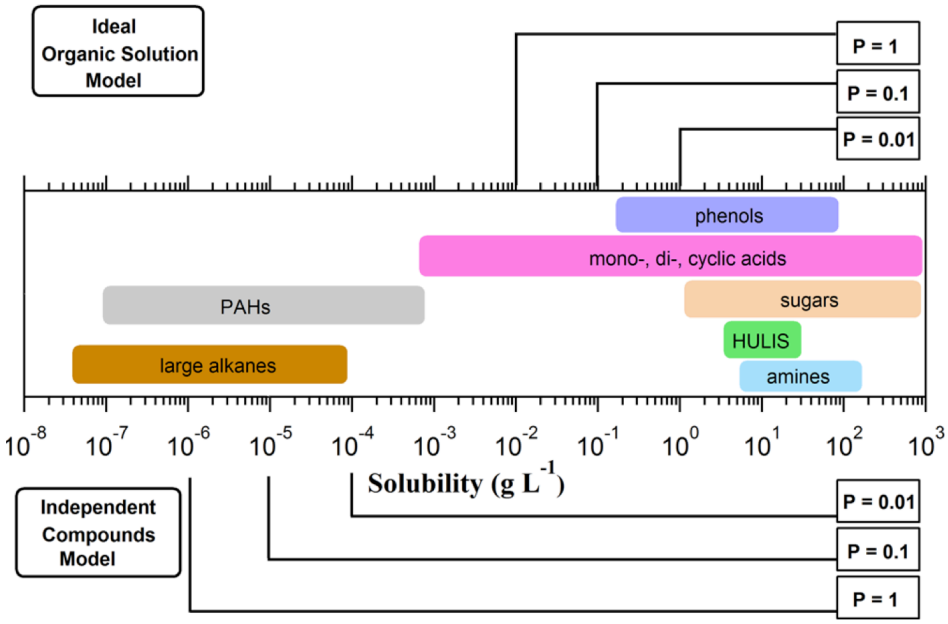

Figure 1.3. Solubility ranges of various organic aerosol compound classes and predicted lower limits of the solubility of compounds for the extraction under the conditions of different *P* parameter values (the ratio of the volume of water used per volume of air sampled on the analyzed filter (cm^3 m^{-3})). Adopted from *Psichoudaki and Pandis*, [2013]

Solid-phase extraction (SPE) techniques can be used for the separation of more organic fractions from extracts with water and organic-solvents than those from a solvent extraction method, according to the polarity of organics. Reversed-phase SPE (i.e., Oasis HLB and C18 columns) have been used in some cases to isolate HULIS from WSOM according to the polarity and/or acidity of the compounds [*Varga et al.*, 2001; *Gysel et al.*, 2004; *Hoffer et al.*, 2006; *Song et al.*, 2012; *Lin et al.*, 2012; *Salma et al.*, 2013; *Utrya et al.*, 2013; *Paglione et al.*, 2014]. An

additional advantage of the reversed-phase SPE is that the isolation of organics from inorganic salts in aerosol water extracts is possible. The isolated organic matter can be characterized without interference from inorganics, for example for the analysis of functional groups using an FT-IR [*Fan et al*., 2013] and the analysis of the hygroscopicity of organics [*Gysel et al*., 2004]. Among organic fractions, WSOM and HULIS were subjected to the characterization of chemical structures, and their properties were investigated in a number of studies [*Hoffer et al*., 2006; *Song et al*., 2012; *Lin et al*., 2012; *Utrya et al*., 2013; *Paglione et al*., 2014]. However, the fraction of WSOM other than HULIS remain poorly characterized, despite the fact that they constitute a large fraction of organics in aerosols. The non-HULIS WSOM is polar and may be closely linked to aerosol hygroscopicity [*Varga et al*., 2001; *Gysel et al*., 2004]. Normal-phase SPE, i.e., the extraction using a silica gel column is useful for the separation of organic compounds in organic-solvent extracts based on the polarity of the organics. Silica gel column was often used for sample pretreatment for the analysis of less polar organic compounds in aerosols, such as aliphatic hydrocarbons, aromatics, fatty alcohols, ketones, aldehydes and acids by gas chromatograph-mass spectrometer (GC/MS) [*Okuda et al*., 2006; *Liu et al*., 2006]. Many individual organic compounds in these less polar aerosol fractions were identified by GC-MS or two-dimensional GC-MS (2D-GC/MS) [*Simoneit et al*., 2004; *Chan et al*., 2013]. The overall structural characteristics of the less polar organic compounds have not been understood [*Willoughby et al*., 2014], although the significant light absorptivity and toxicity of this less polar component in aerosols have been suggested [*Verma et al*., 2012 and 2013; *Zhang et al*., 2013].

1.4 Off-line measurements of organic aerosols

Figure 1.4 summarizes some techniques currently used for the analysis of the organic component in aerosols. Different instruments are compared in views of chemical resolution, the

ability of the quantification, and the time and size resolutions of the chemical analysis of the organics.

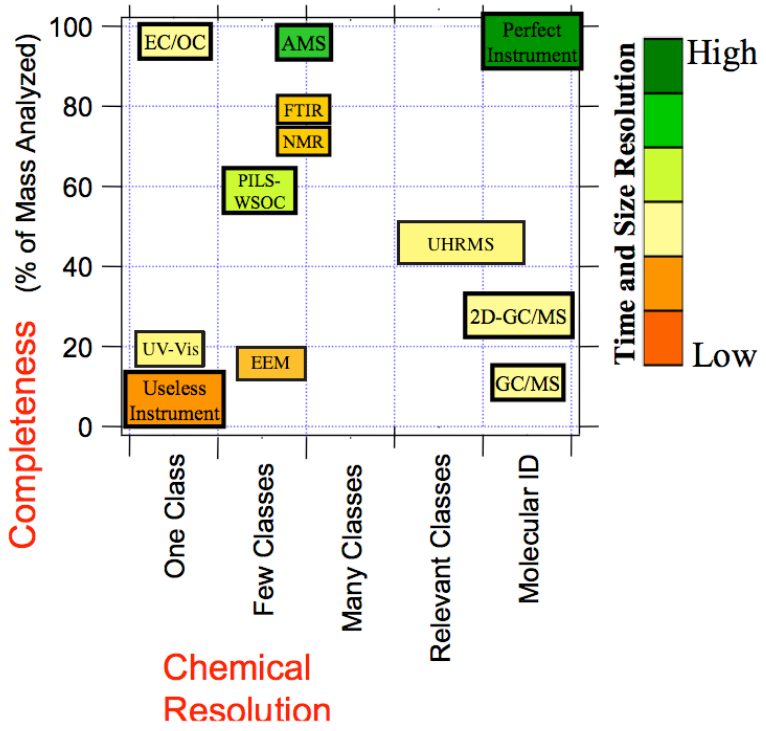

Figure 1.4. Three-dimensional representation of some techniques currently used for the analysis of the organic component of aerosols. Reproduced from *Hallquist et al.*, [2009] (Copyright Authors 2009). EC/OC: EC/OC carbon analyzer; UV-Vis: ultraviolet-visible spectrophotometer; PLIS-WSOC: particle-into-liquid sampler with a total carbon analyzer; EEM: excitation-emission matrix; AMS: aerosol mass spectrometer; FT-IR: Fourier-transform infrared spectrometer; NMR: nuclear magnetic resonance spectrometer; UHRMS: ultrahigh resolution mass spectrometer with soft ionizations; 2D-GC/MS: two-dimensional gas chromatography (2D-GC) coupled with mass spectrometer (MS).

Aerodyne HR-AMS with a certain chemical resolution, high-time resolution and complete quantitative ability [*Hallquist et al*., 2009] have been widely used for online measurements of the concentrations and chemical composition of atmospheric aerosols [*Mohr et al*., 2012; *Paglione et al*., 2014; *Han et al*., 2014; *Huang et al*., 2015], and have also been applied to offline chemical characterization and quantitative analysis of aerosol extracts in combination with a nebulization technique [*Mihara and Mochida*, 2011; *Desyaterik et al*., 2013; *Huang et al*., 2014; *Kaul et al*., 2014]. HR-AMS can be used for elemental analysis and ion-group analysis based on the determination of ion formulas, and can be used to distinguish organic component and inorganic species from HR-AMS spectra using a fragment table [*DeCarlo et al*., 2006; *Aiken et al*., 2008]. An additional advantage of the HR-AMS analysis of organic aerosols is that the overall structural information of complex organic matter is obtained. A number of HR-AMS data of primary organic aerosol (POA) and SOA with different sources and formation processes have been reported in previous works (URL: http://cires.colorado.edu/jimenez-group), which are important references to identify sources and properties of isolated organics from aerosols.

In the cases of chemical analysis of organic aerosols by FT-IR spectroscopy and nuclear magnetic resonance (NMR) spectroscopy, various organic functional groups in aerosols can be identified and quantified. Multiple types of functional groups, i.e., aliphatic C–H (saturated and unsaturated), alcoholic C–OH, non-acidic carbonyl C=O, carboxylic COOH, amine C–NH_2 and organic nitrate C–ONO_2 in ambient organic aerosols were quantified in ambient aerosol filter samples and aerosol extracts by the FT-IR analysis [*Graber and Rudich*, 2006; *Takahama et al*. 2013]. For example, *Graber and Rudich* [2006] showed that the FT-IR spectra of aerosol HULIS was similar to that of Suwannee River fulvic acid. In the case of NMR analysis of organic aerosols, because of the complexity of organic aerosol composition, most individual compounds cannot be identified. Instead, the intensities of the signals in ^{1}H-NMR spectra of aerosol extracts

are usually divided into four chemical shift ranges, i.e., the saturated aliphatic region (H–C–C, δ0.6–δ1.9 ppm), the unsaturated aliphatic region (H–C–C=, δ1.9–δ3.2 ppm), the oxygenated saturated aliphatic region (H–C–O, δ3.2–δ4.5 ppm) and the aromatic region (H–Ar, δ6–δ9 ppm) [*Seaton et al*., 2013; *Chalbot et al*., 2014; *Duarte et al*., 2015].

Ultraviolet-visible (UV-Vis) spectroscopy and excitation-emission matrix (EEM) fluorescence spectroscopy are commonly used to investigate the optical and structural characteristics of chromophores that are responsible for the light absorption and fluorescence by complex organic matter. The MAE and *Å* of BrC can be obtained from UV-Vis spectra of different aerosol extracts. For example, *Zhang et al*. [2013] reported the MAE and *Å* values both of the methanol- and water-soluble BrC in $PM_{2.5}$ particles in Los Angeles based on the UV-Vis analysis of the extracts. More detailed information on the type of chromophores can be obtained from the EEM of aerosol extracts. Components associated with HULIS and protein-like organic matter (PLOM) have been statistically determined for complex organic matter in terrestrial and oceanic systems as well as atmospheric aerosols by parallel factor (PARAFAC) analysis for the EEMs. The method was widely applied to the characterization of water-soluble organic matter in terrestrial and oceanic systems [*Murphy et al*., 2013; *Yu et al*., 2015]. However, it has not been extensively used in the atmospheric aerosol science community [*Mladenov et al*., 2011; *Matos et al*., 2015; *Aryal et al*., 2015]. Although EEMs of organic matter in terrestrial and oceanic systems are relatively well characterized, the results may not be applied to organic matter in the atmosphere because the sources and underlying physical-chemical processes are different [*Duarte et al*., 2007; Matos et al., 2015]. Hence, the relationship between the EEM components and chemical structural characteristics of organic aerosol components must be studied further to understand the chemical structures of chromophores in the atmosphere.

GC/MS or 2D-GC/MS can be used to determine individual organic compounds in aerosols, such as aliphatic hydrocarbons, aromatics, fatty alcohols, ketones, aldehydes and acids [*Simoneit et al*., 2004; *Chan et al*., 2013]. However, the composition of a large mass fraction of organics, including unresolved complex mixtures (branched and cyclic compounds) and nonvolatile or thermally unstable compounds (oxygenated compounds with high molecular weights), have not been characterized well [*Hallquist et al*., 2006; *Simoneit et al*., 2007; *Alama et al*., 2013; *Chan et al*., 2013]. Although the elemental composition of aerosol organic molecules can be obtained by UHRMS analysis of the extracts, the quantitative information of the chemical composition of aerosol organic matter is missing because ionization efficiency of organic compounds largely varied with their chemical structures in the soft ionizations (i.e., ESI, APCI and APPI).

As explained above, to obtain the overall structural information of the complex organic matter, analytical techniques of HR-AMS, FT-IR and NMR can be employed. These analytical techniques in combination with extraction and separation techniques (as described in section 1.3) provide both qualitative and quantitative information on the overall chemical structural characteristics of aerosols with a relatively high chemical resolution.

1.5 Research objectives of this study and the contents of this dissertation

For understanding the chemical structures and optical properties of the highly complex organic mixture in atmospheric aerosols, different aerosol organic components were fractionated according to the solubility and polarity of organics using the methods of multiple solvent extraction and solid phase extraction, and then the chemical structures and optical properties of those fractions were characterized with multiple analytical techniques. The relationships between the chemical structural characteristics of organic aerosols and their optical properties were explored.

Research objectives of this study are to characterize (1) the chemical structures of total organic matter in total suspended particulates (TSP) collected in the city of Nagoya in summer/early autumn and winter; (2) the light-absorption and fluorescence of total organic matter in the TSP samples; (3) the chemical structures and light-absorption of WISOM in the submicron aerosols ($PM_{0.95}$) collected in Nagoya; and (4) the light-absorption and fluorescence of WSOM in $PM_{0.95}$ collected in the urban, forest and marine environments (Nagoya, Kii Peninsula, and the tropical Eastern Pacific). For the first and second objectives, a combination of solvent extraction and reverse-phase SPE was used to extract and fractionate organic compounds with different polarities in TSP samples (WSOM, WISOM, two fractions of humic-like substances, showing neutral and acidic behavior (HULIS-n and HULIS-a, respectively), and the remaining highly-polar part of WSOM). Their chemical structures and optical properties were obtained from the HR-AMS spectra, soft ionization mass spectra, FT-IR spectra, UV-visible absorption spectra and the EEMs. For the third objective, the WISOM in the urban $PM_{0.95}$ were fractionated to six sub-fractions using solvent extraction and normal-phase SPE. The structural and light-absorption characteristics of these sub-fractions were then determined using multiple analytical techniques including HR-AMS and FT-IR analyses. For the fourth objective, structural and optical characteristics of WSOM in the urban, forest and marine $PM_{0.95}$ samples were investigated based on the EEMs and HR-AMS spectra. The origins of water-soluble brown carbon were inferred from the signatures in the HR-AMS spectra and EEMs, and from the comparison of the results from hierarchical cluster analysis and backward air mass trajectory analysis.

This dissertation is composed of seven chapters: *Chapter 1* is about the research background regarding the chemical composition, chemical structural characteristics and optical properties and analysis of organic aerosols; *Chapter 2* explains the experimental methods of this study, i.e.,

aerosol sampling, extraction, instrument analysis and data processing; *Chapters 3-6* are the results and discussion sections. *Chapters 3* and *4* present the structural and optical properties of total aerosol organics in the urban TSP samples. *Chapter 5* presents the structural and light-absorption characteristics of six sub-fractions of WISOM in the urban $PM_{0.95}$. *Chapter 6* presents the chemical and optical properties of water-soluble BrC in the $PM_{0.95}$ collected in the urban, forest and marine environments (Nagoya, Kii Peninsula, and the tropical Eastern Pacific). *Chapter 7* is the conclusions section, in which the major conclusions and potential implications of this study and suggestions for future studies were given.

2 Experimental methods

2.1 Aerosol sampling and extraction and separation of aerosol components

2.1.1 Urban total suspended particulates (TSP, Nagoya)

A total of 16 TSP samples (146–191 h) were collected using a high-volume sampler (HV-700F, Shibata) with a flow rate of 700 L min^{-1} at the Nagoya City Institute for Environmental Sciences, Nagoya, Japan over two periods: from 26 July to 20 September 2011 (summer and early autumn) and from 20 December 2011 to 13 February 2012 (winter). These samples were collected on 8 × 10 inch quartz fiber filters, which were pretreated at 450 ˚C for 2 h in a muffle. Blank filters were also collected. Among sixteen filter samples, twelve were used for the chemical and optical analysis of organic aerosols and the other four were used for the assessment of the analytical method. The TSP filter samples were used for the study of the chemical structures, light-absorption and fluorescence characteristics of total aerosol organic matter. The results are presented in *Chapters* 3 and 4.

A punched piece of TSP filter samples (diameter: 34 mm) was used to extract and separate organic components (Figure 2.1). WSOM was extracted by ultrasonication with 3 g of Fluka water (Sigma Aldrich) three times and was filtered through a 0.2 μm PTFE filter (Millex). After the extraction, WISOM was further extracted from the same filter punch by ultrasonication with 3 g of methanol (MeOH) once and subsequently with 3 g of a dichloromethane (DCM)/MeOH (2/1, v/v) mixture three times. The PTFE filter used to extract the WSOM was used again to filter the extract containing WISOM, to recover organics remaining on the PTFE filters. The sequentially extracted WISOM fractions were combined, dried using a rotary evaporator, and redissolved in 8 g of DCM/MeOH (2/1, v/v). To evaluate the recovery of organics from TSP samples throughout the solvent extraction procedure, we compared the concentrations of

extracted organic carbon (EOC = water-insoluble organic carbons (WISOC) + water-soluble organic carbons (WSOC)) derived from the analysis using HR-AMS and those of TOC derived from the TOC analyzer. As shown in Figure 2.2, the recoveries of OC were calculated to be 92 ± 5.3% (mean ± SD; n = 12; r^2 = 0.93) and 102 ± 11% (mean ± SD; n = 12; r^2 = 0.84) with the application of thermal/optical transmittance (TOT) and reflectance (TOR) methods, respectively, for the analysis using the TOC analyzer. The results suggest that nearly all organics were extracted from the TSP samples.

Two fractions of HULIS, showing neutral and acidic behavior at the elution steps (HULIS-n and HULIS-a, respectively) and high polarity (HP-) WSOM were fractionated from the WSOM fraction using an Oasis HLB (6cc, 200 mg; Waters) in a manner analogous to that described in *Varga et al*. [2001] and *Lin et al*. [2012] as follows:

1) First, the pH of the water extract was adjusted to 7 with 0.01 M NaOH (Sigma-Aldrich, ≥99.99) solution, and it was then passed through the HLB column (200 mg, pre-activated by 6 mL MeOH and 6 ml Fluka water), followed by the addition of 2 × 0.5 ml of Fluka water to wash residual ions/species that were not retained. The HLB column was dried under a N_2 flow by Visiprep DL vacuum manifold (Supelco). Then, adsorbed species were eluted by 2 mL of methanol containing 2 wt% ammonia. The extract was fully dried under a nitrogen flow and redissolved with 6 g of MeOH. This organic fraction is referred to as humic-like substances with a neutral nature in WSOM (HULIS-n), because they favor adsorption on the column, which suggests small abundance of polar carboxylic groups.

2) Second, the effluent in the first step was collected in a 15-mL pre-cleaned sample bottle, and its pH was adjusted to 2 with 1 M HCl solution (Fluka, for trace analysis). The effluent was then passed through the HLB column, followed by the addition the 2×0.5 mL of acidified Fluka water (pH = 2) to the column. The HLB column was dried, and then the species adsorbed on the

column were eluted with 6 mL MeOH. The organics in this effluent are referred to as humic-like substances with an acidic nature in WSOM (HULIS-a), because the pH dependence of the absorption can be explained by different degrees of dissociation of carboxylic groups therein. In the case of organic acids, their acid ionization constants pK_a may range from 2 to 7. The effluent in this step was collected in 15-mL pre-cleaned sample bottles. According to the adsorption mechanism of HLB, this fraction should contain highly polar species. We refer to organics in this fraction as high polarity (HP-) WSOM.

To evaluate the recovery of organics in SPE, the concentrations of WSOM directly determined using HR-AMS and the concentrations of the sum of HULIS-n, HULIS-a and HP-WSOM were compared. The result shows that the recoveries of the SPE procedure were 106 ± 8% (r^2 = 0.94; n = 12) for WSOM and 105 ± 19% (r^2 = 0.96; n = 12) for WSOC, indicating that most of the WSOM were recovered.

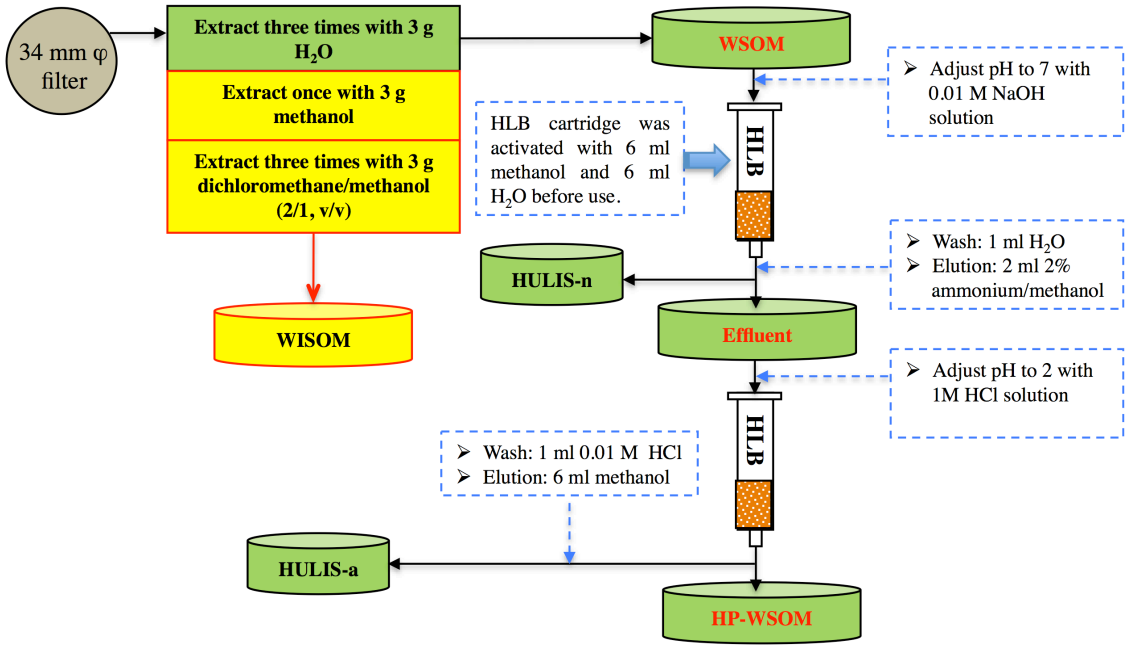

Figure 2.1. The procedure of solvent extraction and SPE for fractionation of organics in TSP samples.

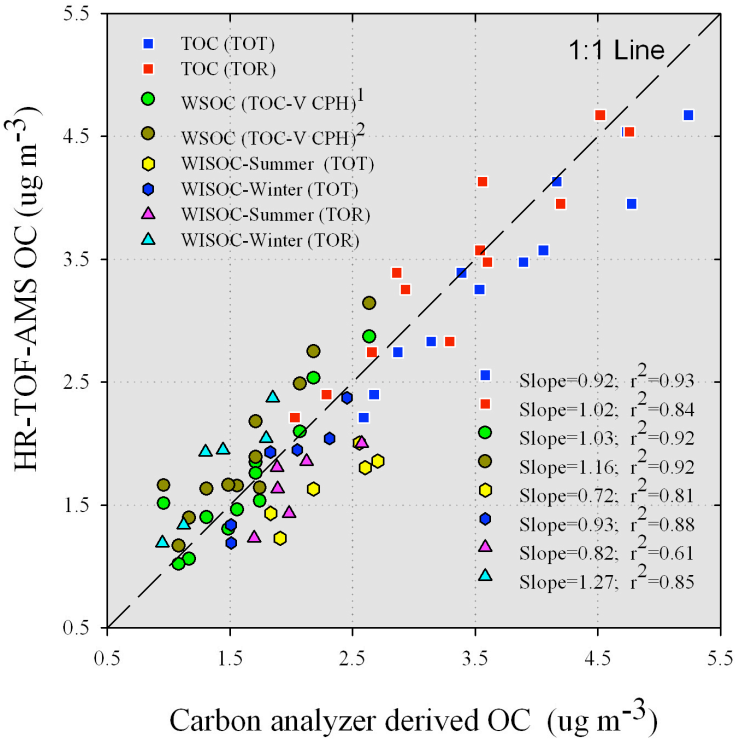

Figure 2.2. OC concentrations from the HR-AMS plotted against those from the TOC analyzer. $WSOC^1$ and $WSOC^2$ in the vertical axis are from HR-AMS-derived WSOM and from HULIS-n, HULIS-a, and HP-WSOM derived from HR-AMS, respectively. The plot for the sample influenced by marine aerosol (8/30-9/3) largely deviated from the 1:1 line and is shown in parenthesis.

2.1.2 Urban submicrometer atmospheric particles ($PM_{0.95}$, Nagoya)

Submicrometer urban atmospheric particles were collected on 8 × 10 inch quartz-fiber filters using a high-volume sampler (MODEL-120B, Kimoto Electric Co. Ltd.) on the rooftop of a building at Nagoya University in Nagoya, Japan. The sampler, equipped with a cascade impactor (TE-230, Tisch Environmental, Inc.), was used to collect particles with an aerodynamic diameter of <0.95 μm. A total of twenty-four samples were collected from 25 August to 28 September

2013 and from 4 March to 7 April 2014. Five blank filters were also collected. The filter samples were stored at −20°C until further analysis. The urban $PM_{0.95}$ filter samples, including four weekly samples (for the main part of the analysis) and twenty two-day samples (for additional analyses using an FT-IR and a UV-visible spectrometer), were used for the analysis of the chemical structures and light-absorption characteristics of water-insoluble aerosol organic mixtures. The results are presented in *Chapter* 5.

Three filter punches (diameter: 34 mm) for each sample were used for the extraction and fractionation of organic components (Figure 2.3). Water-soluble matter (WSM) was extracted by ultrasonicating with 3 g of Fluka water (Sigma Aldrich) three times and filtering through 0.2 μm PTFE membrane filters on a stainless steel syringe filter holder (Millex). After the extraction, WISOM was further extracted from the same filter punches by ultrasonicating continuously with 3 g of MeOH, DCM and *n*-hexane. The PTFE membrane filter used to filter the WSM was used again to filter the extract containing WISOM to recover organics remaining on the PTFE filters.

The extracted WISOM fractions were dried using a rotary evaporator and redissolved in different solvents in the order of 6 ml of *n*-hexane, *n*-hexane/DCM (2/1, v/v), DCM, DCM/MeOH (2/1, v/v), and MeOH and 4 ml of MeOH containing 2 wt% of ammonia for the same samples. These samples were successively placed on the silica gel columns (500 mg, glass hardware, Sigma-Aldrich). The silica gel columns were pre-rinsed with 6 ml MeOH, DCM and *n*-hexane prior to the sample loading. Six fractions, F1, F2, F3, F4, F5 and F6, were successively eluted with *n*-hexane, *n*-hexane/DCM (2/1, v/v), DCM, DCM/MeOH (2/1, v/v), and MeOH and MeOH containing 2 wt% of ammonia and were collected in 15-mL pre-cleaned glass bottles. The concentrations of the extracted organic carbon (EOC = WSOC + WISOC) was on average 1.96 ± 0.16 μg m^{-3} (mean ± SD), which corresponds to 87% ± 5% and 106% ± 10% (mean ± SD)

of the filter TOC derived from the TOC analyzer with the thermal optical transmittance (TOT) and reflectance (TOR) methods, respectively.

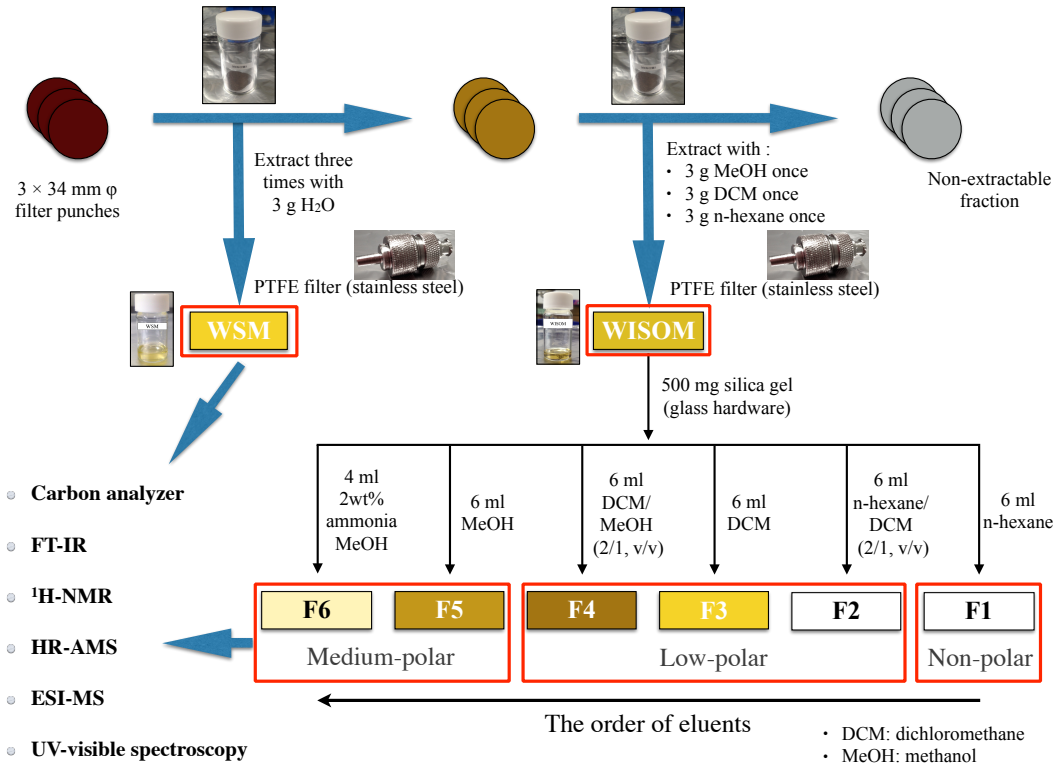

Figure 2.3. The procedure of the solvent extraction, fractionation and analysis of water-insoluble complex organic mixtures in the unban $PM_{0.95}$ samples.

2.1.3 Urban, forest and marine $PM_{0.95}$ samples (Nagoya, Kii Peninsula, and the tropical Eastern Pacific)

Sixty-three $PM_{0.95}$ samples (50% cutoff: 0.95 μm) collected on 8 × 10 inch quartz fiber filters using high-volume samplers in urban, forest and marine environments were used for the characterization of chromophoric water-soluble organics by HR-ToF-AMS analysis and excitation–emission matrix spectroscopy. The results are presented in *Chapter* 6. Twenty-seven samples were collected at an urban site in Nagoya, Japan (Nagoya University; 35.15°N,

136.97°E) from 11 August to 14 September 2013 (sample ID: 1–17), and from 4 to 24 March 2014 (sample ID: 18–27). Sixteen samples were collected at a forest site on the Kii Peninsula, Japan (Wakayama Forest Research Station (WFRS), Kyoto University; 34.07°N, 135.52°E); five from 20 to 30 August 2010 (sample ID: 28–32), and eleven from 28 July to 8 August 2014 (sample ID: 33–43). Twenty samples were collected aboard the NOAA RV Ka'imimoana as part of the Tropical Ocean tRoposphere Exchange of Reactive halogens and Oxygenated VOCs (TORERO) field experiment over the eastern equatorial Pacific ocean during the TORERO/KA-12-01 cruise in February 2012 (sample ID: 44–63). Blank filters were also collected at different sites and periods. Note that the urban $PM_{0.95}$ samples have also been used for the study of chemical structures and light-absorption characteristics of water-insoluble aerosol organic mixtures as detailed in section 2.1.2.

WSOM for the EEM analysis and HR-AMS analysis was extracted by ultrasonication of filter punches (diameter: 34 mm) with Milli-Q water for 1 h, followed by filtration through 0.2 μm PTFE filters (Millex). Different extraction conditions, i.e., the number of filter punches (diameter: 34 mm) and the mass of Mill-Q water, were applied to different samples, as summarized in Table 2.1.

Table 2.1. Filter samples used and the extraction conditions.

Sampling location	Sampling period	Samples			Blank filters	Extraction	
		Number	ID	Sampling time (h)		Filter (cm^2)	Water (g)
Urban (Nagoya)	11 August 2013– 14 September 2013	17	1–17 (Summer)	47–48	5	1 × 9.1	10
	4 March 2014– 24 March 2014	10	18 –27 (Winter)	47–48	5	1 × 9.1	10*
Forest (WFRS, Kii Peninsula)	20 August 2010– 30 August 2010	5	28–32 (WKYM2010QFF)	43–48	3	2 × 9.1	5
	28 July 2014– 8 August 2014	11	33–43 (WKYM2014QFF)	23–24	3	3 × 9.1	5
Ocean (eastern equatorial Pacific)	1 February 2013– 29 February 2013	20	44–63 (TRR)	11–30	3	2 × 9.1	4

* For the analysis of five extracts (sample ID: 18, 22, 24, 25 and 27) using EEM spectroscopy, the extracts were diluted 3 times with Mill-Q water.

2.2 Instrumental analyses

2.2.1 Off-line analysis of organic aerosol extracts using HR-AMS

Aerosol extracts from TSP and $PM_{0.95}$ were atomized with pure air (CO, CO_2 and THC: <0.1 ppm) and argon (purity: 99.9999%), respectively. The generated aerosol was passed through two diffusion scrubbers (one with silica gel and the other with activated carbon mixed with silica gel) to remove water and organic solvent vapors. Then, the aerosol was introduced to the HR-AMS. The HR-AMS spectra were acquired in both V and W modes to quantify OM mass and to analyze the chemical structural characteristics (ion group and elemental analyses) of the organics, respectively. The V- and W-mode data were analyzed using Squirrel v.1.56A and Pika v1.15A Software (http://cires.colorado.edu/jimenez-group/ToFAMSResources/ToFSoftware/), respectively. In the analysis, $(CO_2^+)_{air}$ in the fragment

table was modified to be zero, and $(CO^+)_{org}$ were modified to (CO^+) when argon was used as a carrier gas. The mass concentrations of the extracts were quantified by the internal standard method using phthalic acid [*Mihara and Mochida*, 2011; *Han et al*., 2016]. In the analysis using Pika, all organic ions were classified into six groups of CH, CO (CO+O+HO), CHO_1, $CHO_{>1}$, CHON, and CS for TSP samples and ten groups of C_x, CH, CHO_1, CHO_{gt1}, CHN, CHON, NO, HO, CO, and CO_2 for $PM_{0.95}$ samples, respectively. The elemental analyses to determine the molar elemental ratios (O/C, H/C, and N/C) and the mass ratio of OM to OC were performed as described in *Aiken et al*. [2008] (for N/C) and *Canagaratna et al*. [2015] (for O/C, H/C, and OM/OC).

The reproducibility of the quantification of WISOM, WSOM, HULIS-n, HULIS-a and HP-WSOM was assessed by the extraction and the HR-AMS analysis of an identical TSP sample three times; the relative standard deviation (RSD) of the concentrations of WISOM, WSOM, HULIS-n, HULIS-a and HP-WSOM were 10.8%, 2.8%, 0.6%, 0.5%, and 5.8%, respectively. The blank levels were also assessed with HR-AMS analysis for a blank filter three times; they corresponded to 1.7%, 0.6%, 4.4%, 3.8%, and 1.6% of the lowest concentrations of the solutions of WISOM, WSOM, HULIS-n, HULIS-a and HP-WSOM for the HR-AMS analysis, respectively. The low RSD and low blank levels suggest that the process for quantifying organics, including aerosol sampling, solvent extraction, separation using SPE, and off-line HR-AMS analysis, was reliable. The reproducibility of the ion group and the elemental analyses for the off-line HR-AMS analysis of organics was also examined; the RSD of the relative intensities of six ion groups (CH, CO, CHO_1, $CHO_{>1}$, CHON, and CS) and the elemental ratios (H/C, O/C, and N/C) were, respectively, in the ranges of 0.5% to 17.5% and 0.2% to 10.1% for WISOM, WSOM, HULIS-n, HULIS-a and HP-WSOM (n = 3 for respective fractions).

2.2.2 Diffuse reflectance FT-IR analysis

FT-IR were used for the study of chemical functional groups of organics in the extracts include WISOM, HULIS-n, HULIS-a and HP-WSOM in the unban TSP samples and the six sub-fractions of WISOM in the urban $PM_{0.95}$. The liquid extracts were concentrated to ~0.5 mL under N_2, and then 0.1 g or 0.2 g of KBr (FT-IR grade, Sigma Aldrich) was added and concentrated to be fully dried. The extracts containing HP-WSOM were completely dried using a rotary evaporator and then redissolved with 2 g of MeOH prior to the process described above. The mixture of the extracts and KBr was ground in an agate mortar for analysis by FT-IR spectrometry.

An FT-IR spectrometer (6100, JASCO) with a diffuse reflectance accessory (DR PR04 10-M, JASCO) was employed to quantify the chemical functional groups in the extracts. The FT-IR spectra in the range of 400–4000 cm^{-1} were recorded 64 times, with a resolution of 4 cm^{-1}. The spectrum baseline was determined by analyzing pure KBr before analysis of the aerosol extract samples. Six types of functional groups, i.e., aliphatic C-H (saturated and unsaturated), alcoholic C-OH, non-acidic carbonyl C=O, carboxylic COOH, amine C-NH_2 and organic nitrate C-ONO_2, were identified and then quantified (see section 2.3.1).

2.2.3 Analysis of functional groups using ^{1}H-NMR

Extracts of respective water-insoluble organic fractions from the urban $PM_{0.95}$ samples (the weekly samples only) were combined, dried under a nitrogen flow, and redissolved in 0.6 mL of chloroform-d ($CDCl_3$) and 0.75 ml of methanol-d_4 (99.8 atom % D, Sigma-Aldrich) for fractions F1–F4 and F5, respectively; 0.03% (v/v) of TMS in chloroform-d and methanol-d_4 served as internal standards for the ^{1}H-NMR measurements. The ^{1}H-NMR spectra of different extracts in 5

mm NMR tubes were recorded 1024 times on a JEOL JNM ECA-600 spectrometer equipped with a 5-mm FG/HCN probe.

The baseline and phase corrections and the data integration were performed using matched software (JEOL). The peaks in the ^{1}H-NMR spectra of blank samples were subtracted from the ^{1}H-NMR spectra of the samples. The intensities of the signals in four chemical shift ranges, i.e., the saturated aliphatic region (H–C–C, δ0.6–δ1.9 ppm), the unsaturated aliphatic region (H–C–C=, δ1.9–δ3.2 ppm), the oxygenated saturated aliphatic region (H–C–O, δ3.2–δ4.5 ppm) and the aromatic region (H–Ar, δ6–δ9 ppm), were integrated [*Seaton et al*., 2013; *Chalbot et al*., 2014; *Duarte et al*., 2015]. For the identification of specific molecular structures that correspond to the peaks in the ^{1}H-NMR spectra and the ^{1}H-^{1}H correlation spectra (COSY), online tools at nmrdb.org were employed [*Banfi et al*., 2008].

2.2.4 Analyses of molecular weight distribution using ESI/APCI-MS

A high-performance quadrupole time-of-flight mass spectrometer (micrOTOF-QII, Bruker) equipped with either of two soft ionization sources, electrospray (ESI) or atmospheric pressure chemical ionization (APCI), was employed to investigate the molecular-weight distributions (MWD) of fractionated organics of WIOSM, HULIS-n, HULIS-a and HP-WSOM in the unban TSP samples and the fourth fraction of WISOM (F4) in the urban $PM_{0.95}$ (the weekly samples only). The extracts were directly injected from a syringe pump into an ionization source. The spray voltage was set to –3.5 and 4.5 kV for the ionization of organics in negative and positive modes, respectively. The voltage of the collision cell RF was set to 120 and 620 Vpp for the acquisition of the signals of ions with mass-to-charge ratios (m/z) in the ranges of 50–1000 (low-molecular weight method) and 300–2000 (high-molecular weight method), respectively. The signals of ions were recorded for ~8 min and preprocessed to eliminate some peaks with a signal

to noise ratio (S/N)≤10 or those present in blank samples. The m/z axis was calibrated using ESI Taning mix and APCI-Low concentration Taning mix (Agilent Technologies). The accuracy of the mass was <5 ppm, and the resolution reached 5000–18000 (FWHM), according to external calibrations and measurements of the samples. To characterize the possible MWD of the fractionated organics, the number-average molecular weight (M_n) and mass-average molecular weight (M_w) were estimated according to the following formulas [*Mané et al*., 2007]:

$$M_n = \frac{\sum_i (m/z)_i I_i}{\sum_i I_i} , \quad (1)$$

$$M_w = \frac{\sum_i (m/z)_i^2 I_i}{\sum_i (m/z)_i I_i} , \quad (2)$$

where $(m/z)_i$ and I_i are, respectively, the m/z and the signal intensity of the i-th peak and the m/z of ions is approximated to be equal to the molecular weight of corresponding organic molecules.

2.2.5 UV-visible absorption spectra and EEM fluorescence spectra

All extracts (i.e., WISOM, WSM, HULIS-a, HULIS-n and HP-WSM in the unban TSP samples, WSM and the six sub-fractions of WISOM in the urban $PM_{0.95}$, WSM in the forest and marine $PM_{0.95}$ samples) in a 1-cm path-length quartz cell was subjected to the analysis using a UV-visible spectrophotometer (V-570, JASCO). Further, the extracts of WISOM, WSM, HULIS-a, HULIS-n and HP-WSM in the unban TSP samples and WSM in the urban, forest and marine $PM_{0.95}$ samples in a 1-cm path-length quartz cell was subjected to the analysis using a fluorescence spectrophotometer (FP-6600, JASCO). The UV-visible absorption spectrum in the range from 200 to 800 nm was recorded in triplicate with an interval of 0.5 nm and a scan speed

of 400 nm min^{-1}. The UV-visible absorption spectra of blank extracts were also recorded to subtract their contributions from the extract spectra.

For the TSP extracts, the EEMs were measured in the range from 235 to 500 nm for excitation and from 300 to 600 nm for emission with a scan speed of 600 nm min^{-1}. The wavelength increments of the scans for excitation and emission were 5 nm and 2 nm, respectively. The excitation and emission slit widths were 5 nm. For the $PM_{0.95}$ extracts, the EEMs were measured in the range from 200 to 400 nm for excitation, and 250 to 650 nm for emission, at a scan speed of 1000 nm min^{-1}. The band-passes for excitation and emission were both set as 10 nm [*De et al.*, 2013]. The EEMs of blank extracts were also recorded and subtracted from those of the sample extracts.

The reproducibility and the blank levels of the analysis of the WISOM, WSM, HULIS-n, HULIS-a, and HP-WSM by the UV-visible absorption spectrophotometer and the EEM fluorescence spectrophotometer were assessed by the triplicate extraction and analysis of an identical aerosol sample and a blank filter (TSP sample). The relative standard deviation (RSD) of the EEM fluorescence volumes of the WISOM, WSM, HULIS-n, HULIS-a and HP-WSM (over the wavelength range of 235–400 nm for excitation and 300–600 nm for emission) varied in the range of 0.7%–5.4% and those of the absorbance of the five components (in the wavelength range of 250–350 nm for the HP-WSM and 250–500 nm for the other extracts) varied in the range of 0.5%–14.3%. Note that the light-absorption of the WSM and the summed light-absorption of the HULIS-n, HULIS-a and HP-WSM were similar (<11% differences on average in the range of 210–500 nm), which indicates that the light-absorptive compounds were largely not lost in the separation procedure using the SPE. The blank levels of the absorbance for the WSM, HULIS-n, HULIS-a and HP-WSM in the wavelength range of 250–600 nm were <4% of the lowest absorbance of the sample solutions. The average blank levels of the absorbance in

the wavelength ranges of 250–400 nm and 400–600 nm for the WISOM varied in the ranges of 1%–3.3% and 7.7%–12% of the absorbance for the sample solutions, respectively. The intensities of the fluorescence peaks of the blank samples for the WISOM, WSM, HULIS-n, HULIS-a and HP-WSM were <6.8% of the lowest fluorescence intensity of the sample solutions over the wavelength ranges of 235–400 nm for excitation and 300–600 nm for emission (except for the signals of the primary and secondary Raman and Rayleigh-Tyndall scattering). The fluorescence volumes (235–400 nm for excitation and 300–600 nm for emission) of those blank extracts were <3.6% of the lowest fluorescence volumes of the sample solutions.

2.2.6 Analysis of carbonaceous components and ions

EC and OC in filter samples were quantified using a carbon analyzer with thermal optical transmittance (TOT) and thermal optical reflectance (TOR) methods and with the IMPROVE temperature protocol. For the quantification of OC in six water-insoluble organic fractions, F1, F2, F3, F4, F5 and F6, extracted from the weekly samples (the urban $PM_{0.95}$ samples) were dried under a nitrogen flow and redissolved in 100 μL of corresponding solvents for the analysis of carbonaceous components. Then, 20-μL aliquots of the extracts were dropped onto 1 × 1.5 cm pre-baked quartz-fiber filters, and the solvents were allowed to volatilize for ~25 minutes. The prepared filter samples were analyzed using a carbon analyzer with the IMPROVE temperature protocol. In the analysis, three blank samples for each fraction were also analyzed to correct for blank levels.

WSOC was quantified using a TOC analyzer (TOC-V CPH, Shimadzu). Ions (anions: NO_3^-, SO_4^{2-}, Cl^-, and oxalate; cations: Na^+, K^+, Ca^{2+}, Mg^{2+}, and NH_4^+) were analyzed using ion chromatography (ICS-1600 and ICS-2100, DIONEX). In the analyses using the carbon analyzer,

the ion chromatograph, and the TOC analyzer, blank filters were also analyzed to correct for background levels.

2.3 Data processing

2.3.1 FT-IR data analysis

For the quantitative analysis of the chemical functional groups using diffuse reflectance FTIR spectroscopy, DRIFTS data were represented by Kubelka-Munk (K-M) units [*Sirita et al*., 2007]:

$$f(R_\infty) = \frac{k}{s} = \frac{(1-R_\infty)^2}{2R_\infty} \propto \frac{\varepsilon c}{s} \quad , \tag{3}$$

where R_∞ is the intensity of scattered IR divided by that of the incident radiation, k is the sample absorption, s is the scattering coefficient, ε is the absorptivity, and c is the concentration of the material that absorbs IR. The Kubelka-Munk conversion was performed using matched software (JASCO).

For the quantification of organic functional groups, the FTIR spectra were integrated in a manner analogous to that described in previous reports [*Sax et al*., 2007; *Russell et al*., 2009; *Day et al*., 2010; *Takahama et al*., 2013]. A linear combination of a series of Gaussian distribution functions was used to represent the absorption of multiple functional groups (alcohol CO-H, aromatic C-H, alkene C-H, alkane C-H, carbonyl C=O, amines C-NH_2, organonitrate C-ONO_2 and unidentified groups in Table 2.2), and peak patterns of carboxylic COH (from *Takahama et al*., [2013]) and ammonium (from NH_4NO_3) were used to represent their absorption at the 1500–4000 cm^{-1} region. A least squares optimization method for the determination of peak parameters was performed to minimize the error:

$$Error = (Abs(\lambda) - F(\lambda))^2$$
$$F(\lambda) = \sum_i \alpha_i \cdot C_i(\lambda) + \sum_j \beta_j \cdot \exp[-\frac{(\lambda - \mu_j)^2}{2 \cdot \sigma_j^2}] \quad , \quad (4)$$

where $Abs(\lambda)$ is the observed absorption in the KM unit; $F(\lambda)$ is the fitted curve; $C_i(\lambda)$ is the line shapes for carboxylic COH and ammonium N-H; α_i is the scaling factor; β, μ and σ are parameters of the Gaussian function; and j denotes different chemical functional groups.

The areas of fitted peaks were used to quantify different functional groups. The peak area of non-carboxylic C=O was calculated as the total peak area of carbonyl C=O minus the peak areas of carboxylic COOH at the 1710–1740 cm^{-1} region [*Takahama et al*., 2013]. Similarly, the peak area of amine C-NH_2 at the 1630–1640 cm^{-1} region was calculated as the total peak area minus the peak area of organonitrate C-ONO_2 [*Day et al*., 2010]. Organonitrate C-ONO_2 was quantified directly from the peak area at the 1265–1300 cm^{-1} region [*Sax et al*., 2005]. The relative contents of different chemical groups in organics were also used to determine the elemental ratios and OM/OC in accordance with *Takahama et al* [2013]. The absolute mass concentrations of the fractionated organics were not quantified from the FT-IR data. Instead, relative contents of different chemical groups in fractionated organics were calculated based on previously reported absorptivity in Table 2.2.

The uncertainty of quantification of transmittance FT-IR spectroscopy were reported to be 21% and 33% for carboxylic COOH and ketonic C=O, respectively, and 5%–21% for other functional groups [*Russell*, 2003; *Maria* et al., 2003; *Gilardoni et al*., 2007; *Takahama et al*., 2013]. The reproducibility of the functional group analysis based on the FT-IR analysis in this study was examined by the extraction and the FT-IR analysis of an identical aerosol sample (an TSP sample) three times; the RSD of the mass percentage of the C-OH, COOH, C=O, C-NH_2, C-ONO_2, and C-H groups of WISOM, HULIS-n and HULIS-a were, respectively, 7–32%, 5–13%,

2–32%, 51–76%, 11–19%, and 1–11%. The RSD of O/C, H/C, and OM/OC from the FT-IR analysis were in the ranges of 6.3–12.2%, 0.5–0.9%, and 0.7–5.4%, respectively (n = 3 for WISOM, HULIS-n and HULIS-a, respectively). The RSD of the FT-IR-derived mass of organics (in ∑(KM-area/absorptivity)) for WISOM, HULIS-n and HULIS-a were 13.0%, 14.1% and 5.0%, respectively (n = 3).

Table 2.2. Fitting parameters and absorptivity of chemical groups.

Peak no.	Functional group	Constraints		1/Absorptivity [a]
		μ (cm^{-1})	σ (cm^{-1})	
1	Carboxylic COH	Lineshape; 2400–3400 [d]		0.015 [d, e]
2	Ammonium NH_4 [b]	Lineshape; 2500–3500 [c]		-
3	Alcohol COH—1	3400–3600	30–100	0.057 [d, e, f]
4	Alcohol COH—2	3200–3350	30–75	0.057 [d, e, f]
5	Unidentified—1[2]	3136–3142	10–20	-
6	Unidentified—2	3070–3076	10–20	-
7	Aromatic CH	3030–3070	3.5	8.7 [d, e]
8	Unidentified—3	3014–3008	10–25	-
9	Alkene CH	2980–3010	3.5	3.8 [d, e]
10	Alkane (CH_3) CH—1	2940–2960	5–15	0.6 [e, f]
11	Alkane (CH_2) CH—2	2920–2930	10–40	0.6 [e, f]
12	Alkane (CH_3) CH—3	2873–2886	10–40	0.6 [e, f]
13	Alkane (CH_2) CH—4	2830–2858	5–25	0.6 [e, f]
14	Alkane CH—5	2805–2811	10–20	0.6 [e, f]
15	Carbonyl CO Carboxylic CO	1710–1740	10–40	0.067 [e, f, j] 0.034 [l]
16	Amine CNH_2—1 Organonitrate $CONO_2$—1	1627–1640	5–30	0.112 [d, e, g, h] 0.037 [j, k]
17	Amine CNH_2—2	1587–1610	3–30	-
18	Organonitrate $CONO_2$—2	1265–1300	-	0.075 [k]
19	Organonitrate $CONO_2$—3	850–870	3–30	-

[a] Absorptivity is the unit of peak area (in absorbance) per micromole of functional group.

[b] This peak may be contributed by amines.

[c] An absorption profile of ammonium from NH_4NO_3.

[d] *Takahama et al*., 2013; [e] *Russell et al*., 2009; [f] *Gilardoni et al*., 2009; [g] *Gilardoni et al*., 2007; [h] *Maria et al*., 2002; [l] *Allen et al*., 1994; [j] *Day et al*., 2010; [k] *Sax et al*., 2005.

2.3.2 Analysis of UV-visible absorption spectra

The mass absorption efficiency (MAE, $m^2\ g^{-1}$ OC or OM) of the organics in the extracts was calculated using the following equation [*Zhang et al*., 3013]:

$$MAE_{\lambda} = (Abs_{\lambda} - Abs_{700})\ \ln(10)/\ C_{\mathrm{OC\ or\ OM}}\ , \tag{5}$$

where Abs_{λ} and Abs_{700} are the light absorption coefficients (m^{-1}) of the extract solutions at λ and 700 nm, respectively, and $C_{\mathrm{OC\ or\ OM}}$ is the concentration of organic carbon or organic mass of the extracts. Because the cut-off wavelengths of the *n*-hexane, DCM and MeOH were 230 nm and 210 nm, respectively, the MAEs of the extracts with solvent of *n*-hexane, DCM and MeOH were calculated from 700 nm to 200 nm, 230 nm and 210 nm, respectively. Because ammonium sulfate and ammonium nitrate in aqueous solutions can absorb the ultraviolet light in the wavelength range <250 nm, the MAEs of the aerosol water extracts was calculated from 700 nm to 250 nm.

The MAE of the organics in the aerosols is generally expressed as a function of *Å*:

$$MAE(\lambda) = a \cdot \lambda^{\AA}\ , \tag{6}$$

where *a* is a constant that is related to the light-absorptivity. We derived *Å* in the wavelength range of 200–600 nm and also in the following four sub-ranges: 210–300 nm (UV-I), 300–400 nm (UV-II), 400–500 nm (Visible-I) and 500–600 nm (Visible-II) for the unban TSP samples.

The relative contribution of each aerosol extract to the total light-absorption by the organics and EC was assessed. The total light-absorptions of the different aerosol extracts and EC were calculated from the MAEs of the organics and EC and their atmospheric concentrations using

$$Abs(\lambda)_{\mathrm{total}} = \sum_{i} MAE(\lambda)_i \cdot C_i' + MAE(\lambda)_{\mathrm{EC}} \cdot C_{\mathrm{EC}}\ , \tag{7}$$

where C_i' is the concentration of the organics in extract *i* (i.e., WISOM, WSM, HULIS-n, HULIS-a and HP-WSM in the unban TSP samples or WSM and six sun-fractions of WISOM in unban $PM_{0.95}$ samples) when they were in the atmosphere (μg m^{-3}). The concentrations of C_{EC} were derived from a carbon analyzer with the TOR method and with the IMPROVE temperature protocol. The MAE of EC in the range of 250–600 nm was calculated using Eq. (2), with the

MAE of EC at 550 nm and the parameter *Å* assumed to be 7.5 m^2 g^{-1} and 1, respectively [*Andreae and Gelencsér*, 2006; *Bond and Bergstrom*, 2006; *Bergstrom et al.*, 2007].

The contributions of polycyclic aromatic hydrocarbons (PAHs) to the total light absorption of the WISOM (f_{PAHs}) in the unban TSP samples were estimated by

$$f_{PAHs} = \frac{\frac{\varepsilon \cdot 10^{-1}}{\overline{MM}} \cdot C_{PAHs}}{MAE_{WISOM}}, \quad (8)$$

where MAE_{WISOM} is the mass absorption efficiency of the organics in the WISOM, C_{PAHs} is the mass fraction of PAHs in the WISOM, $\overline{MM}$ is the average molar mass of the PAHs, which herein is assumed to be 250 g mol^{-1} (typical molar mass based on *Dzepina* et al. [2007]: 200–300 g mol^{-1}), and ε is the average molar absorption coefficient of the PAHs, which herein is assumed to be 5×10^4 *l* mol^{-1} cm^{-1} at 245 nm (typical molar absorption coefficient based on *Zhan et al.* [1997]: (1–10) × 10^4 *l* mol^{-1} cm^{-1}). The maximum contribution of the PAHs to the light absorption of the WISOM was calculated with the maximum of ε of 10×10^4 *l* mol^{-1} cm^{-1} and the minimum of $\overline{MM}$ of 200 g mol^{-1} for the PAHs.

2.3.3 Post-processing of the fluorescence spectra

The EEMs collected using a fluorescence spectrophotometer were calibrated according to the procedures described in *Lawaetz and Stedmon* [2009] and *Murphy* [2010]. The spectral correction factors were acquired from the manufacturer of the spectrometer (JASCO), which were used for the first calibration of the EEMs. This was followed by an inner filter correction based on the corresponding UV-visible absorbance spectra of the extracts. The highest light absorbance in the calibrated wavelength range was not greater than 2 (mostly below 1 at 235 nm), which is appropriate for the inner filter corrections of the EEMs [*Gu and Kenny*, 2009]. Then,

the EEMs were normalized so that their unit is RU [*Lawaetz and Stedmon*, 2009]. This was performed by using the Raman peak of water, which was extracted from the EEMs of the water at an excitation wavelength of 348 nm over the emission wavelength range from 380 nm to 410 nm.

The fluorescence index (FI), biological index (BIX), and humification index (HIX), which are the ratios of the fluorescence intensity at excitation/emission wavelengths (Ex/Em) of 370/470 nm to that at 370/520 nm, the intensity at 310/380 nm to that at 310/430 nm, and the intensity at 255/434–480 nm (average of the values on the line between 255/434 and 255/480 nm) to that at 255/300–344 nm (average of the values on the line between 255/300 and 255/344 nm), respectively, were obtained from the EEMs [*Birdwell and Engel*, 2010; *Birdwell and Valsarai*, 2010]. To compare the fluorescence efficiency of different extracts, the fluorescence volumes over the excitation wavelength of 200–400 nm and the emission wavelength of 250–650 nm were normalized by the OC or OM concentration of the extracts (abbreviated to NFV, RU-nm^2 [mg L^{-1} OC or OM]$^{-1}$).

2.3.4 PARAFAC analysis for EEMs

The PARAFAC model was used to resolve the EEM compounds and to analyze the chromophores in the aerosol samples. PARAFAC analysis with non-negativity constraints of EEMs was performed with the drEEM toolbox version 0.2.0 for MATLAB (http://www.models.life.ku.dk/dreem) *[Murphy et al*., 2013]. The details of the data analysis are given in the tutorial of PARAFAC [*Murphy et al*., 2013].

(1) PARAFAC analysis for EEMs of different extracts from TSP samples

The EEMs (n = 12) of the extracts in the respective types of fractions (WISOM, WSM, HULIS-n, HULIS-a and HP-WSM) and the EEMs of all of the extracts (n = 60) were used for

the PARAFAC analysis. Using all 60 EEMs in the analysis, a 5-component PARAFAC solution was adopted by comparisons of the residual errors, by split-half analysis and by visual inspection for the 2- to 7- component PARAFAC model (Figure 2.4) [*Murphy et al*., 2013]. The 5-component model explains >98.8% of the variations within the dataset. Although the model has low core consistencies (8.8%), it should be acceptable for models with five or more components [*Murphy et al*., 2008 and 2013]. One of the PARAFAC components (compound 5 in Figure 2.4) is similar to those reported previously by *Murphy et al*. [2008] and *Mendoza and Zika* [2014], which have been identified as a component from an instrument artifact [*Mendoza and Zika*, 2014]. In this study, this component (which contributes to 14.8% of the total variations) was excluded from the analysis. The high contribution of the remaining four components to the total variation (84.2%) suggests that they explain most of the fluorescence from the extracted organics.

(2) PARAFAC analysis for EEMs of water extracts in the urban, forest and marine $PM_{0.95}$

Sixty-three EEMs of water-soluble extracts of the urban, forest and marine $PM_{0.95}$ were used for the PARAFAC analysis. The three-component PARAFAC model was the optimal solution among two- to ten-component PARAFAC models validated through comparisons of residual errors, split-half analysis and visualization of spectral loadings according to the PARAFAC tutorial (Figures 2.5 and 2.6) [*Murphy et al*., 2013]. The seven-component PARAFAC solution, which shows the best result in the residual analysis among four- to ten-component PARAFAC solutions, was also used to obtain more detailed information on chromophores. The seven-component PARAFAC solution passes the split analysis with the split style of '$S_3C_3T_3$', indicating that the solution is stable.

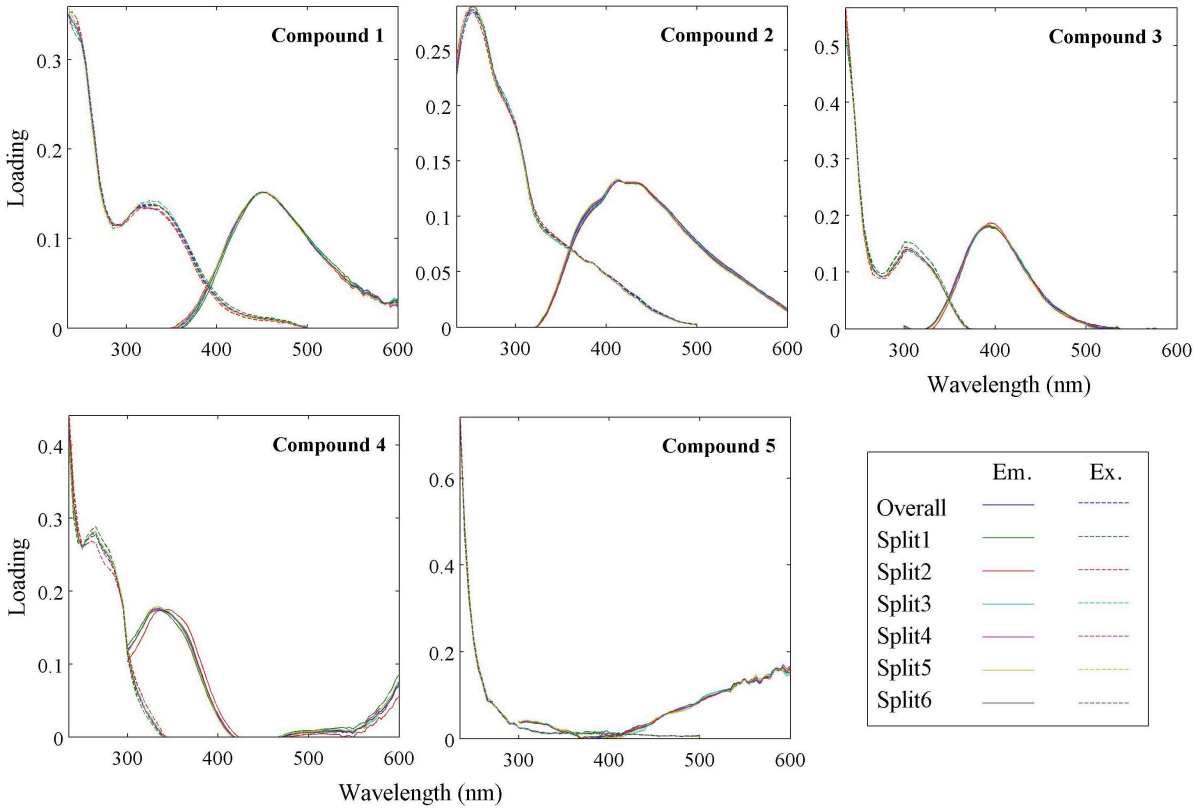

Figure 2.4. Split half validation of the 5-component solutions obtained by the split style of '$S_4C_6T_3$' for the entire dataset (EEMs of WISOM, WSM, HULIS-n, HULIS-a and HP-WSM extracted from the TSP filter samples, n = 60). The solid and dashed lines represent the spectra against excitation and emission wavelengths respectively.

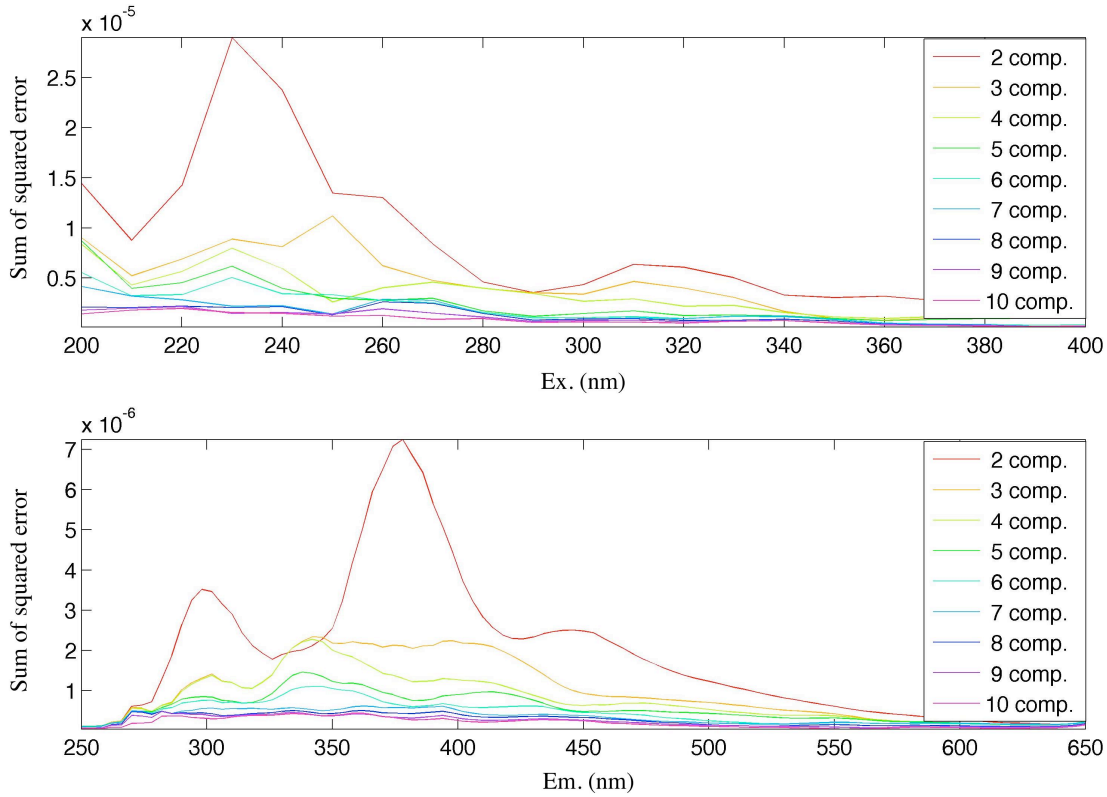

Figure 2.5. Residual analysis of two- to ten-component PARAFAC models for the sixty-three EEMs of the urban, forest and marine $PM_{0.95}$ water extracts.

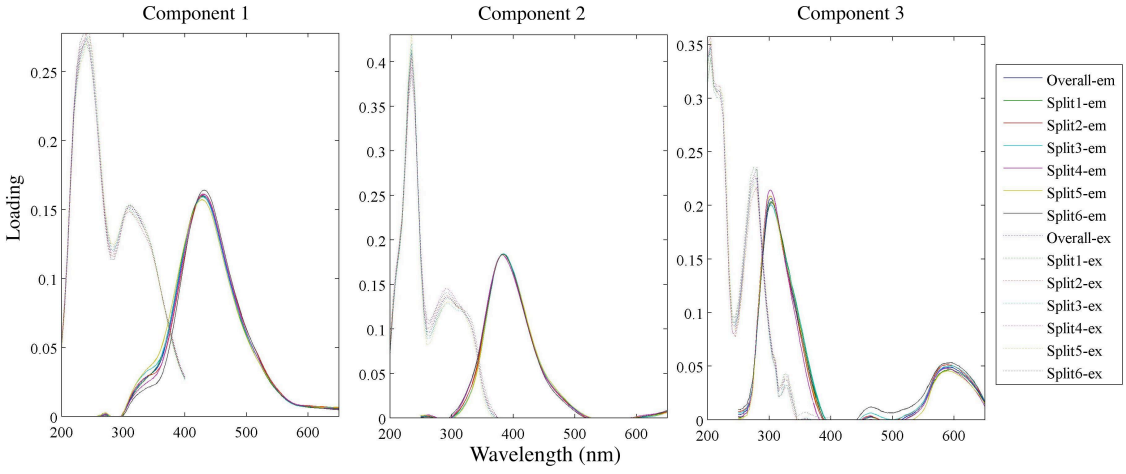

Figure 2.6. Split half analysis of three-component PARAFAC model with the split style of '$S_4C_6T_3$' for the sixty-three EEMs of the urban, forest and marine $PM_{0.95}$ water extracts.

2.3.5 Factor analysis for HR-AMS spectra

Non-negative matrix factorization (NMF) analysis was performed for the HR-AMS dataset of the sixty-three EEMs of the urban, forest and marine $PM_{0.95}$ water extracts using the NMF toolbox version 1.4 in MATLAB (https://sites.google.com/site/nmftool/) [*Li and Ngom*, 2013]. First, a gradient-descent-based multiplicative algorithm was used to find solutions from multiple random starting values, and then a least-squares active-set algorithm was used to find final solutions from the first solutions. To find a final solution, the model was run 100 times with a different starting point each time. The four-factor NMF model was validated through comparisons of residual errors, split analysis and visualization of spectral loadings.

2.3.6 Hierarchical cluster analysis

A hierarchical cluster method was performed to classify aerosol samples of the sixty-three EEMs of the urban, forest and marine $PM_{0.95}$ based on the relative contributions of PARAFAC components and NMF factors to the respective samples. The Euclidean distance was used to evaluate the distances between samples, and the centroid method was chosen for the hierarchical cluster analysis by comparing the multiple correlation coefficients for nearest neighbour, farthest neighbour, median neighbour and Ward's method. Six clusters were determined for EEMs and HR-AMS data, and were named clusters *A-F* and clusters *a-f*, respectively.

3 Chemical characteristics of total organic matter in urban total suspended particulates

3.1 Composition and concentrations

The concentrations of chemical components of the TSP collected in Nagoya, Japan are shown in Figure 3.1. The AMS-derived concentrations of extracted organic matter (EOM = WISOM + WSOM) and organic carbon therein were on average 5.5 ± 1.4 (mean ± SD) and 3.4 ± 0.8 μg m^{-3}, respectively. The concentrations of EOM were comparable to those of the sum of the EC and the quantified inorganic species (mean ± SD: 11.1 ± 1.8 μg m^{-3}) and accounted for 35 ± 4% of the sum of the quantified components in summer and early autumn and 31 ± 3% (mean ± SD) of the sum of the quantified components in winter. Among the isolated organic fractions, the most abundant fraction in the EOM was WISOM (mean ± SD: 41 ± 7%). The contribution of this fraction on a carbon basis was even larger (mean: 64%), indicating a large contribution of hydrophobic substances to urban TSP. The mean concentrations of WISOM were similar in summer and early autumn (2.1 μg m^{-3}) and in winter (2.3 μg m^{-3}). Conversely, the mean concentration of WSOM in summer and early autumn (4.1 μg m^{-3}) was markedly higher than that in winter (2.5 μg m^{-3}).

The concentration of HULIS-n in summer was 1.75 ± 0.57 μg m^{-3} (mean ± SD), which was slightly higher than that observed in winter (1.50 ± 0.25 μg m^{-3}). HULIS-n, the most hydrophobic fraction of WSOM, accounted for 51 ± 11% (mean ± SD) of WSOM and 30 ± 4% of EOM, respectively; the findings are similar to those of previous studies in urban environments [*Salma et al*., 2007; *Krivácsy et al*., 2008]. The mean concentrations of HULIS-a, a medium polarity fraction of WSOM, were 1.1 μg m^{-3} in summer and early autumn and 0.5 μg m^{-3} in winter. The mean concentrations of HP-WSOM, the most polar portion of WSOM, were 1.4 μg

m^{-3} in summer and early autumn and 0.7 μg m^{-3} in winter. The concentrations of HULIS-a and HP-WSOM in summer and early autumn were on average 1.8 and 2 times higher than those in winter, respectively. The seasonal changes suggest the photochemical formation of HULIS-a and HP-WSOM in summer and early autumn. This finding is supported by the seasonal change in oxalate concentrations: The concentrations in summer and early autumn (mean ± SD: 0.45 ± 0.10 μg m^{-3}) were on average 4.1 times higher than those in winter (0.11 ± 0.03 μg m^{-3}).

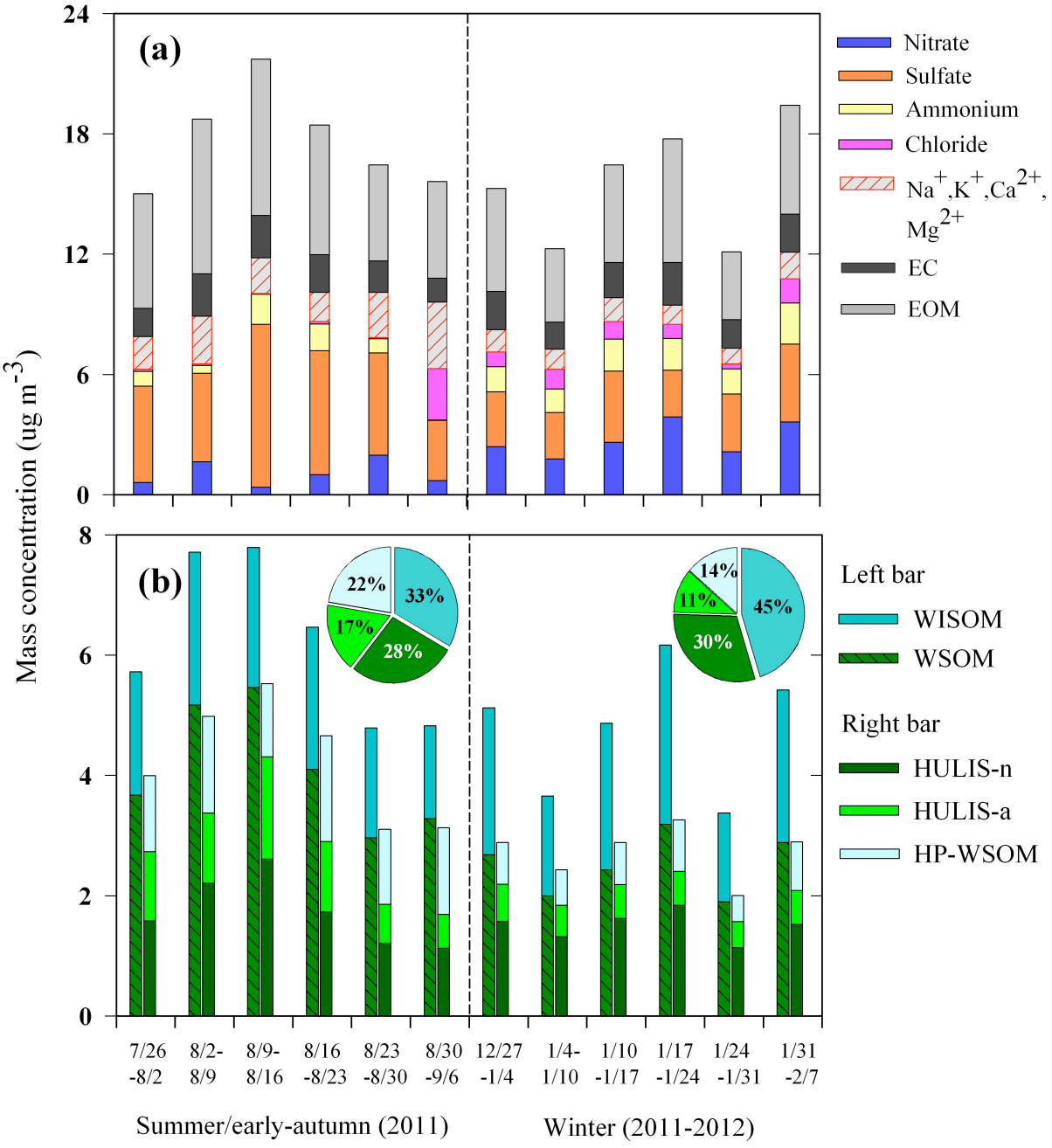

Figure 3.1. Concentrations of (a) inorganic species and extracted organic matter and (b) fractionated organic matters in total suspended particulates over Nagoya, Japan in summer/early autumn and winter. The pie charts in panel (b) represent the mean mass percentages of fractionated organic matter (WISOM, HULIS-n, HULIS-a and HP-WSOM).

3.2 Analysis of functional groups using FT-IR spectroscopy

The FT-IR spectra of WISOM, HULIS-n, HULIS-a and HP-WSOM are presented in Figure 3.2. Typical functional groups, i.e., aliphatic C-H, alcoholic C-OH, non-acidic carbonyl C=O, carboxylic COOH, amine C-NH_2 and organic nitrate C-ONO_2, in the fractions were identified and quantified as follows.

Aliphatic C-H groups on average accounted for 77%, 47%, and 32% of the OM in WISOM, HULIS-n and HULIS-a, respectively. The peaks at 2950 cm^{-1} and 2925 cm^{-1} in the FT-IR spectra of WISOM and HULIS-n could be distinguished clearly and were assigned to the bands of C-H asymmetric stretching vibrations of methyl (-CH_3) and methylene (-CH_2) groups, respectively. Based on comparison with reference IR spectra in the NIST library (http://webbook.nist.gov/chemistry/form-ser.html), the molar ratios of -CH_2 to -CH_3 were estimated to be 5.5 ± 1.1 (mean ± SD) and 0.6 ± 1.0 for WISOM and HULIS-n, respectively. The high ratio of WISOM suggests that WISOM consists of long-chain or cyclic structures with fewer side-chains than those of HULIS-n. By contrast, the small molar ratio of -CH_2 to -CH_3 for HULIS-n suggests abundant branched structures. The intensity ratios of -CH_2 to -CH_3 in the FT-IR spectra of WISOM (1.89 ± 0.07) were similar to the ratio in the FT-IR spectra of the fossil fuel standard of diesel (2) and were higher than that of the standard of gasoline (1.2) [*Guzman-Morales et al.*, 2014]. In the case of the spectra of HULIS-a and HP-WSOM, the peaks of -CH_2 and -CH_3 cannot be distinguished.

The strong absorption of the alcoholic (C-OH) groups was observed for HULIS-n and HULIS-a and on average corresponds to 35% and 36% of the organic mass quantified from FT-IR spectra, respectively. The spectra of HULIS-n contain three clear peaks: 1027 cm^{-1} (primary alcohol), 1128 cm^{-1} (tertiary alcohol) and 1253 cm^{-1} (primary alcohol). The results suggest that HULIS-n contains abundant alcohols and that the alcohols are dominated by primary alcohols,

followed by tertiary alcohols. In the cases of WISOM and HULIS-a, absorption in the range of 1000-1320 cm^{-1}, typically corresponding to the C-O stretching vibration of alcohols and esters and an alcohol O-H deformation vibration, was observed, and no clear peak corresponding to primary/tertiary alcohols was observed.

Carboxylic (COOH) groups in WISOM, HULIS-n and HULIS-a on average account for 2%, 4%, and 10%, respectively, of the OM quantified from FT-IR spectra. The mass percentages of non-acidic carbonyl (C=O) were on average 7%, 9% and 18% for WISOM, HULIS-n and HULIS-a, respectively. The positions of the peaks of C=O absorption for WISOM, HULIS-n and HULIS-a seemed different, suggesting that the main forms of their C=O structures were different: i.e., aldehydes/ketones (peak position: 1715–1730 cm^{-1}), ketones (1712–1715 cm^{-1}) and carboxylic acids (1720–1735 cm^{-1}), respectively. A conjugated C=O, such as that in quinones, was presumably not abundant regardless of the organic fraction because a shift of the peaks corresponding to C=O to <1700 cm^{-1} in the presence of electron-donating groups (such as quinones) was not evident.

The FT-IR spectra further suggest the presence of nitrogen-containing groups. An intense peak at 1589 cm^{-1} was observed for HULIS-n, while the peak was weak in the case of other organic fractions. This peak has generally been attributed to the absorption by aromatic C=C and an N-H scissoring vibration of amines and/or a C=N stretching vibration of heterocyclic amines [*Bekircan et al*., 2005; *Ki et al*., 2007; *Sundaraganesan et al*., 2007; *Popovicheva et al*., 2014]. An abundance of C-ONO_2 was observed in WISOM and HULIS-n, as shown by the peaks at 1280 cm^{-1} and 863 cm^{-1} [*Kirchner et al*., 2000; *Bruns et al*., 2010; *Liu et al*., 2012]. The percentages of C-ONO_2 mass in WISOM, HULIS-n and HULIS-a were calculated to be 1.3 ± 0.5%, 1.7 ± 0.2% and 0.5 ± 0.1% (mean ± SD), respectively, from the peak at 1280 cm^{-1} [*Sax et al*., 2005]. Furthermore, based on the area of the peak at 1630 cm^{-1}, with the subtraction of the

contributions from C-ONO_2, the mass percentages of C-NH_2 in WISOM, HULIS-n and HULIS-a were estimated to be 2.5 ± 0.4%, 4.1 ± 1.4% and 4.6 ± 0.1% (mean ± SD), respectively [*Sax et al.*, 2005; *Day et al.*, 2010].

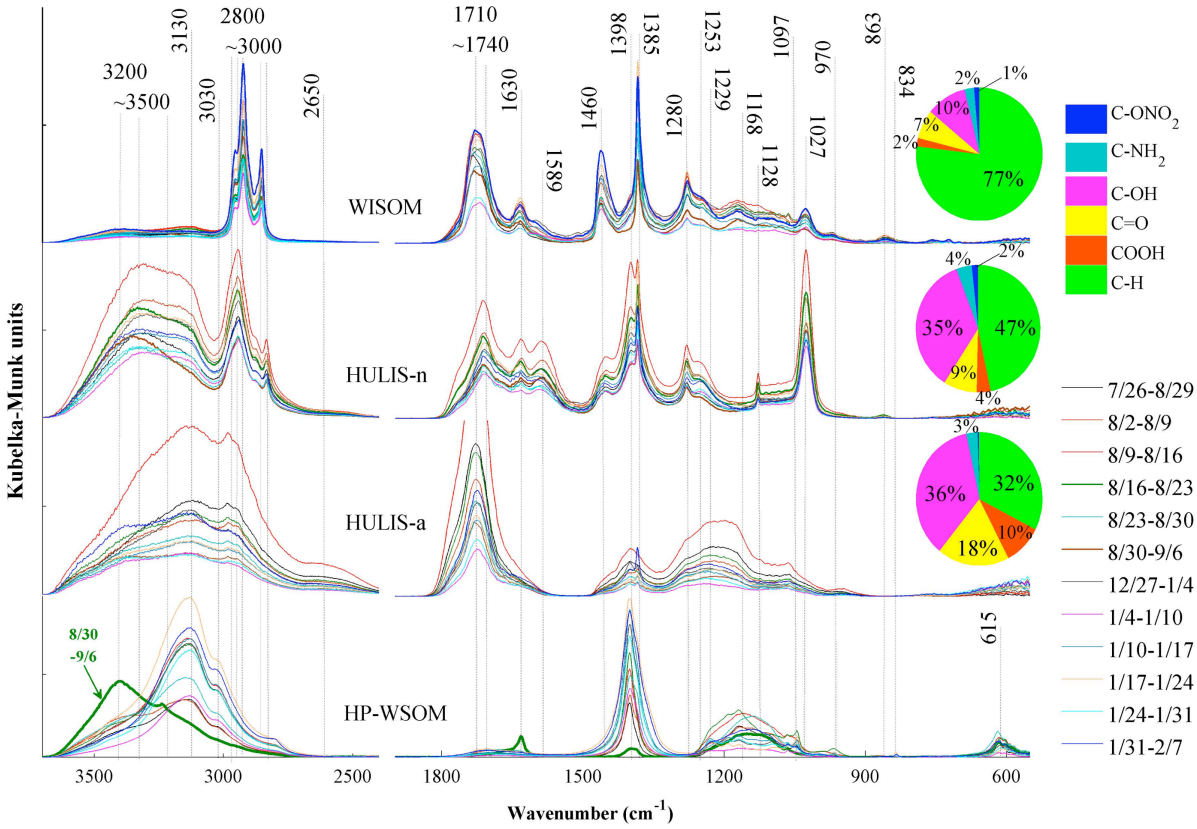

Figure 3.2. FT-IR spectra of WISOM, HULIS-n, HULIS-a, and HP-WSOM. The assignments of major peaks to functional groups are summarized in Table 2.2. The pie charts represent the mass fractions of the major functional groups in WISOM, HULIS-n, and HULIS-a. The bold line in dark green for HP-WSOM represents a spectrum of the sample that was presumably strongly influenced by maritime air (8/30–9/6).

The FT-IR spectra of HP-WSOM seem to be strongly influenced by the presence of inorganic species (NH_4^+, NO_3^- and SO_4^{2-}); hence, it is difficult to quantify the organic functional

groups, which however can be quantified using HR-AMS as described in the next section. We found that the FT-IR spectrum of one HP-WSOM sample (30 August - 6 September) at the time of high concentrations of Cl^- (2.57 μg m^{-3}) and Na^+ (2.4 μg m^{-3}) was very similar to that attributed to a marine aerosol in a previous study [*Hawkins et al.*, 2010]. The sample is characterized by a large fraction of alcohols, as inferred from significant absorption at 3200–3500 cm^{-1} (Figure 2). Organic nitrates and/or amines may also contribute considerably to this HP-WSOM sample, as inferred from an intense peak at 1630 cm^{-1}.

3.3 HR-AMS characteristics of various organic extracts

The chemical structural characteristics (ion species and groups) and elemental composition of WISOM and HULIS-n, HULIS-a, and HP-WSOM were further suggested from the HR-AMS spectra (Figure 3.3). The $C_xH_y^+$ ions in the spectra are presumably attributed to aliphatic hydrocarbons. The fractions in the mass spectra of WISOM were large and accounted for an average of 79% of the ions from organics. The percentage was significantly higher than that of WSOM (33%). In the case of HULIS-n, the most hydrophobic portion of WSOM, the fraction of $C_xH_y^+$ ions was on average 48%, higher than that in the other hydrophilic WSOM portions of HULIS-a and HP-WSOM. This result suggests that WISOM and HULIS-n contain an abundance of aliphatic hydrocarbon structures, whereas other chemical structures were more abundant in the case of HULIS-a and HP-WSOM. The signal patterns of $C_xH_y^+$ ions in the HR-AMS spectra of WISOM were similar to those of vehicle organic aerosol (VOA) in the Gubrist Tunnel, Switzerland (r^2 = 0.98) and those of hydrocarbon-like organic aerosol (HOA) identified in road traffic emissions in Barcelona, Spain (r^2 = 0.85), whereas the correlations with biomass burning organic aerosols (BBOA, r^2 = 0.52) and cooking organic aerosol (COA, r^2 = 0.61) were less stronger[*Mohr et al.*, 2012]. Hence, WISOM may be attributable primarily to fossil fuel

combustion rather than BBOA or COA. A contribution of lubricating oils to WISOM in the TSP of Nagoya City is likely, given the dominance of lubricating oil in POA emitted from motor vehicles [*Dallmann et al*., 2014; *Worton et al*., 2014].

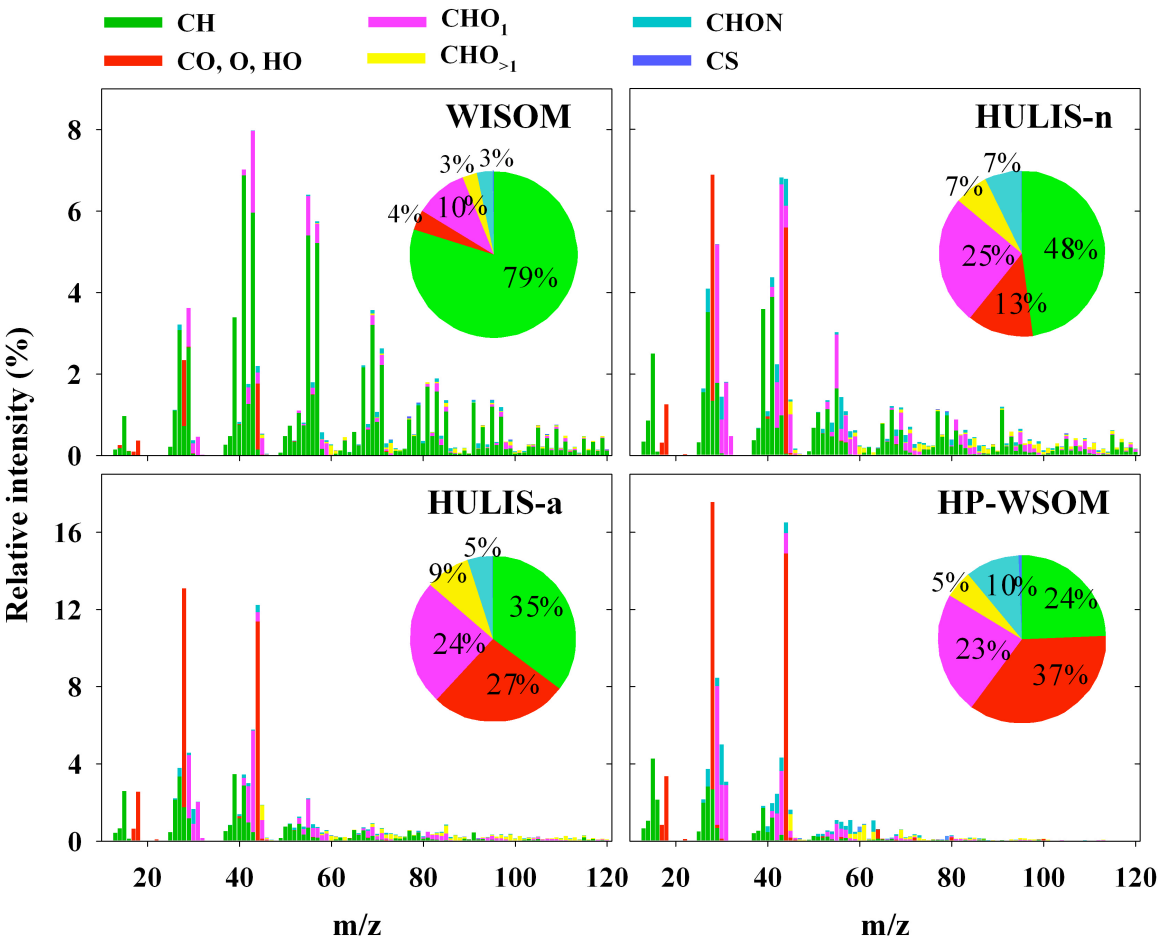

Figure 3.3. The average HR-AMS spectra for WISOM, HULIS-n, HULIS-a, and HP-WSOM, which were derived from W-mode data (n = 12). The pie charts of the mass fractions of CH, CO, CHO_1, $CHO_{>1}$, CHON and CS ion groups are also presented.

The CO and CHO groups in the HR-AMS spectra presumably originated from carboxylic acids, alcohols and carbonyl compounds. The contributions of fragment ions containing oxygen to the AMS spectra were large in the case of WSOM (mean: 58%) and were small in the case of

WISOM (mean: 17%). The CO and CHO groups accounted for 3.9% and 13.3% of WISOM, respectively. The higher fraction of CHO groups than of CO groups is a characteristic of WISOM, suggesting that the marked contributions of alcohols, ketones/aldehydes, and esters, to the overall structure of WISOM. The CHO group (mean: 32%) was abundant in the mass spectra of HULIS-n, and the abundance of this group was much higher than that of the CO groups (mean: 13%). By contrast, the fractions of CO group ions in HULIS-a and HP-WSOM (mean: 27% and 37%, respectively) were comparable to those of CHO group ions (mean: 33% and 28%, respectively). This result indicates marked contribution of non-carboxylic oxygenated species to the overall structure of HULIS-n and that of carboxylic acids to the structures of HULIS-a and HP-WSOM.

The CHON group ($C_xH_yO_zN_q^+$ and $C_xH_yN_q^+$), a nitrogen-containing group in the HR-AMS mass spectra, is presumably attributed to amines and organic nitrates. The fractions in the mass spectra of HULIS-n and HP-WSOM were large and accounted for an average of 7.1% and 10.4% of the ions from organics, respectively. The $C_xH_yN_q^+$ ions, attributed to amines, were abundant and accounted for an average of 5.2% and 9.1% of the ions from HULIS-n and HP-WSOM, respectively. The signal ratios of NO^+/NO_2^+ in the HR-AMS spectra of WISOM, HULIS-n and HULIS-a were 6, 5.7 and 7 on average, respectively, which were obviously higher than the ratio derived from NH_4NO_3 (2.4). The higher NO^+/NO_2^+ abundance is presumably due to the presence of organic nitrates [*Liu et al*., 2012; *Farmer et al*., 2010; *Hao et al*., 2013]. Assuming that the relative ionization efficiency of organic nitrates is equal to that of inorganic nitrates (1.1), we estimated that NO_3 in organics accounted for 1.4 ± 0.3%, 1.9 ± 0.2%, and 0.5 ± 0.4% (mean ± SD) of the masses of WISOM, HULIS-n and HULIS-a, respectively.

The results from the HR-AMS agree well with those from the FT-IR analysis (Figures 3.2 and 3.3). The mass percentages of the CH, CHO and CO group ions in the HR-AMS spectra of

WISOM, HULIS-n and HULIS-a were on average very similar to the mass percentages of the functional groups of C-H, C-OH and the sum of COOH and C=O from the FT-IR spectra, respectively, and they showed high positive correlations (r^2 from the data for all organic fractions: 0.98, 0.96 and 0.92, respectively). This result suggests that the CH, CHO and CO groups in the HR-AMS spectra originated primarily from aliphatic hydrocarbons, alcohols, and carbonyl/carboxylic compounds, respectively. In the case of WISOM, the mean mass percentage of CO groups in the HR-AMS spectra was 3.9%, which was significantly lower than the sum of the mass percentages of acidic and non-acidic C=O (mean: 8.9%). A possible explanation for this result is that a large fraction of carbonyl compounds contributed to CHO group ions rather than CO group ions in the HR-AMS spectra of WISOM.

As presented in Figure 3.4, the HR-AMS-derived O/C ratios of WISOM, HULIS-n, HULIS-a, WSOM, and HP-WSOM were 0.12 ± 0.02, 0.41 ± 0.02, 0.67 ± 0.03, 0.76 ± 0.10 and 0.99 ± 0.06 (mean ± SD), respectively, and agreed with those estimated from the FT-IR spectra. The O/C and H/C ratios of HULIS-n and HULIS-a determined in this study were, respectively, similar to those of SV-OOA and LV-OOA identified in the PMF analysis of AMS datasets [*Ng et al*., 2010] and were also similar to those of aerosol HULIS analyzed in earlier studies (Figure 3.4a) [*Kiss et al*., 2002; *Fan et al*., 2013; *Salma et al*., 2007]. However, the H/C ratios of aerosol HULIS from both present and previous studies (1.4–1.8) are obviously higher than those of model humic substances of Suwannee River Fulvic Acid and Nordic Lake fulvic acid (0.91–0.99) [Dinar et al., 2006]. This result suggests that aerosol HULIS has a lower aromatic moiety content than those aquatic environments do.

The ratios of OM/OC are summarized in Figure 3.4b, which shows a wide range of OM/OC ratios (1.3–2.7), in accordance with the polarity of organics. Based on the OM/OC ratios of WISOM and WSOM from the HR-AMS data, the OM/OC of EOM was estimated to be 1.7 ± 0.1

(mean ± SD). In addition, using HR-AMS-derived O/C and H/C ratios, the densities of WISOM, HULIS-n, HULIS-a, WSOM, and HP-WSOM were predicted to be 943 ± 21, 1190 ± 17, 1395 ± 32, 1495 ± 76 and 1598 ± 45 kg m^{-3} (mean ± SD), respectively [*Kuwata et al*., 2012]. From the results for WISOM and WSOM, the density of EOM was estimated as 1211 ± 75 kg m^{-3} (mean ± SD).

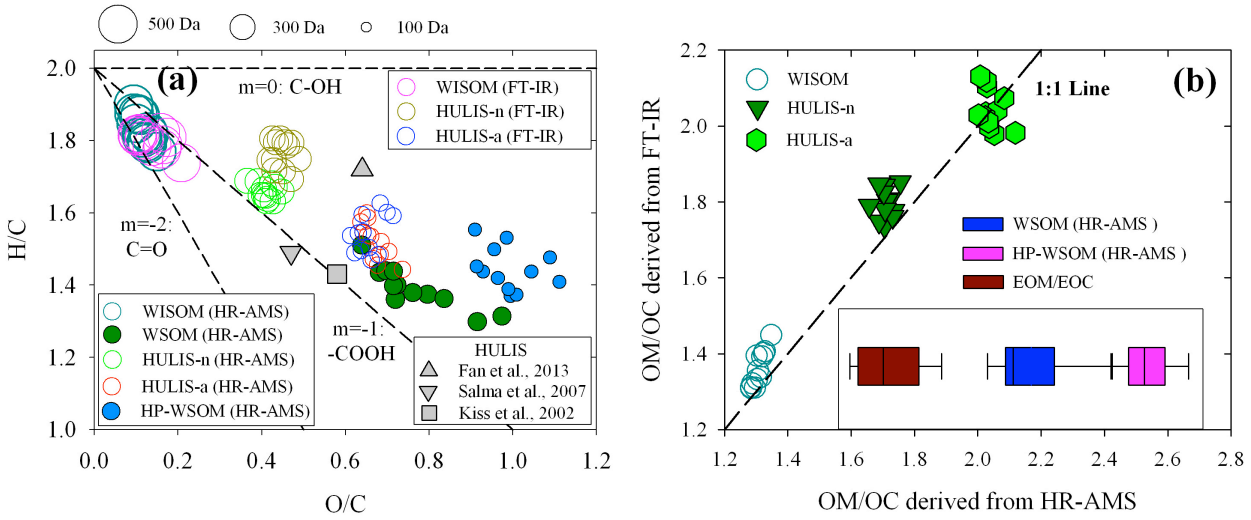

Figure 3.4. (a) Van Krevelen diagram of fractionated organics and (b) the mass ratios of the OM/OC ratio of fractionated organics derived from both HR-AMS spectra and FT-IR spectra. The dashed line in panel (b) is the 1:1 line. Panel (b) also shows the ratio of WSOM, HP-WSOM and EOM/EOC as box plots, which were calculated based on the HR-AMS spectra only (EOM: the sum of WIOM and WSOM; EOC: the carbon mass of EOM). In panel (b), the box plots show the 25th, 50th, and 75th percentiles (box outlines) and the minimum to maximum ranges of the values (bars).

3.4 Molecular-weight distributions

The average molecular weights of WISOM, HULIS-n, HULIS-a and HP-WSOM were obtained from APCI and ESI spectra and are summarized in Table 3.1. The result shows that the M_n of WISOM was much higher than that of the other fractions: 417 ± 41 Da in APCI positive mode and 501 ± 25 Da in ESI negative mode. Based on the M_n and the elemental composition (C/H and C/O) derived from the HR-AMS, the molecular formula of WISOM is represented on average by $C_{26–32}H_{48–58}O_{3–4}$. The results from the molecular formula and the FT-IR-derived structural characteristics suggest that a single molecule of WISOM has an average of 2-3 groups of C-OH and one or two groups of C=O in ketone, aldehyde, and ester compounds. As explained above, the carbon number of WISOM was estimated to be 26-32 on average. Lubricating oils from vehicle emissions contain high MW hydrocarbon mixtures from C_{14} to C_{45} and an average MW corresponding to ~C_{32} [*Kweon et al*., 2003; *Sakurai et al*., 2003], which explains the observed MWD of WISOM.

The M_n values of HULIS-n derived from ESI positive (summer 298 Da; winter 259 Da) and negative (summer 296 Da; winter 250 Da) modes were similar. The M_n values of HULIS-n in this study are similar to the previously reported molecular weight of HULIS in aerosols, with a range of 200–300 Da and a maximum of less than 500 Da [*Kiss et al*., 2003; *Samburova et al*., 2005; *Lin et al*., 2012]. The M_n values of HULIS-n in summer were on average 40–46 Da higher than those in winter. This result is related to the findings of *Samburova et al*., [2005] who found that the maximum molecular weight of HULIS is positively correlated with HULIS generated secondarily in summer, whereas such correlations were not found in winter. Based on the calculated molecular formula, the majority of the compounds in HULIS-n may contain 9–18 carbon atoms (20%–80% of the cumulative intensity in negative mode). This is within the range of 3–24 reported in a study using UHRMS [*Lin et al*., 2012].

Table 3.1. Characteristic parameters (M_n, M_w, and *PI*) of molecular-weight distributions for different organic fractions.[a]

Ion mode [b]	Sample type (Number of samples)	M_n (Da)		M_w (Da)		*PI* [c]	
		Mean	SD	Mean	SD	Mean	SD
Positive	WISOM (*n*=12)	417	41	468	57	1.12	0.03
	HULIS-n (*n*=12)	279	22	321	25	1.15	0.01
	HULIS-n; summer (*n*=6)	298	13	342	16	1.15	0.01
	HULIS-n; winter (n=6)	259	6	300	8	1.16	0.01
	HULIS-a (*n*=12)	218	8	248	12	1.14	0.02
	HP-WSOM (*n*=12)	231	18	269	35	1.16	0.06
	WSOM/EOM [d]	251/317		288/359		1.15/1.13	
Negative	WISOM (*n*=12)	501	25	554	23	1.11	0.02
	HULIS-n (*n*=12)	273	26	291	26	1.07	0.01
	HULIS-n; summer (*n*=6)	296	12	314	13	1.06	0.01
	HULIS-n; winter (*n*=6)	250	8	268	9	1.07	0.00
	HULIS-a (*n*=12)	182	15	192	16	1.05	0.01
	HP-WSOM (*n*=12)	163	9	176	13	1.08	0.02
	WSOM/EOM [d]	217/330		228/357		1.05/1.08	

[a] The obtained molecular weights may be influenced by the instrument settings and the dependence of the ionization efficiency on molecules.

[b] The data for WISOM were obtained with APCI positive mode and ESI negative mode; the data for HULIS-n, HULIS-a and HP-WSOM were obtained from ESI with both positive and negative modes.

[c] The polydispersity index (*PI*) was calculated by $PI = M_w/M_n$ [*Mané et al*., 2007].

[d] M_n of WSOM was calculated from M_n of HULIS-n, HULIS-a and HP-WSOM; M_n of EOM was calculated from M_n of WSOM and WISOM.

The M_n values of HULIS-a and HP-WSOM from ESI negative mode were 182 ± 15 Da (20%–80% of the cumulative intensity corresponds to C_6–C_{10}) and 163 ± 9 Da (C_4–C_6), respectively. The M_n values of the hydrophilic fractions of WSOM (HULIS-a and HP-WSOM) were on average ~100 Da lower than those of the hydrophobic fractions of WSOM (HULIS-n). The M_n of HP-WSOM from the positive mode was 231 ± 18 Da, ~20–40 Da higher than that from the negative mode. This result may have been due to the formation of adduct molecular ions such as $[M+Na]^+$, $[M+NH_4]^+$ from HP-WSOM fractions in the ESI positive mode.

4 Light-absorption and fluorescence characteristics of total organic matter in urban total suspended particulates

4.1 Characteristics of the optical properties of aerosol extracts

Figure 4.1 shows the UV-visible absorption spectra, the EEMs and the results of the AMS-derived ion-groups for various aerosol extracts. A common characteristic of the absorption spectra of the aerosol extracts was the monotonic decrease of MAE as the wavelength increases (Figure 4.1a). The MAE at 266 nm of the WISOM and HULIS-n, which are regarded as relatively less polar organic fractions based on the extraction procedure, were 1.73 ± 0.51 (mean ± SD) and 1.89 ± 0.55 $m^2 g^{-1}$, respectively. These values are on average substantially higher than more polar fractions of the organics: HULIS-a and HP-WSM (mean ± SD: 1.15 ± 0.39 and 0.35 ± 0.09 $m^2 g^{-1}$, respectively). In the visible region, the MAE showed a decreasing trend with wavelength regardless of the fraction type, and those at 532 nm were ≤0.03 $m^2 g^{-1}$. These values are hundreds of times lower than those of amorphous carbon spheres/tar balls [*Alexander et al*., 2008; *Hoffer et al*., 2016] and 2–5 times lower than those of HULIS and water- and MeOH-soluble BrC in BBOA [*Hoffer et al*., 2006; *Chen and Bond*, 2010]. They are also lower than those of BrC over the cities of Beijing and Los Angeles [*Yang et al*., 2011; *Zhang et al*., 2011; *Cheng et al*., 2011], where large contributions from anthropogenic sources are expected. However, they are similar to those of aerosols that are predominantly of biological origin, as found over Atlanta and the rural background site of Kpuszta [*Zhang et al*., 2011; *Utry et al*., 2013]. The MAE of the extracts in the visible region decreased along with their polarity in the order WISOM, HULIS-n, HULIS-a and HP-WSM. This result contrasts the finding that the MAE of the SOA generated in a chamber increased with the O/C ratio [*Lambe et al*., 2013]. Conversely, in the case of atmospheric aerosols over the Gulf of Mexico, most of the oxidized

OA has been reported to be non-absorbing (467–660 nm) [*Lack et al*., 2008]. A reasonable explanation is that the light absorptivity of organics in aerosols may not increase monotonically with their oxidation level [*Kameel et al*., 2014]; rather, such chromophores tend to bleach as the photochemical oxidation proceeds.

In general, the ratio of MAE at 250 nm to that at 365 nm (E_2/E_3) is related to the total aromaticity and the averaged molecular weight of organic aerosol components [*Peuravuori and Pihlaja*, 1997; Duarte et al., 2005; *Heal and Hammonds*, 2014]. Figure 4.4c presents the temporal variations of E_2/E_3 for the extracts with different polarities. A comparison among different fractions (WISOM, WSM, HULIS-n, HULIS-a, and HP-WSM) shows that the respective mean values of M_n (i.e., the number-average molecular weight) have a decreasing trend as E_2/E_3 increases (with an r^2 value of 0.74 between E_2/E_3 and the natural logarithm of the mean of measured M_n). This result agrees with that reported by *Peuravuori and Pihlaja* for aquatic humic substances [1997]. The E_2/E_3 values of WISOM, HULIS-n, HULIS-a, WSM and HP-WSM were, respectively, 5.8 ± 0.4 (mean ± SD), 6.8 ± 0.5, 11.2 ± 1.4, 5.8 ± 0.5 and 10.5 ± 2.6 (Figure 4.2c). The E_2/E_3 of the WISOM and HULIS-n in winter were, on average, 0.91 and 0.90 times those in summer, respectively. The lower ratios in winter suggest their higher aromaticity or higher molecular weight, which is similar to the results reported for the urban background in Edinburgh, UK [*Heal and Hammonds*, 2014]. The E_2/E_3 increased with the polarity of the extracts, indicating that less polar organics probably have higher aromaticity and higher molecular weight.

As seen in Figure 4.1c, the EEMs of the different extracts clearly have different profiles. Four common peaks were found in most of the EEMs: P1 (excitation: ~240 nm; emission: ~430 nm), P2 (~240 nm; ~390 nm), P3 (~275 nm; ~325 nm) and P4 (~320 nm; ~430 nm). A comparison with previous studies suggests that P1 and P2 relate to low-UV absorber HULIS

[*Birdwell and Engel*, 2010]. Furthermore, P3 generally accounts for protein-like components [*Sierra et al*., 2005; *Huguet et al*., 2009], and P4 are from marine HULIS or photodegradation products [*Sierra et al*., 2005]. P4 was also close to the peaks in the EEMs of the SOA from the ozonolysis of α-pinene [*Le et al*., 2013]. The relative fluorescence intensity of the HULIS-n at P3 was higher than those in other extracts, suggesting the large abundance of protein-like components in the forms of amines and other nitrogen-containing compounds. The intensity ratios of P1/P4 (usually denoted A/M in previous studies) in the EEMs of the WISOM were, on average, 1.5, which is lower than those of the WSOM (mean: 3.1). Low ratios indicate higher proportions of conjugated and/or aromatic compounds [*Santos et al*., 2013]. It is thus likely that the WISOM possessed large conjugated systems more abundantly than the WSOM.

To compare the fluorescence efficiencies from different types of extracts, the fluorescence volumes over the excitation wavelength of 235–400 nm and the emission wavelength of 300–600 nm were normalized by the mass concentrations of the organics (abbreviated to NFV). As seen in Figure 4.4d, the NFV of the WISOM was $7.4 \pm 2.5 \times 10^2$ (mean ± SD) RU-nm^2 [mg/L OM]$^{-1}$, which was higher than that of the WSOM. In particular, the NFV of the HP-WSM was only 21 ± 11 (mean ± SD) RU-nm^2 [mg/L OM]$^{-1}$. This result suggests that hydrophobic organics have stronger fluorescence than hydrophilic organics.

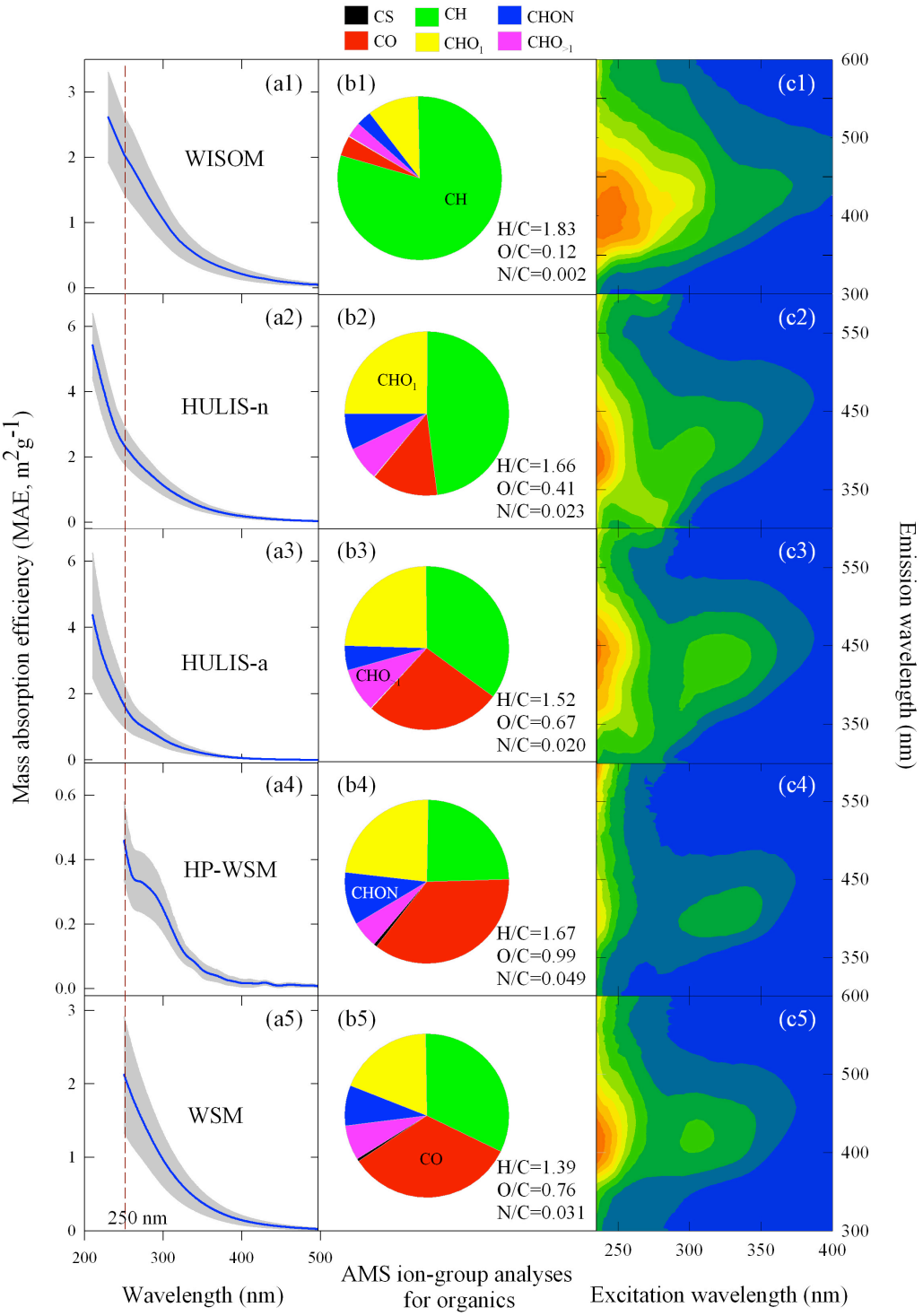

Figure 4.1. UV-visible absorbance spectra, excitation–emission matrix fluorescence spectra (the highest intensity is scaled to be unity) and results from the AMS ion-series analysis for aerosol extracts. The solid lines and shaded areas in panels a1–a5 indicate the mean values and the ranges within standard deviation from the mean, respectively.

4.2 Relative contributions of total light-absorption for aerosol organics

Figure 4.2 presents the relative contributions of each of the aerosol extracts to the total light-absorption of the studied organics. The total light-absorption of the WISOM and WSM at 300 nm was 10.6 Mm^{-1}, which was 0.23 times the estimated light-absorption by BC. In the low-UV region (at 250 nm), the total light-absorption of the WISOM, HULIS-n and HULIS-a was as large as 21.9 Mm^{-1}, which is 0.39 times the light-absorption by BC. Although the significant UV absorption at wavelengths below 300 nm may not be important for the transfer of total solar radiation in the troposphere, the presence of light-absorbing organic aerosols may cause a reduction in UV photolysis and the near-surface ozone mixing ratios [*Barnard et al*., 2008]. By contrast, the total light-absorption of the WISOM and WSM in the visible region at 400 and 500 nm, for example, were, on average, 1.8 and 0.2 Mm^{-1}, respectively, both of which were 0.05 times the BC light absorption. This result suggests that the light absorption of the organics in the visible region cannot be neglected for these aerosols. The light absorption by the organics was mainly contributed by the WISOM and HULIS-n, the less polar fractions of the organics; the sum of the light absorption by the two components at 250 and 400 nm accounted for approximately 75% and 84% of the light absorption by the total organics, respectively. In contrast, the light absorption of the HP-WSM was small and contributed only 4% and 2% of the light absorption by the total organics at 250 and 400 nm, respectively.

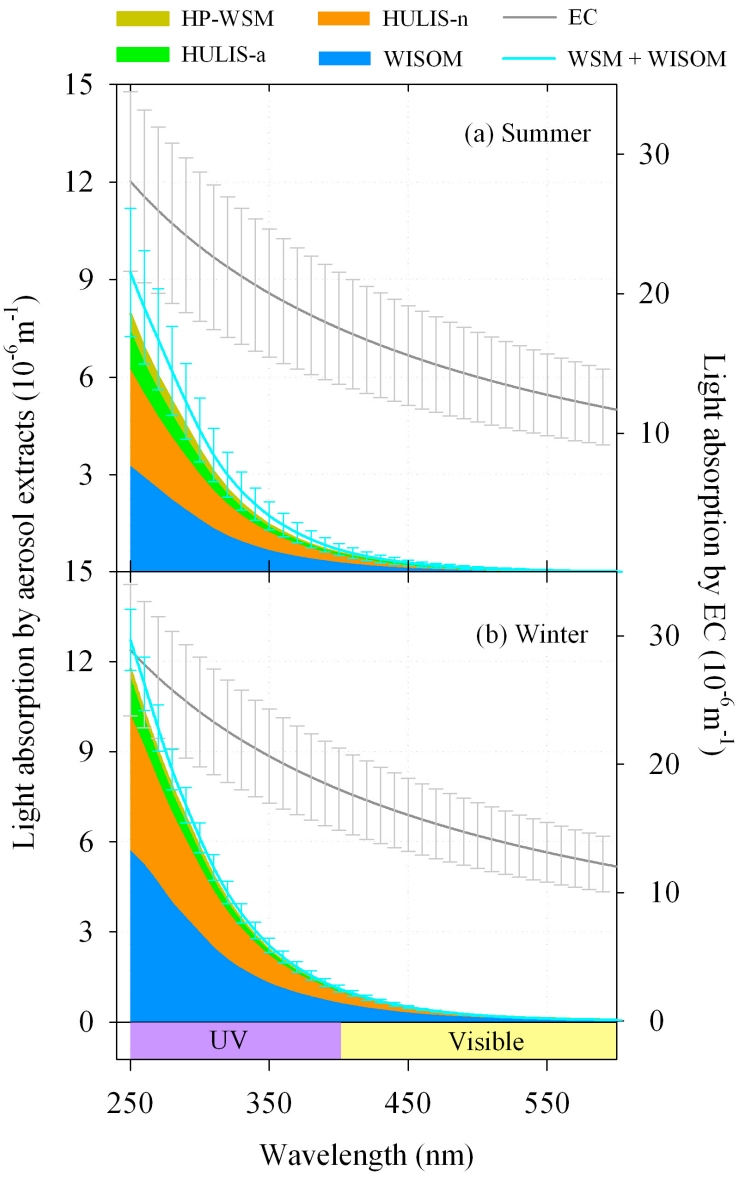

Figure 4.2. Calculated wavelength-resolved contributions of the aerosol extracts and BC to the light-absorption of the studied atmospheric aerosols. The bars indicate the standard deviation.

PAHs have large electron-conjugated systems that lead to large MAE values [*Zhan et al.*, 1997]. The contributions of the PAHs to the total light absorption of the WISOM were estimated (the details of which are given in section 2.3.2). The estimated contributions of the PAHs to light absorption are only 31 ± 4% (mean ± SD) and 19 ± 1% of the total absorption of the WISOM in the summer/early-autumn and winter, respectively. Thus, the BrC other than the PAHs in the

WISOM should be an important light absorber, particularly in winter when most light absorption of the WISOM cannot be explained by the presence of the PAHs. Polycyclic aromatic compounds containing oxygen, nitrogen or sulfur that are formed by atmospheric or combustion processes, such as aromatic organosulfates, quinones and phenolic compounds, may account for most of the water insoluble BrC [*Cory and McKnight*, 2005; *Chang and Thompson*, 2010; *Mladenov et al*., 2011; *Staudt et al*., 2014].

4.3 Ångström exponents for different aerosol organics

Figure 4.3 presents the values of *Å* for different extracts and wavelength ranges. Fits using a single value of *Å* over 300 nm to 600 nm were made for the average spectra of the WISOM, HULIS-n, HULIS-a, HP-WSM and WSM, giving *Å* values of 6.4, 7.2, 8.8, 5.0 and 7.6, respectively. However, the fitted curves largely deviate from the actual absorption spectra (up to 40% at 300 nm). These results illustrate the problems associated with using a single *Å* value for the characterization of the light absorption of aerosol BrC over across the UV and visible ranges (300–600 nm), particularly in the UV range. A similar result was reported for the methanol extracts from wood combustion aerosols; the *Å* values in that case were 0.95–1.3 times higher in the UV range than those in the visible range [*Chen and Bond*, 2010].

The *Å* values increased with the increase of the wavelength ranges. In the range of 300–400 nm, the *Å* of the WISOM, HULIS-n, HULIS-a and WSM were 5.6 ± 0.3, 6.5 ± 0.3, 8.3 ± 0.6 and 6.8 ± 0.4 (mean ± SD), respectively, which are similar to those of methanol- and water-soluble BrC of urban aerosols over Los Angeles and Beijing, respectively [*Cheng et al*., 2011; *Zhang et al*., 2013]. The *Å* values for the WSM were much lower than those of the water extracts from BBOA [*Chen and Bond*, 2010]. In the wavelength range of 400–500 nm, the *Å* of the WISOM, HULIS-n, HULIS-a and WSM increased to 7.2 ± 0.7, 7.7 ± 0.2, 8.3 ± 0.6 and 8.1 ± 0.7 (mean ±

SD), respectively. These values are comparable with those of the methanol extracts (mean ± SD: 7.9 ± 0.3) of wood combustion aerosols [*Chen and Bond*, 2010]. The *Å* values did not further increase in the visible range of 500–600 nm.

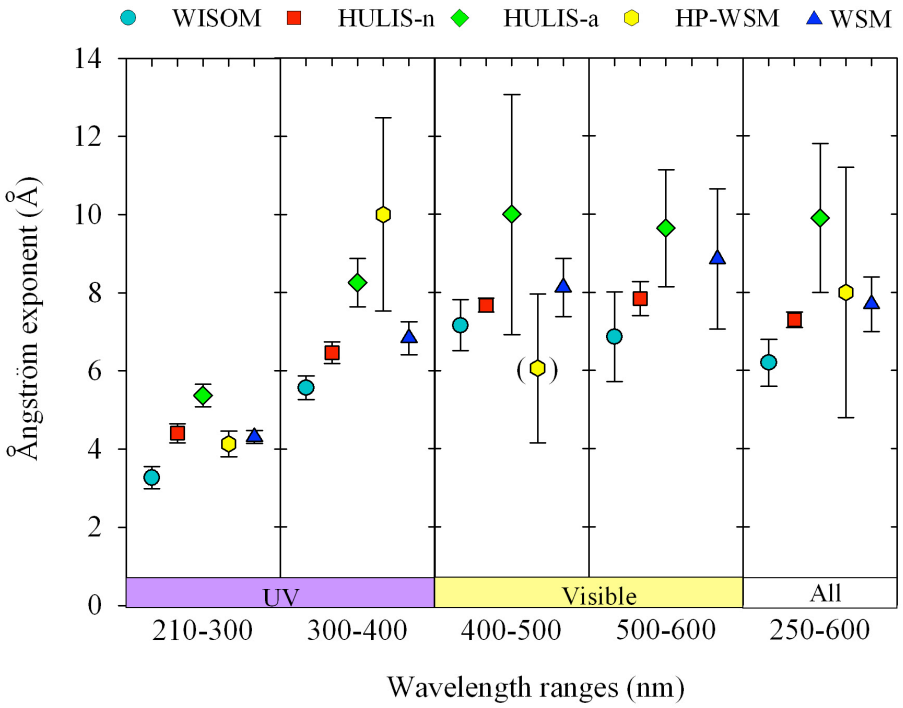

Figure 4.3. The Ångström exponent (*Å*) of the aerosol extracts. The brackets indicate that the values of *Å* may not be reliable because the absorbances of the HP-WSM in the visible ranges were close to those in the blanks. The bars indicate the standard deviation.

Figure 4.3 also shows that *Å* varied depending on the extracts, with the tendency to increase with an increase of their polarity, except for the HP-WSM; the *Å* values of the WISOM, HULIS-n, WSM and HULIS-a in the wavelength range of 250–600 nm were 6.2 ± 0.6, 7.3 ± 0.2, 7.7 ± 0.7 and 9.9 ± 1.9 (mean ± SD), respectively. This result agrees with that from *Zhang et al*. [2013], who reported substantially different *Å* values of the methanol- and water-soluble BrC in Los

Angeles in the wavelength range of 300–700 nm (4.8 and 7.6, respectively). The authors suggested that chromophores tend to be hydrophobic in urban aerosols, which may also explain the result from the extracted organics in this study.

4.4 Variations of the optical properties and chemical structures

The light absorption and fluorescence efficiency (i.e., MAEs and NFVs) for five different types of extracts from aerosols in the summer/early-autumn and winter are plotted in Figure 4.4. Except for the HP-WSM, the MAEs and NFVs of the extracted fractions from the winter aerosols were significantly higher than those from the summer/early-autumn aerosols, according to a 5% two-sided Welch's test. Specifically, the MAEs for the WISOM, WSM, HULIS-n and HULIS-a in winter were, on average, 1.91 (at 365 nm) times higher than those in summer/early-autumn, and the NFV in winter was 2.4 times higher than those in summer/early-autumn. These results suggest that the proportion of BrC in the total organics and/or their light absorptivity was larger in winter, which may have resulted from the changes in the sources and formation processes of the organics from summer/early-autumn to winter. Biomass burning is potentially an important source of BrC in ambient aerosol [*Utry et al*., 2013; *Lack et al*., 2013], and may have contributed to the higher values of MAEs in winter. The relative intensity of $C_2H_4O_2^+$, an ion that is associated with organics from BBOA sources [*Lee et al*., 2010], in the AMS spectra of the WSM in the winter (mean ± SD: 0.54 ± 0.1%) were higher than those in summer/early-autumn (0.24 ± 0.02%). Further, the relative intensity of $C_2H_4O_2^+$ was positively associated with the MAE of the WSOM ($r^2 = 0.80$, $p < 0.01$) and WISOM ($r^2 = 0.78$, $p < 0.01$) at 365 nm, and the NFV of the WISOM ($r^2 = 0.81$, $p < 0.01$) and WSOM ($r^2 = 0.66$, $p < 0.01$). This result suggests that the proportion of the BBOA in winter was generally higher than that in summer/early-autumn and that the organics from the BBOA were probably a major BrC source in winter that

was responsible for the increase of the MAEs and NFVs of both the water soluble and insoluble BrC. Backward air mass trajectory analysis suggests the influence of the outflow of aerosols from the Asian continent in winter. Hence, long-range transport of biomass burning aerosols may have contributed to the observed high MAEs of organic aerosols in the season. The large enhancement of the MAEs and NFVs in winter may also be attributable to the relatively greater partitioning of aromatic compounds, including those of anthropogenic origin, into the particle phase in the cold season [*Cheng et al*., 2011; *Heal and Hammonds*, 2014].

The differences in the MAEs and NFVs in the summer/early-autumn and winter were further examined based on the relationship between the optical properties and ion-groups in the HR-AMS spectra of the summer/early-autumn and winter extract samples (Figure 4.5 and Table 4.1). The relative intensities of the CHO_1N and $CHO_{>1}N$ ion-groups showed strong positive correlations with the MAEs in <400 nm and NFVs for the HULIS-n, HULIS-a and HP-WSM. Additionally, the relative intensity of the $CHO_{>1}N$ ion-groups ions correlated positively with the MAE of the WISOM, especially in the long-wavelength range. The results suggest that organic compounds with O and N atoms contributed largely to the total light absorption and fluorescence of the organic aerosol components and that these molecules were responsible for the enhancements of the MAE in winter. Both the MAE at 266 nm and NFV for different extracts (WISOM, HULIS-n and HULIS-a, and HP-WSM) correlated positively with the relative intensity of the CH group (r>0.63, p<0.001) and negatively to that of the CO group (r<–0.77, p<0.001). This result indicates that the chromophores may have been degraded by photochemical reactions, which is a possible reason for the relatively low values of the MAEs and NFVs of the organics in the summer/early-autumn [*Kieber et al*., 2012; *Lee et al*., 2014]. This is consistent with the results from the correlation analyses of the optical properties and the relative intensity of the chemical groups in the FT-IR spectra of the WISOM, HULIS-n and HULIS-a (Figure 4.6

and Table 4.2). The result shows that, in most cases, the MAEs and NFVs correlated positively with the aliphatic C–H groups and negatively with non-acidic carbonyl C=O and carboxylic COOH groups. Furthermore, the amine C–NH_2 group correlated positively with the MAEs and NFVs in some cases, whereas the organic nitrate C–ONO_2 group was not correlated with the MAEs and NFVs with strong significance.

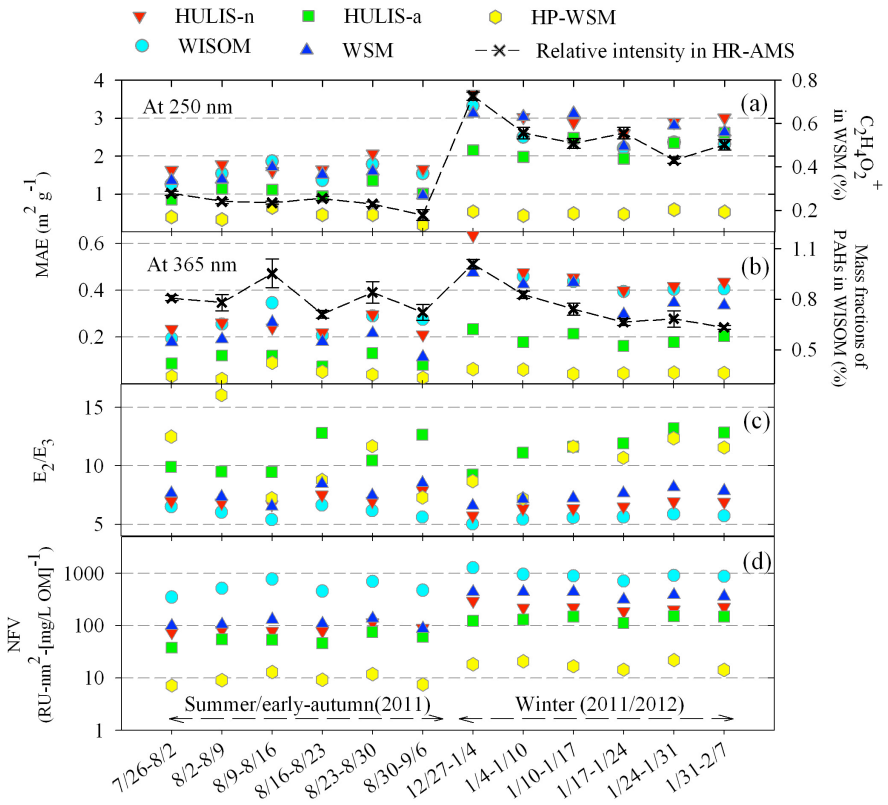

Figure 4.4. Temporal variations of the mass absorption efficiency (MAE) at 250 and 365 nm, E_2/E_3 (the ratio of MAE at 250 nm to that at 365 nm), and fluorescence volume of aerosol extracts normalized by the organic mass concentration (NFV) for the WISOM, WSM, HULIS-n, HULIS-a and HP-WSM, relative peak intensity of $C_2H_4O_2^+$ ion in the HR-AMS spectra of the WSM and calculated mass fractions of the PAHs in the WISOM. The bars indicate the standard deviation.

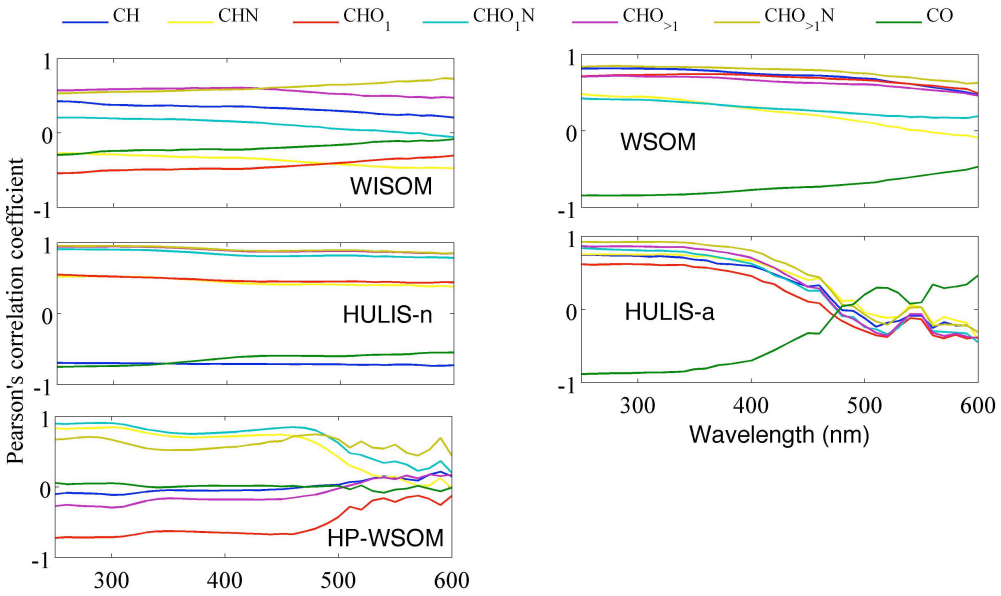

Figure 4.5. Pearson's correlation coefficients between the MAEs at different wavelengths and the relative intensities of the AMS ions (n = 12).

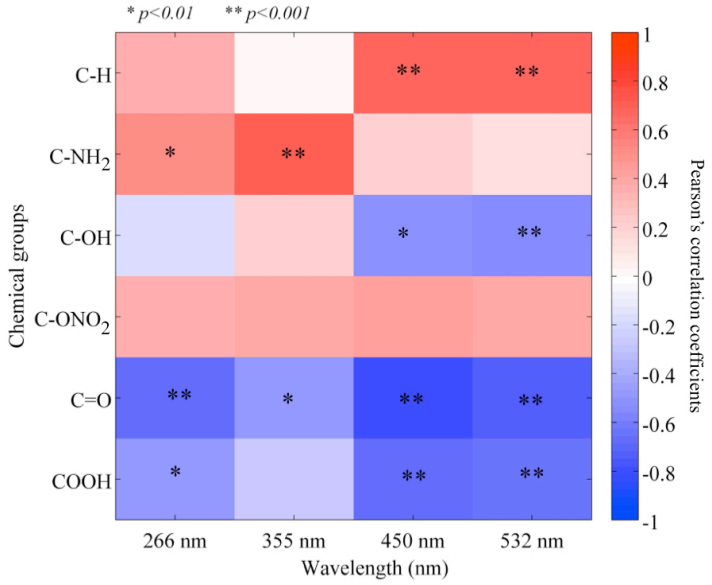

Figure 4.6. Pearson's correlation coefficients between the MAEs at different wavelengths and the relative intensities of the chemical groups in the FT-IR spectra of the WISOM, HULIS-n and HULIS-a (n = 36).

Table 4.1. The Pearson's correlation coefficients (r) and significance levels (p, two-sided t-test) from the correlation analysis between the relative intensities of the ion-groups in the AMS spectra and the normalized fluorescence volumes for the different extracts (n = 12).[a]

Ion-groups	WISOM	WSM	HULIS-n	HULIS-a	HP-WSM
CH	—	0.79*	–0.73*	0.80*	
CHN	—	—	—	0.82*	0.86*
CHO_1	—	0.67	—	0.59	–0.80*
CHO_1N	—	—	0.93*	0.87*	0.95*
$CHO_{>1}$	0.58	0.63	0.96*	0.84*	—
$CHO_{>1}N$	—	0.79*	0.95*	0.93*	0.80*
CS	—	—	0.73*	—	—
CO	—	–0.82*	–0.75*	–0.92*	—

[a] The r values with significance levels p greater than 0.05 are not shown. * p<0.01.

Table 4.2. Pearson's correlation coefficients (r) and significance levels (p, two-sided t-test) from the correlation analysis between the relative intensities of the chemical groups in the FT-IR spectra and the normalized fluorescence volumes for the different extracts (n = 12).[a]

Ion-groups	WISOM	HULIS-n	HULIS-a	All (n = 36)
C–H	—	—	—	0.88*
$C–NH_2$	—	0.85*	0.73	—
C–OH	—	—	0.83*	–0.87*
$C–ONO_2$	—	—	—	—
C=O	—	–0.76	–0.81	–0.64*
COOH	—	—	—	–0.62*

[a] The r values with significance levels p greater than 0.01 are not shown. * p<0.001.

4.5 Fluorescent components

Four fluorescent components (C1, C2, C3 and C4) were identified from the different types of fractions. Their profiles and relative contents are shown in Figure 4.7. Based on a comparison with previous studies, the four fluorescent components were identified to the short-wavelength-light absorber (HULIS-1), long-wavelength-light absorber (HULIS-2) and protein-like organic matter (PLOM-1 and -2), respectively [*Chen et al*., 2003; *Dubnick et al*., 2010; *Yu et al*., 2015; *Santos et al*., 2013]. The NFVs of these four components in the different extracts correlated positively to their MAEs over the visible region (400–600 nm, $p<0.01$, Figure S4), suggesting that the fluorescent compounds in the extracts may associate with compounds that absorb light in the visible region.

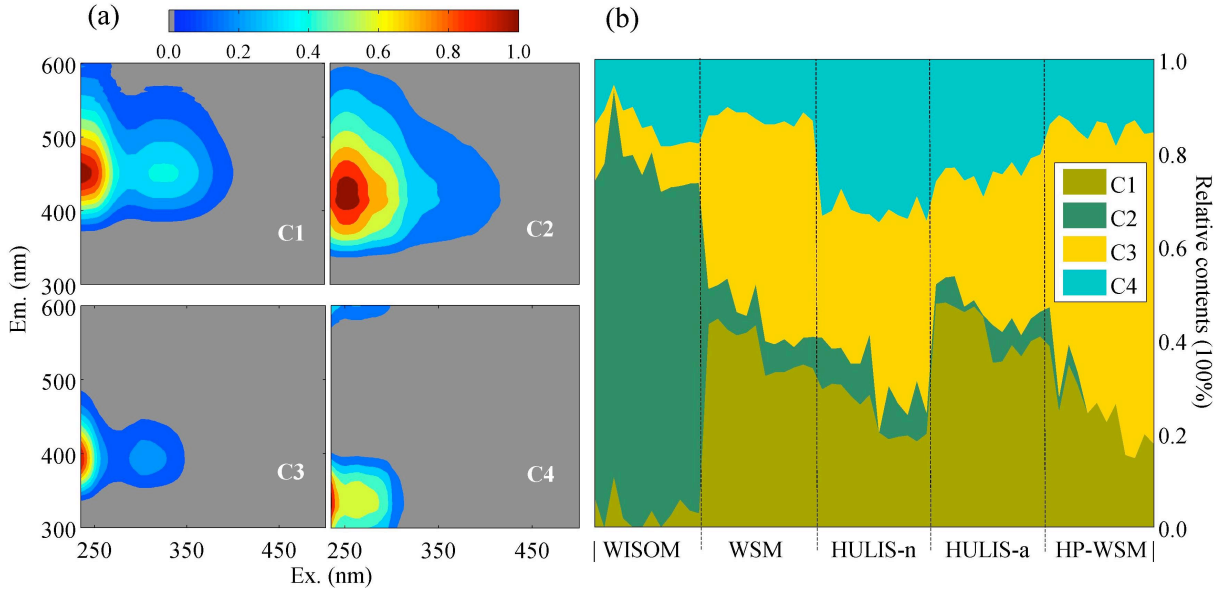

Figure 4.7. (a) The EEM components (C1, C2, C3 and C4) that were identified using the PARAFAC model for all of the samples (n = 60) and (b) their relative contributions to the different aerosol extracts.

The correlation analysis between the relative intensity of the AMS ions and the relative contents of the PARAFAC components was performed to infer possible chemical structures that contribute to the observed fluorescence (Table 4.3). The HULIS-1 and PLOM-1 from the PARAFAC model correlated positively with those of the oxygen-containing ions (CO and CHO) and negatively with those of the CH ions ($p<0.01$). Conversely, the HULIS-2 correlated positively with the CH ions ($p<0.001$) and negatively with the other ions (except for the CS ions: $p<0.01$). The results suggest that the HULIS-2 is associated with hydrocarbons and that the HULIS-1 and PLOM-1 are associated with oxygen-containing compounds. This finding is consistent with the results shown in Figure 4.7b; the HULIS-1 and PLOM-1 were abundant in the water-soluble fractions, whereas the HULIS-2 was abundant in the WISOM. The PLOM-1 correlated strongly with the CHN ions ($r = 0.92$, $p<0.001$), indicating that the PLOM-1 is closely related to nitrogen-containing compounds, probably atmospheric amines and amides, which have been identified as protein-like compounds in terrestrial and oceanic systems [*Yu et al*., 2015; *Hunt and Ohno*, 2007]. The larger percentages of the PLOM-1 for the water-soluble fractions suggest that the WSOM contained an abundant amount of nitrogen-containing compounds, which is in contrast to the WISOM. The CNH ion-group did not correlate with the PLOM-2 ($p>0.65$), although the PLOM-2 was also composed of protein-like compounds in terrestrial and oceanic systems [*Yu et al*., 2015; *Hunt and Ohno*, 2007]. Instead, the PLOM-2 component correlated positively with the CHO ion-groups ($p<0.01$). This result suggests that most of the PLOM-2 were comprised of oxygen-containing compounds rather than protein-like compounds. Additionally, the PLOM-2 may be comprised of phenol- and naphthalene-like substances, as inferred from the similarity of the position of the fluorescence peak [*Mladenov et al*., 2011; *Laurentiis et al*., 2013]. In contrast to terrestrial and oceanic systems, the biotic activity of microbes in the atmosphere should not be active, which may have resulted in this feature.

A correlation analysis between the relative intensity of the chemical groups in the FT-IR spectra and the relative contents of the PARAFAC components was performed for the WISOM, HULIS-n and HULIS-a (Table 4.4). The results showed that the HULIS-1, HULIS-2, PLOM-1 and PLOM-2 correlated positively with the oxygenated functional groups (non-acidic carbonyl C=O and carboxylic COOH groups), aliphatic C–H group, amine C–NH_2 and alcohol C–OH groups, respectively. This result is consistent with the results that were obtained from the correlation analysis based on HR-AMS. This study successfully associated the PARAFAC components from the extracts of different fractions with specific AMS ions and chemical groups of organics in the FT-IR spectra.

Table 4.3. Pearson's correlation coefficients (r) and significance levels (p, two-sided t-test) from the correlation analysis between the relative intensities of the ion-groups in the AMS spectra and the relative contents of the EEM components derived from the PARAFAC model (n = 60).[a]

Ion-groups	C1	C2	C3	C4
	HULIS-1	HULIS-2	Protein-like-1	Protein-like-2
CH	–0.76*	0.93*	–0.84*	—
CHN	—	–0.64*	0.92*	—
CHO_1	0.65*	–0.84*	0.54*	0.56*
CHO_1N	0.34	–0.34	0.37	—
$CHO_{>1}$	0.79*	–0.77*	0.38	0.41
$CHO_{>1}N$	—	–0.41	0.40	—
CS	—	—	0.46	–0.40
CO	0.67*	–0.74*	0.75*	—

[a] The r values with significance levels p greater than 0.01 are not shown. * p<0.001.

Table 4.4. Pearson's correlation coefficients (r) and significance levels (p, two-sided t-test) from the correlation analysis between the relative intensities of the chemical groups in the FT-IR spectra and the relative contents of the EEM components derived from the PARAFAC model (n = 36 for the WISOM, HULIS-n, and HULIS-a).[a]

Chemical groups	**C1** HULIS-1	**C2** HULIS-2	**C3** Protein-like-1	**C4** Protein-like-2
C–H	–0.94*	0.94*	–0.78*	–0.61*
$C–NH_2$	—	—	0.67*	0.54
C–OH	0.82*	–0.96*	0.90*	0.76*
$C–ONO_2$	–0.55	—	—	—
C=O	0.88*	–0.60*	—	—
COOH	0.88*	–0.66*	—	—

[a] The r values with significance levels p greater than 0.01 are not shown. * p<0.001.

5 Structural and light-absorption characteristics of water-insoluble organic mixtures in urban submicron aerosols

5.1 Carbon concentrations and carbon fractions

The concentrations of carbon in the aerosols and the six sub-fractions of WISOM therein were determined using the thermal-optical method (Tables 5.1 and 5.2). The thermograms from the thermal-optical analysis for the extracted organic carbon are shown in Figure 5.1. The ratio of E-WISOC to WSOC was on average 0.41 ± 0.02 (mean ± SD), indicating that a substantial part of organic compounds in $PM_{0.95}$ was insoluble. On average, one-half of E-WISOC (50%) was found in F4, a low-polar fraction of WISOM. By contrast, relatively small fractions of carbon were detected in the non-polar fraction of F1 (mean: 9%), low-polar fractions of F2 (15%) and F3 (18%), and medium-polar fractions of F5 (6%) and F6 (2%).

The carbon-mass percentages of thermally derived carbon fractions (OC1–4 and EC1–3) in the six sub-fractions of WISOM were obtained (Figure 5.1). The relative abundances of OC2, which is associated with high-volatility compounds (≤250°C), for non-polar fraction F1 and low-polar fraction F2 were obviously higher than those for other fractions. This result indicates that the organic compounds with non-polar and low-polar properties in E-WISOC tended to have relatively high volatility. Furthermore, the thermal decomposition of organic compounds during the analysis was evident from the decrease in the laser signals during the steps to analyze OC3 and OC4, and a large fraction of organic carbon was found to be pyrolyzed organic carbon. There was a positive correlation between the mass fractions of carbon detected during the steps to analyze EC and the average O/C ratios of organics in each of fractions F1–F6 that derived from the HR-AMS spectra ($r = 0.88$, $p < 0.05$). This result suggests that oxygenated organic compounds in E-WISOC were prone to be charred.

Table 5.1. Concentrations of extractable organic carbon and total organic carbon in the four weekly aerosol samples and the mass ratios of E-WISOC to WSOC and EOC to TOC.[a]

	Concentration (μg-C m^{-3})					Ratio		
	E-WISOC	WSOC	EOC	TOC_R	TOC_T	E-WISOC/ WSOC	EOC/ TOC_R	EOC/ TOC_T
Mean	0.57	1.39	1.96	1.85	2.26	0.41	1.06	0.87
SD	0.03	0.13	0.16	0.23	0.17	0.02	0.10	0.05

[a] E-WISOC: the extracted water-insoluble organic carbon (the sum of OC in the six sub-fractions of WISOM); EOC: the sum of E-WISOC and WSOC; TOC_T: TOC in filter samples derived from the TOC analyzer with the thermal optical transmittance (TOT) method; TOC_R: same as TOC_T but determined with the total optical reflectance (TOR) method.

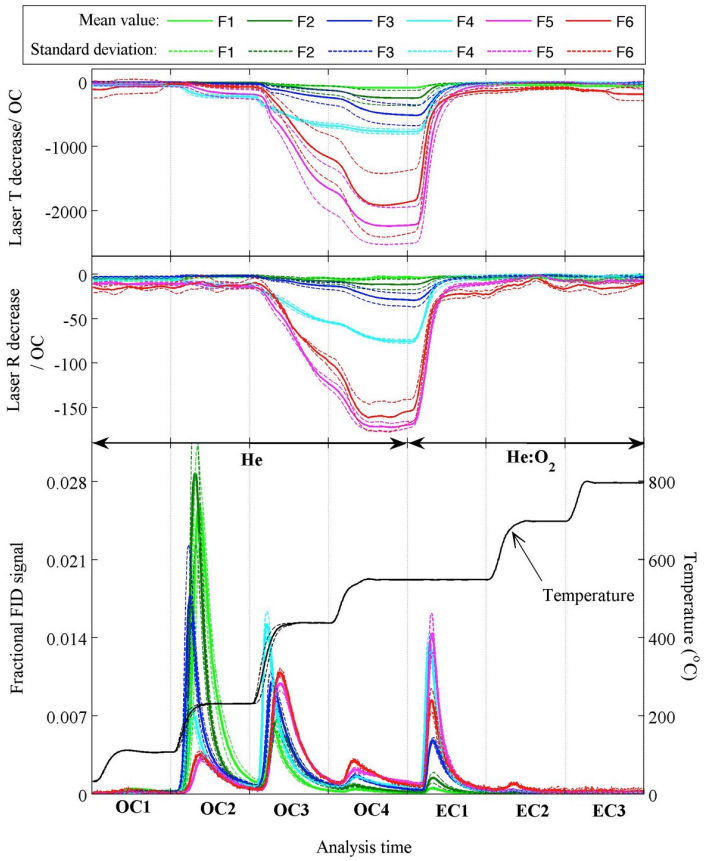

Figure 5.1. Thermal-optical analysis of fractionated organic matters with the IMPROVE temperature protocol. The solid and dashed lines indicate the mean and ranges within SD, respectively.

5.2 Analysis of functional groups using FT-IR spectroscopy

The FT-IR spectra of the organic fractions studied are presented in Figure 5.2. The main peaks and their assignments are shown as color bars in the top part of the figure. The relative contents of the organic functional groups are also presented. Nearly all of the quantified organic functional groups in F1 were aliphatic C–H groups (mean: 98%), suggesting that they were mainly aliphatic hydrocarbons. A weak absorption in the range of 1000–1100 cm^{-1} was observed, typically corresponding to the C–O stretching vibration of alcohols, ethers and esters. However, absorption from esters (C–O–C=O) was unlikely because the peaks of carbonyl (C=O) groups were absent in the FT-IR spectra. Hence, a small mass fraction of alcohols (mean: <2%) and/or ethers was present in F1.

The FT-IR spectra of F2 exhibited strong absorption peaks at 1728, 1280, 1125 and 1073 cm^{-1}. They originated from stretching vibrations of C=O and C-O. The peaks at 1600 and 1580 cm^{-1}, which are generally assigned to aromatic C=C ring vibrations, were also observed. The peak at 744 cm^{-1} corresponded to H–Ar plane bending vibration, indicating that phenyl rings in this fraction were ortho-substituted. The above peak assignments and the comparison of the spectra to those of the IR spectra of phthalate esters (PAEs) in the NIST library (http://webbook.nist.gov) and previous studies suggest that F2 contained abundant PAEs [*Das and Mahiuddin*, 2005; *Salim et al*., 1010; *Toja et al*., 2012].

An abundant C–ONO_2 in F3 was indicated by the peaks at 1630, 1280 and 863 cm^{-1} [*Bruns et al*., 2010; *Liu et al*., 2012]. The mass percentages of C–ONO_2 in F3 were estimated to be on average 15%, which was obviously higher than the percentages in other fractions. This result suggests that F3 contained abundant organic nitrates. In addition, the peaks at 1720 cm^{-1} (C=O)

and in the range of 1000–1200 cm^{-1} (C–O–C) suggest that F3 may also have contained abundant aliphatic esters.

Strong absorptions of C–OH (3100–3600 cm^{-1}), C=O (1720 cm^{-1}) and C–O–C (1000–1200 cm^{-1}) groups were observed for F4, indicating that the organics were primarily esters, alcohols, ketones and/or ethers. The peaks at approximately 1635 cm^{-1} corresponded to nitrogen-containing groups, which were presumably organic nitrates and/or amines. A peak at 1580 cm^{-1} was also observed, suggesting that this fraction contained aromatics [*Popovicheva et al*., 2014]. The peaks at 1384 and 1462 cm^{-1} were attributed to the C–H deformation of methyl (CH_3) and methylene (CH_2) groups; the high intensity ratio of CH_3/CH_2 for F4 (mean: 2.9) was obviously higher than that in fractions F1 (mean: 0.2), F2 (mean: 0.5) and F3 (mean: 0.8), indicating abundant branched structures.

The FT-IR spectra of F5 were characterized by the high relative abundance of alcohols, which was indicated by strong absorptions in the wavenumber ranges of 3100–3600 and 1100–1200 cm^{-1}. Significant absorptions at approximately 1715, 1675 and 1580 cm^{-1}, which are generally assigned to saturated and unsaturated carbonyl (C=O) groups and aromatics (C=C), were also observed [*Ramesh and Sampath*, 2014]. Substantial parts of the C–OH (mean: 35%) and C=O (mean: 5%) functional groups were not in carboxylic acids because carboxylic COOH in F5 was not abundant (mean: 3%). Fraction F5 may have contained abundant phenolic compounds and quinones and resulted in the observed spectra.

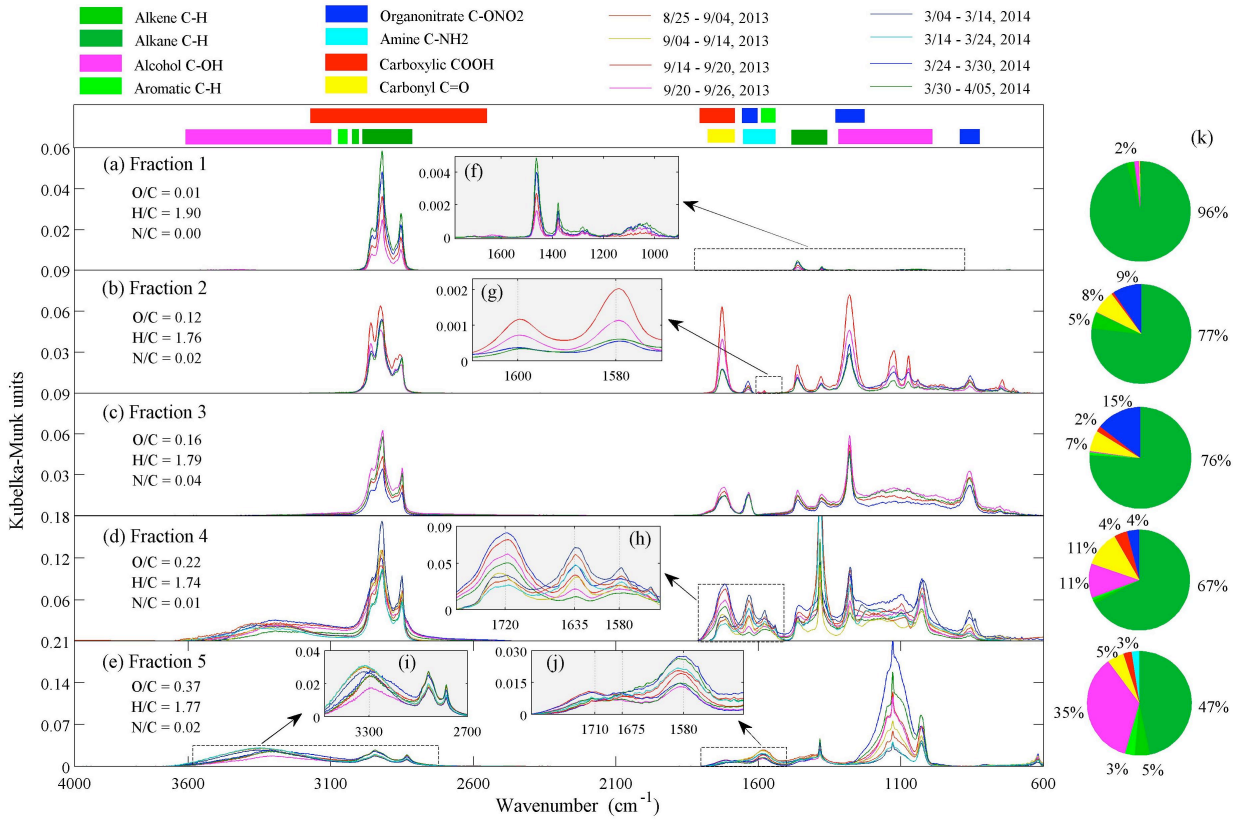

Figure 5.2. (a–e) FT-IR spectra of five fractionated organic matter. Because the signals of the organics in the FT-IR spectra of fraction F6 were low, the result is not presented. (f–j) Enlarged views of the spectra. (k) Pie charts of the mass fractions of the quantified functional groups in organic matter.

5.3 Analysis of functional groups using ^{1}H-NMR spectroscopy

The structural characteristics of complex water-insoluble organic matter were further investigated from the ^{1}H-NMR spectra (Figure 5.3). A few sharp peaks in the chemical-shift range of δ_H <1.9 ppm were observed regardless of the fractions; they are generally attributed to aliphatic protons (H–C) from methyl (C–C–H_3), methylene (C–C–H_2) and methine (C–C–H) groups. The total aliphatic protons in the ^{1}H-NMR spectra accounted for 92%, 83%, 74%, 73% and 48% of the protons of organics in fractions F1, F2, F3, F4 and F5, respectively. Obvious

signals at $\delta_H \approx 1.1$ ppm were observed for fractions F1 to F3, suggesting that a portion of methyl protons was influenced by the γ-C=C structure.

The chemical shift range of $\delta_H = 1.9–4.5$ ppm was characterized by many small peaks and continuous unresolved profiles, indicating the complex composition of the organic matter. The signals in the unsaturated aliphatic region of $\delta_H = 1.9–3.2$ ppm are generally attributed to aliphatic protons on carbon atoms adjacent to double bonds, i.e., allylic H–C–C=C and carbonyl H–C–C=O. A few peaks were observed in the regions of $\delta_H = 2.1–2.2$ ppm and $\delta_H = 2.2–2.5$ ppm, implying that some protons were in H–C–C=C and H–C–C=O groups, respectively, which together accounted for 4%, 6%, 15%, 16% and 27% of the protons from organics in fractions F1, F2, F3, F4 and F5, respectively. Long-chain ester or ketone structures were identified in F4 based on the ^{1}H-^{1}H correlation spectra (COSY) (Figure 5.4) [*Seaton et al.*, 2013]. The oxygenated saturated aliphatic region of $\delta_H = 3.2–4.5$ ppm corresponded to H–C–O proton resonances from aliphatic forms of alcohols, esters and ethers. The signals in this range accounted for 3%, 7%, 8%, 8% and 20% of total proton signals for fractions F1, F2, F3, F4 and F5, respectively. Several peaks at approximately $\delta_H = 3.6$ and 4.2 ppm were observed, which most likely originated from alcohols and esters.

The aromatic protons ($\delta_H = 6–9$ ppm) were found abundantly in fractions F2 and F5, consistent with the assignment of compound groups from the FT-IR spectra. Each of them accounted for on average 5% of total protons in organics, which was significantly higher than the percentages of other fractions (≤2%). Multiple signals at $\delta_H \approx 7.71$, 7.53, 4.22 and 1.69 ppm were identified in the ^{1}H-NMR spectra of F2 (marked as a-d in panel (b) of Figure 5.3), which are assigned to protons from PAE molecules.

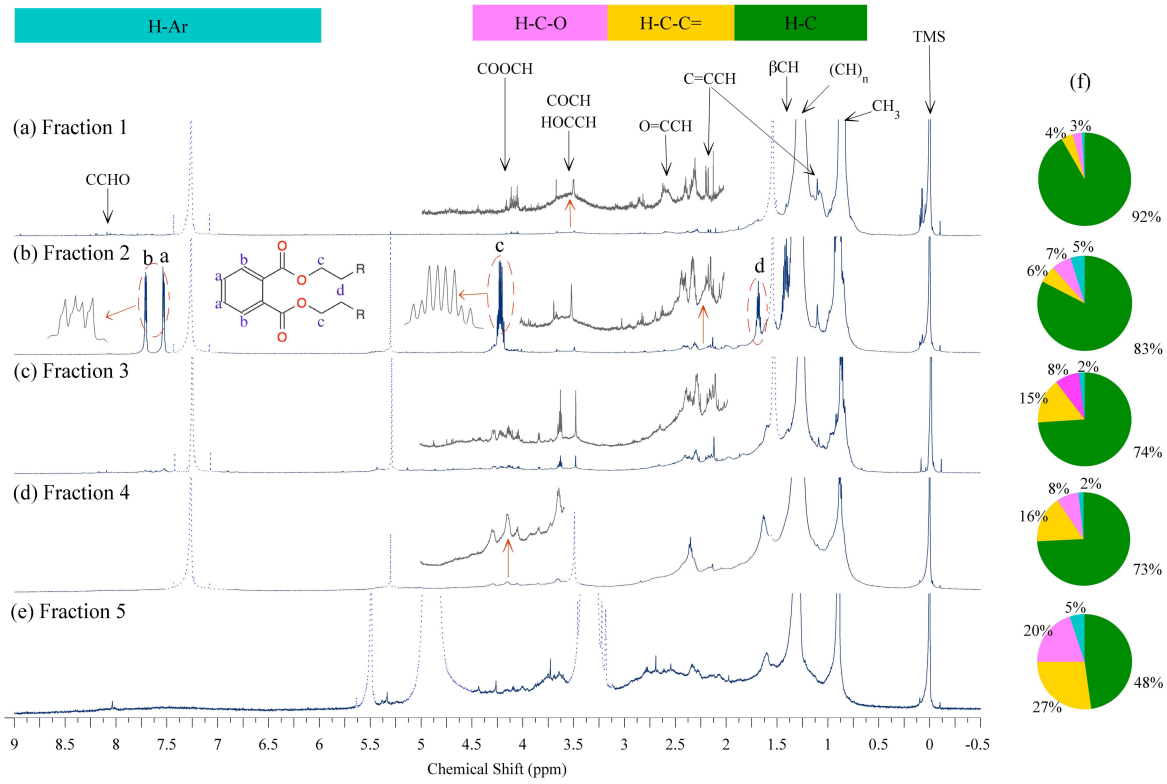

Figure 5.3. (a–e) ^{1}H-NMR spectra of five fractionated organic matter. Because the signals of the organics in the ^{1}H-NMR spectra of fraction F6 were low, the result is not presented. (f) The pie charts represent the mass fractions of the quantified functional groups in respective fractions.

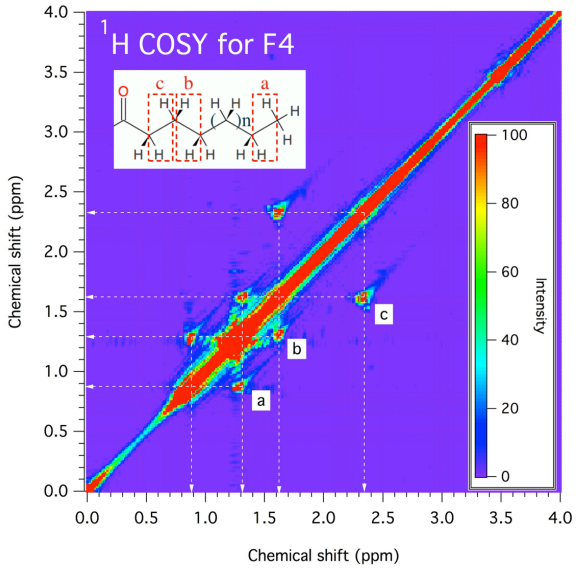

Figure 5.4. The ^{1}H-^{1}H correlation spectra (COSY) of the organic matter in fraction F4.

5.4 HR-AMS characteristics of various organic fractions

The HR-AMS spectra provide the bulk chemical structural characteristics of complex organic matter in aerosols, e.g., element ratios, including those not identified by FT-IR and ^{1}H-NMR analysis. Figure 5.5b shows the HR-AMS spectra obtained at the standard AMS operation temperature of ~600˚C. Based on the high-resolution analysis (m/z <130) of the HR-AMS spectra for fractions F1, F2, F3, F4, F5 and F6, their respective O/C ratios were determined to be on average 0.01, 0.06, 0.13, 0.20, 0.69 and 0.79, respectively.

The ions in the mass spectra of non- and low-polar fractions F1 to F4 were primarily $C_xH_y^+$, which are presumably attributed to aliphatic hydrocarbon structures. The $C_xH_y^+$ ions accounted for an average of 97%, 82%, 63% and 55% of the total mass of fractions F1, F2, F3 and F4, respectively. Conversely, the ions of $C_xH_yO_z^+$, CO_2^+, CO^+ and $H_yO_z^+$ in the mass spectra of medium-polar fractions F5 and F6 accounted for more than 70% of the total signals, indicating a large abundance of oxygenated functional groups. The CO_2^+ ion generally originates from acids and esters in the HR-AMS spectra [*Canagaratna et al*., 2015]. The high relative intensity of CO_2^+ in the HR-AMS spectra of fractions F5 and F6 (on average 20% and 25%, respectively) suggests that carboxylic acids and/or carboxylate esters are abundant in the fractions. Because the carboxylic acid group was not found abundantly in F5 by the FT-IR analysis, a large fraction of CO_2^+ signals form F5 may have originated from carboxylate esters and other oxygenated compounds such as organic hydroperoxides [*Lim and Turpin*, 2015].

Nitrogen-containing ions $C_xH_yO_zN_m^+$, $C_xH_yN_m^+$ and $N_mO_z^+$ were observed in the HR-AMS spectra of the extracts. The $C_xH_yN_m^+$ ions, attributed to amines, accounted for on average <0.1%, 0.1%, 0.2%, 0.7%, 2.2%, and 3.2% of the ions from organics in the mass spectra of fractions F1, F2, F3, F4, F5 and F6, respectively, showing the increase with the increase in the O/C of the

extracted organics. Furthermore, the ratios of NO^+/NO_2^+ in the HR-AMS spectra of the fractionated organic matter (5.1 ± 0.4) were obviously higher than those of NH_4NO_3 (2.4 ± 0.2), suggesting the presence of organic nitrates [*Farmer et al*., 2010; *Hao et al*., 2013]. The percentage of ions from organic nitrates was highest in the case of F3 (mean: 4%); this result agrees with that from the FT-IR spectra.

Specific molecules of PAEs and PAHs in the extract were investigated based on the HR-AMS spectra. High-resolution analysis of the mass spectra for F2 showed the high signal intensities of the $C_7H_4O^+$ (m/z 104), $C_8H_5O_3^+$ (m/z 149), $C_8H_6O_3^+$ (m/z 150) and $C_8H_7O_4^+$ (m/z 167) ions. These ions in the EI mass spectra are generally attributed to PAEs [*Wu et al*., 2012]. The prominent fragment ion of $C_{16}H_{23}O_4^+$ from bis(2-ethylhexyl) phthalate (DEHP) was found, which should have contributed, at least in part, to the signals at m/z 279. The result indicates that DEHP, which were previously detected as the predominant PAE in the atmospheric environment [*Net et al*., 2015], may have been abundant in F2. Furthermore, the possible fragment ions of PAHs in fractionated organic matter were investigated with a minor modification of the fragment table of organics and PAHs in the *m/z* range of 198–479 after Dzepina et al. [2007] PAH marker signals, including those at m/z 202, 215, 239, 252, and 276, were separated from the HR-AMS spectra of fractions F1 to F4 (Figure 5.6). The ion-formula analysis indicated that at least a part of these signals was attributed to the $C_{16}H_{10}^+$, $C_{17}H_{11}^+$, $C_{19}H_{12}^+$, $C_{20}H_{12}^+$ and $C_{22}H_{12}^+$ ions (Figure 5.7). The analysis showed that PAHs accounted for on average 0.26%, 0.13%, 0.14% and 0.11% of the masses of fractions F1, F2, F3 and F4, respectively. The PAHs ions in the mass spectra for fractions F3 and F4 likely originated from oxygenated-PAHs or nitro-PAHs because the organics in the fractions must have a certain degree of polarity [*Musa Bandowe et al*., 2014].

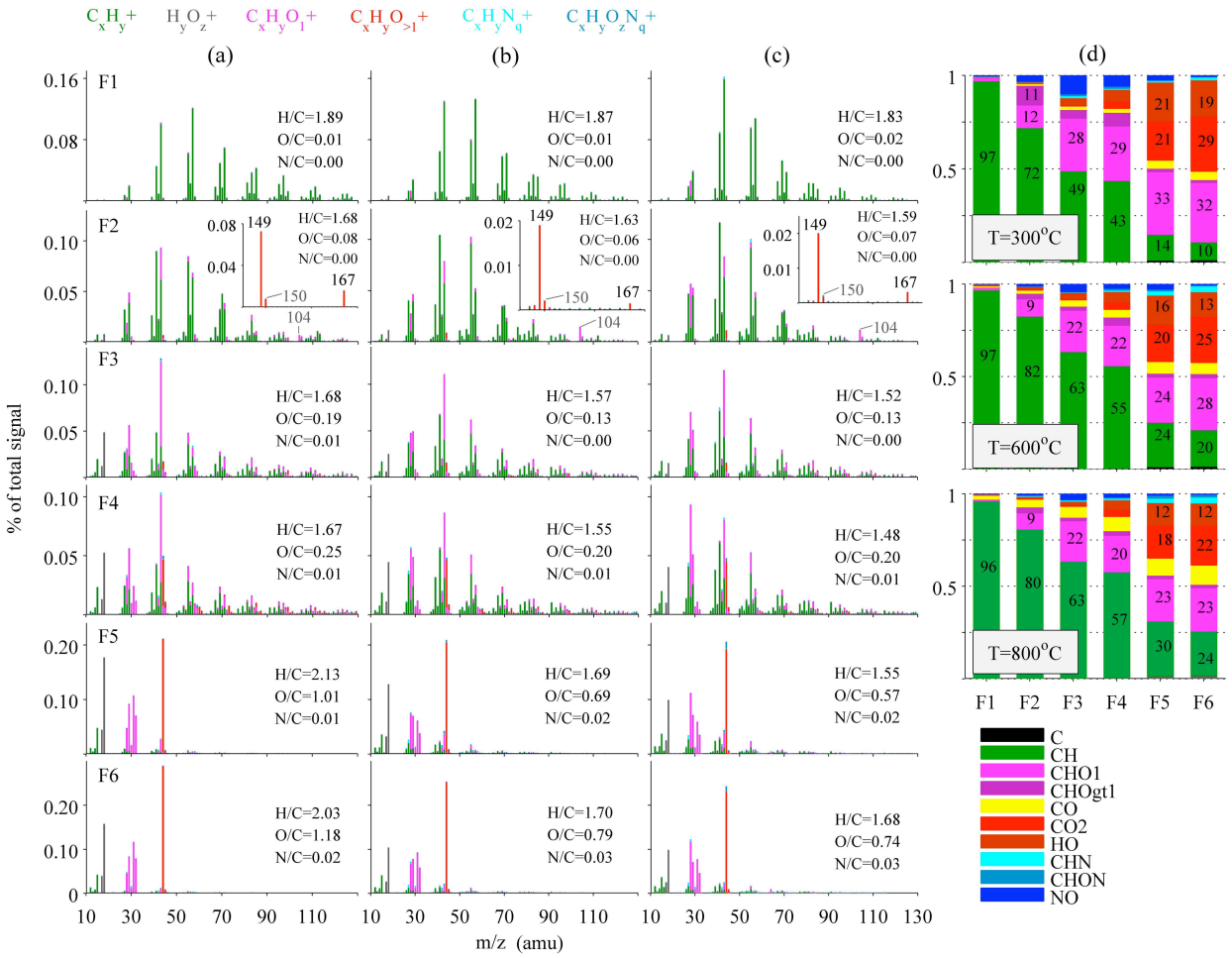

Figure 5.5. (a–c) The average HR-AMS spectra collected in the W-mode for fractionated organic matter at vaporizer temperature of (a) ~300˚C, (b) 600˚C, and (c) 800˚C. (d) Mass fractions of ion groups in the HR-AMS spectra.

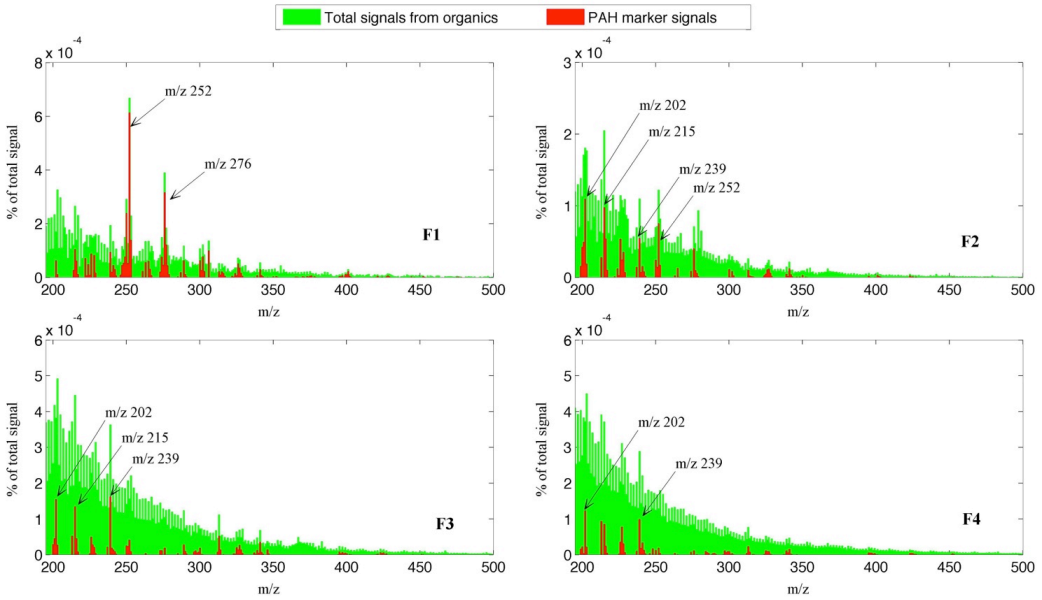

Figure 5.6. The PAH marker signals in the HR-AMS spectra of fractions F1–F4.

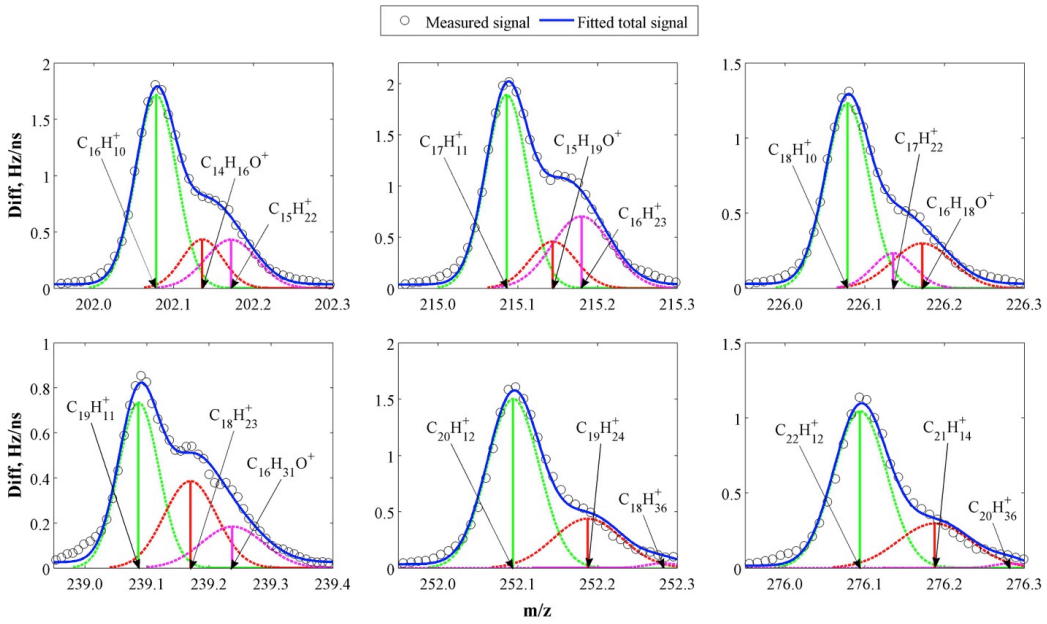

Figure 5.7. High-resolution analysis of possible PAH marker signals in the HR-AMS spectra of fractions F1 and F2. The $C_{16}H_{10}^+$, $C_{17}H_{11}^+$, $C_{18}H_{12}^+$, $C_{19}H_{12}^+$, $C_{20}H_{12}^+$ and $C_{22}H_{12}^+$ ions in the figure are associated with PAH molecules.

5.5 Light-absorption characteristics of extracts and their relationship to the chemical structures

The fractionation method in this study determined important light-absorption organic groups in WISOM. Figure 5.8 presents the average UV-visible spectra of different aerosol extracts and the relative contributions to the total light absorption by the extracted organics from the weekly samples. This result indicated that the relative contributions of light absorption were markedly different between different extracts and wavelengths. In the wavelength range of 250–400 nm (UV region), the light absorption by organics was dominated by that from the water-soluble fraction, which accounted for an average of 66% of total light absorption of the extracts at 300 nm. By contrast, the light absorption in the wavelength range of 400–600 nm (visible region) was primarily contributed by extracted water-insoluble fractions F1–F6, the total of which accounted for on average 64% of the light absorption by the extracts at 600 nm. Hence, the WISOM accounted for a large part of total light absorption by organics, and the contribution was higher than that of water-soluble organics in the visible region. This finding is in line with a previous report by *Zhang et al*. [2013]: The water-insoluble fraction of OC in methanol extracts was on average 4.2 times more light absorbing than WSOC in ambient aerosols in Los Angeles.

The light absorption of WISOM was dominated by the more polar fractions F4, F5 and F6. The sum of the light absorption by the three components in the visible region (≥400 nm) on average accounted for more than 90% of the light absorption by fractions F1–F6. In particular, on average 62% of the light absorption by WISOM was attributed to F4. Furthermore, the MACs of fractions F4, F5 and F6 at 365 nm (on average 0.77, 2.3 and 1.3 $m^2\ g^{-1}$, respectively) were much higher than those of fractions F1–F3 and of water-soluble extracts (<0.4 $m^2\ g^{-1}$). The results show that low- and medium-polar fractions F4, F5 and F6 were strong light-absorbing

substances that were comparable to the BrC in BBOA reported from previous studies (on average 2.2 m^2 g^{-1} at 365 nm) [*Yang et al*., 2009; *Chen and Bond*, 2010]. The high MAC for those low- and medium-polar fractions were most likely associated with the aromaticity and polar functional groups containing O and/or N in the organic matter, because these functional groups were more abundant in fractions F4, F5 and F6 than in other extracts, as shown by the structural characteristics identified by the FT-IR, ^{1}H-NMR and HR-AMS analysis (Table 5.2). The heteroatomic (O and/or N) and aromatic groups in molecules can form conjugated systems such as quinone and nitrophenol structures and lower excitation energies of electrons in the molecules, leading to light absorption in the visible range. In particular, F5 had the highest MAC value. This result was likely due to the large contribution by phenolic compounds and quinones, the presence of which is suggested from the FT-IR spectra, given that they are considered an important BrC in atmospheric particulates [*Cory and McKnight*, 2005; *Chang and Thompson*, 2010; *Mladenov et al*., 2011]. Note that large contributions of WISOM and their sub-fractions F4 and F5 to the light-absorption in the visible region were further confirmed by the analysis of a set of two-day samples (Figure 5.9). This result suggests that their contributions are generally large, at least in the studied urban area.

Light absorption by the studied organics may also be caused by charge transfer (CT) interactions. In the case of WSM in Athens, USA, CT complexes that formed from interactions between alcohol and carbonyl moieties was found to account for approximately 50% of the absorption (300–600 nm) based on reduction experiments using $NaBH_4$ [*Phillips and Smith*, 2014 and 2015]. Similar experiments were performed for F4 from two samples, resulting in 20%–60% decreases in the light absorption in the wavelength range of 300–600 nm. Our result suggests 20%–60% contributions of the CT complexes to light absorption by F4 because the decrease of the absorption was likely caused by the loss of CT complexes as a result of the

reduction of the electron acceptor carbonyl groups. As seen in Figure 5.2k, fraction F4 contained abundant aromatic and oxygenated groups (primarily C=O and C-OH); the CT complexes may have formed between carbonyl groups as electron acceptors and other groups, e.g., phenolic and aliphatic hydroxyl groups as electron donors in the molecules. The CT complexes in F4 may have been associated with high molecular weights and branched structures of organics. Abundant branched structures in F4 were identified from the FT-IR spectra, and the ESI mass spectra of fraction F4 showed that the number-average molecular weight of organic compounds with the m/z in a range of 50–1000 was higher (464–516 Da) than that in WSOM (316–372 Da) (Figure 5.10). The branched and large molecular structures of organics in F4 with aromatic and oxygenated groups may have led to the abundant presence of CT complexes and may have contributed to the light absorption in the visible range.

Table 5.2. Concentrations of organic carbons (mean ± SD) and the marker signals in the FT-IR, ^{1}H-NMR and HR-AMS spectra and suggested major organic compounds in different water-insoluble organic fractions.

Fractions	Concentration (ng-C m^{-3})	Marker signals in different analysis			Major organic compounds
		FT-IR	^{1}H-NMR	HR-AMS	
F1	52 ± 13	C-H	H-C	$C_xH_y^+$; PAHs ions $C_{20}H_{12}^+$ and $C_{22}H_{12}^+$	Aliphatic hydrocarbons (contain PAHs)
F2	85 ± 12	C=O; C-O; C=C in Ar; Ar–H	PAE markers: δH ≈ 7.71, 7.53, 4.22 and 1.69 ppm	PAE ions: $C_7H_4O^+$, $C_8H_5O_3^+$, $C_8H_6O_3^+$; $C_8H_7O_4^+$; $C_{16}H_{23}O_4^+$	Phthalic acid esters
F3	101 ± 23	C–H; C–ONO_2	H-C	$N_xH_y^+$; $C_xH_y^+$	Aliphatic nitrates and esters
F4	284 ± 12	C–OH; C=O; C=C in Ar; C–ONO_2 or C-NH_2	H–C–C=O; H–C–O	$C_xH_yO_z^+$; $C_xH_yN_m^+$; $C_xH_yO_zN_m^+$	Esters, alcohols, ethers and ketones (with aromatic and N-containing groups)
F5	35 ± 2	C–OH; C=O and C=C in Ar	H–Ar; H–C–C=O; H–C–O	$C_xH_yO_z^+$; $C_xH_yN_m^+$	Phenols and quinones (with N-containing groups)
F6	11 ± 1	- - -	- - -	CO_2^+; $C_xH_yO_z^+$; $C_xH_yN_m^+$	Carboxylic acids and carboxylate esters (with N-containing groups)

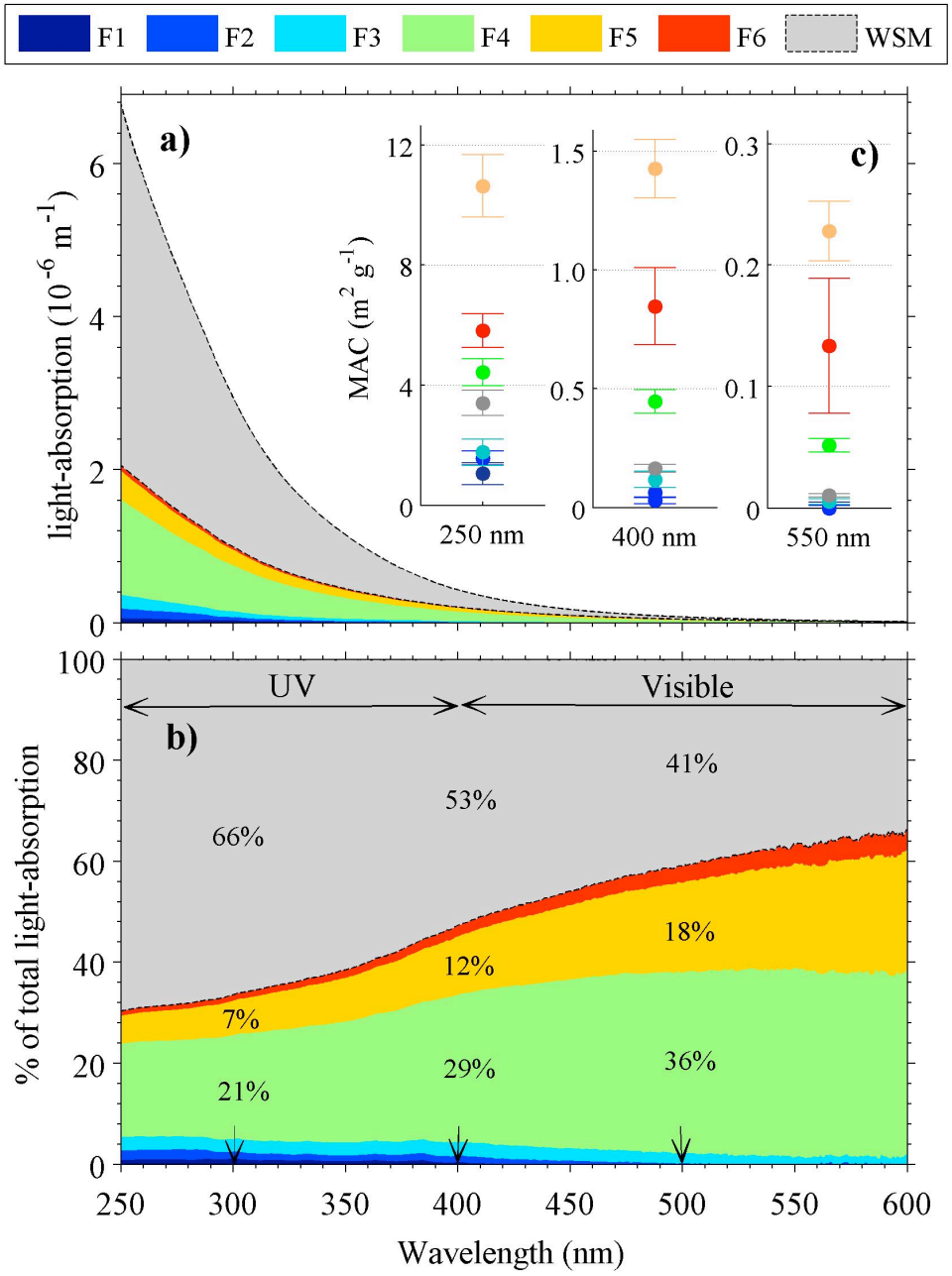

Figure 5.8. (a) Average light absorption and (b) relative contributions of aerosol extracts to total light absorption. (c) Mass absorption coefficient (MAC) of aerosol extracts at wavelengths of 250, 400 and 550 nm. The error bars indicate SD.

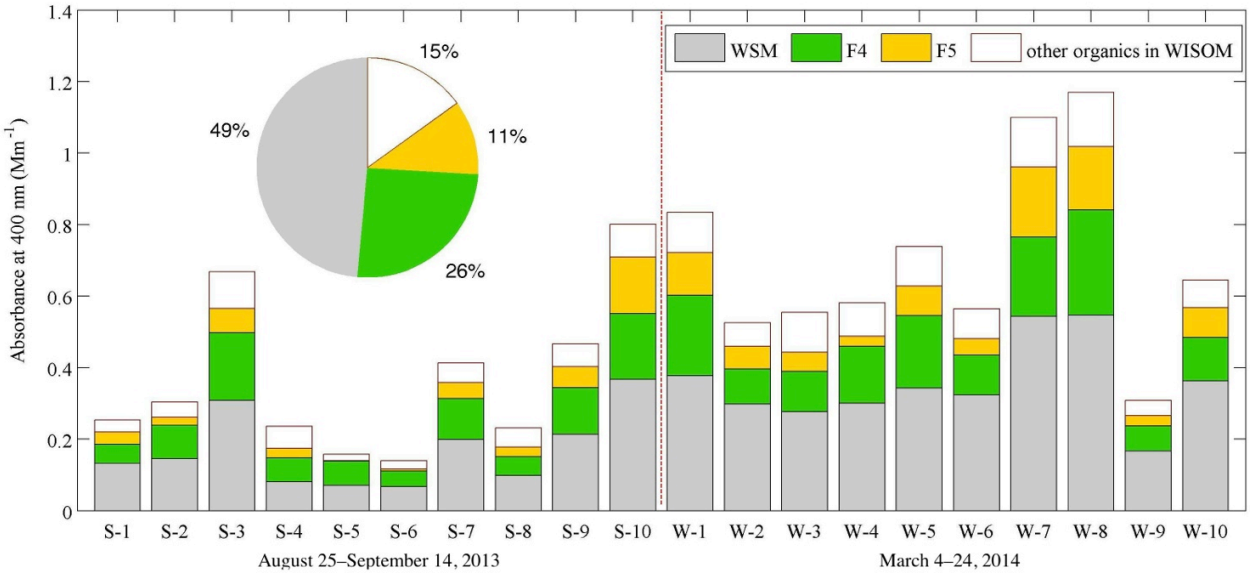

Figure 5.9. Light absorbance of WSM, fractions F4 and F5 and other water-insoluble organics at 400 nm for a set of two-day samples. The absorbance of the other organics in WISOM was calculated by subtracting the absorbance by F4 and F5 from the total absorbance by WISOM. The pie charts in the figure represent the proportion of the mean absorbance of fractionated organic matter (WSM, F4, F5 and the other organics in WISOM).

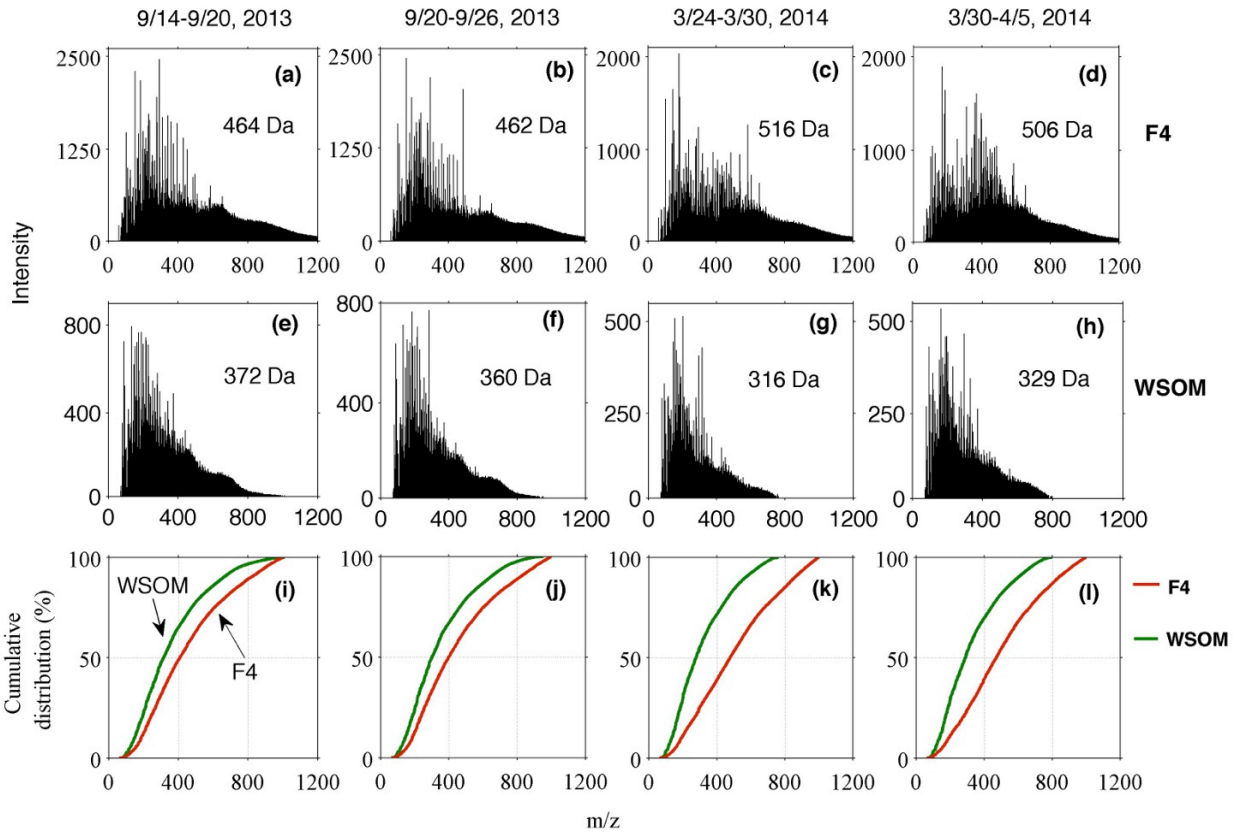

Figure 5.10. (a-h) ESI-QTOF mass spectra of fraction (a-d) F4 and (e-h) WSOM acquired at collision cell RF of 120 Vpp. The number-average molecular weights in panels (a-h) were estimated from the intensity of ions in the range of m/z 50–1000 according to equation (1). (i-l) The cumulative distributions of the mass spectrum signals versus the m/z in the range of 50–1000 for organic fractions F4 and WSOM.

6 Characterization of chromophoric water-soluble organic matter (CWSOM) in urban, forest and marine submicron aerosols

6.1 EEMs and PARAFAC components

To identify and quantify the underlying chemical components of chromophores in aerosols, the PARAFAC model was applied to separate EEMs of independently varying fluorescence components. Figure 6.1 presents the EEM profiles of the three- (3CM-C1~3) and seven- (7CM-C1~7) component PARAFAC solutions. The profiles of 3CM-C1~3 are similar to those identified from water and alkaline soluble matter in urban aerosols in Granada, Spain and in Aveiro, Portugal [*Mladenov et al*., 2011; *Matos et al*., 2015]. Based on a comparison with three fluorescence components defined for terrestrial and oceanic organic matter by *Yu et al*. [2015], the fluorescent components of 3CM-C1, -C2 and -C3 are named HULIS-1, HULIS-2 and PLOM, respectively, in this study. Note that the origins and chemical structures of HULIS and PLOM chromophores studied are not necessarily similar to those of the chromophores with same names in terrestrial and oceanic organic matter. The origins and chemical structures of the chromophores in atmospheric aerosols are discussed below.

The seven-component PARAFAC solution provides more detailed information on the chromophores. Through comparison of the emission wavelengths with the maximum fluorescence of the three-component PARAFAC solution and correlation analysis of the relative abundance of the three and seven components, 7CM-C1 and 7CM-C3 are assigned to HULIS-1, 7CM-C2, 7CM-C4 and 7CM-C5 are assigned to HULIS-2, and 7CM-C6 and 7CM-C7 are assigned to PLOM. Among the seven components, 7CM-C1, 7CM-C3 and 7CM-C5 have peaks at emission wavelengths of >400 nm (Figure 6.1); they are thought to originate from conjugated systems, e.g., via quinonoid n-π^* transition [*Cory et al*., 2005]. This claim is supported by the

result that the emission wavelength of 7CM-C3 (~470 nm) was similar to that of the quinone-like component identified in aerosol WSOM in Granada, Spain [*Mladenov et al*., 2011]. Based on the definition of fluorescent components of terrestrial and oceanic organic matter, 7CM-C6 and 7CM-C7 can be assigned to tryptophan-like and tyrosine-like components, respectively [*Murphy et al*., 2013; *Yu et al*., 2015]. However, non-nitrogen-containing species may account for a major portion of the chromophores of 7CM-C6 and 7CM-C7 in atmospheric aerosols, as discussed below.

The relative intensities of different fluorescent components in different types of aerosols were highly variable depending on the sampling site and period, as shown in Figure 6.2a. This result suggests that the chemical composition of CWSOM differs markedly from sample to sample. HULIS-1 (7CM-C1 and –C3) was the substance with most intense fluorescence in all samples, and, on average, accounted for 46% of the total fluorescence intensity of all samples. The high mass fractions of HULIS were observed in an area similar to that of the marine aerosol sampling, supporting the particularly intense fluorescence of HULIS-1 in the marine aerosols studied [*Deng et al*., 2014]. The fluorescence of HULIS-2 (7CM-C2, -C4 and –C5) was intense in the case of terrestrial aerosols (urban and forest aerosols) (mean: 47% of the total fluorescence intensity of the extracts), particularly in forest aerosols (mean: 51%). Conversely, the fluorescence of HULIS-2 in marine aerosols was weak (mean: 23%). This result suggests that HULIS-2 primarily had a terrestrial origin. The marine aerosols were enriched in the PLOM components (7CM-C6 and –C7, mean: 19%), which should be attributed to marine biological materials [*Fu et al*., 2015; *Yu et al*., 2015]. The fluorescent components assigned to PLOM were also present in the urban aerosols, among which the fluorescence of tryptophan-like substances (7CM-C6) was the strongest. Accordingly, these aerosols differ from the marine aerosols, in which the relative contents of tryptophan-like and tyrosine-like components (7CM-C7) were

nearly equal. This result indicates that PLOM in urban and marine aerosols can be attributed to different chemical structures and origins.

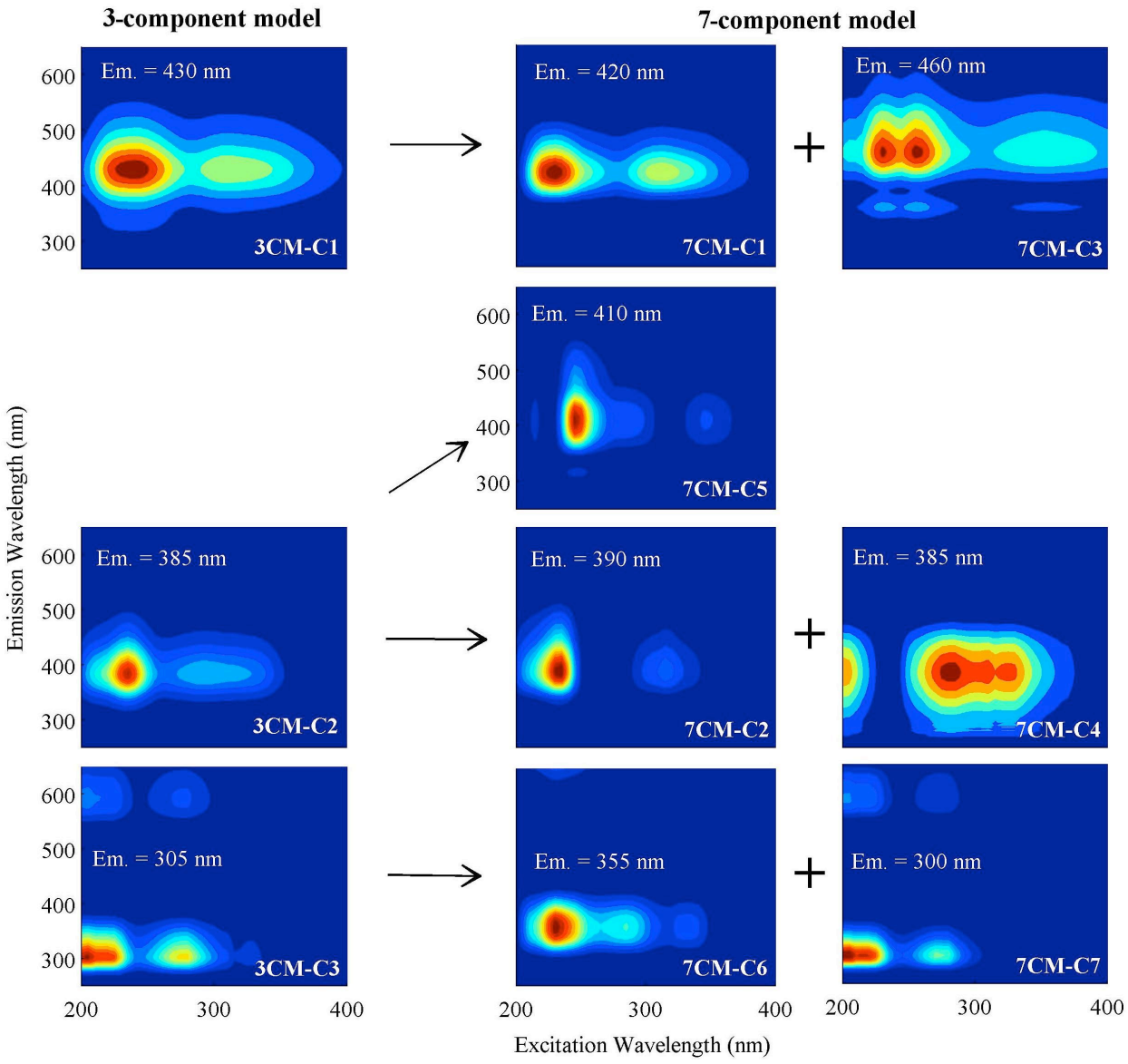

Figure 6.1. EEM components identified by the three- and seven-component solutions of the PARAFAC model for the sixty-three water extracts of the urban, forest and marine $PM_{0.95}$. The three-component PARAFAC solutions of 3CM-C1, -C2 and -C3 were named as HULIS-1, -2 and PLOM, respectively. The arrows represent combinations of three- and seven-component solutions with high positive correlations (r>0.5, p<0.01).

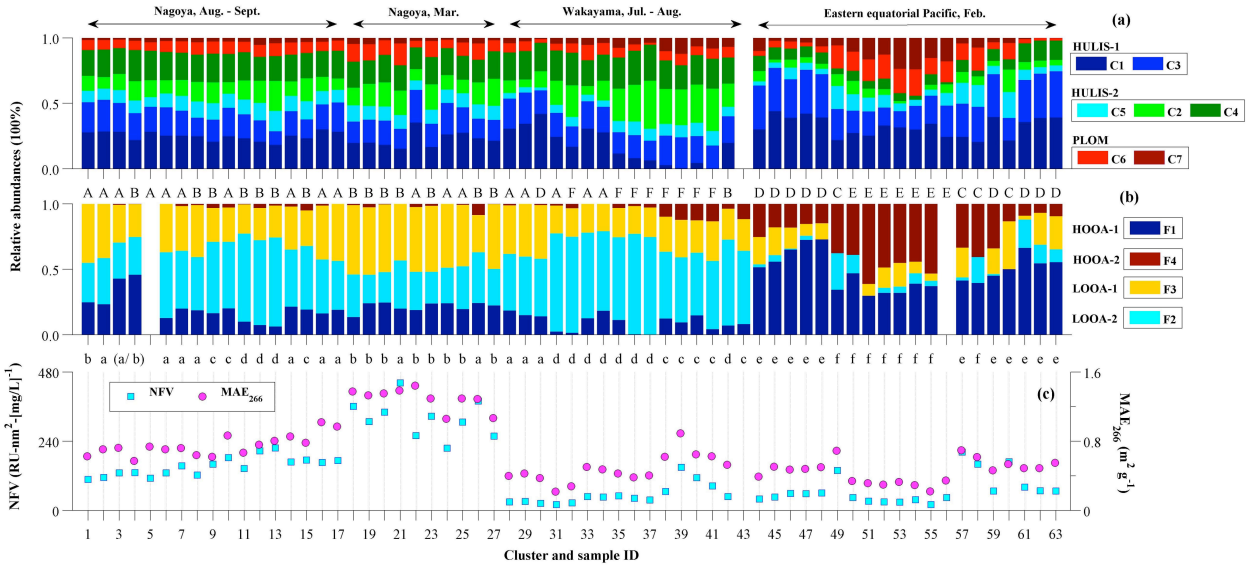

Figure 6.2. (a and b) Relative abundances of (a) the PARAFAC derived components (7CM-C1 and -C3 are associated with HULIS-1; 7CM-C2, -C4 and -C5 are associated with HULIS-2; 7CM-C6 and -C7 are associated with PLOM) and (b) NMF derived fractions (HOOA-1: F1; HOOA-2: F4; LOOA-1: F3; LOOA-2: F2) of WSOM of different samples, as well as different clusters (label on the horizontal axis: *A–F* and *a–f*) classified by hierarchical cluster analysis. (c) The normalized fluorescence volume (NFV, normalized to a WSOC concentration of 1 mg L^{-1}) and the mass absorption efficiency at 266 nm (MAE_{266}) for different samples. The sample IDs correspond to different types of aerosols as follows: ID 1-17: the urban aerosols in August and September; ID 18-27: the urban aerosols in March; ID 28-43: the forest aerosols; ID 44-63: the marine aerosols.

6.2 HR-AMS spectra and the NMF factors

The chemical characteristics of WSOM in aerosols were obtained on the basis of the HR-AMS spectra of the extracts in various samples. Four factors were determined from the HR-AMS spectra of the NMF model; their mass spectra and relative abundances in different types of

aerosols are presented in Figures 6.3 and 6.2b, respectively. Based on the degrees of oxidation (O/C ratio) of organics, four factors were identified as highly oxygenated organic aerosols (HOOA-1 and HOOA-2), and low oxygenated organic aerosols (LOOA-1 and LOOA-2) as follows.

The HOOA-1 factor has a high O/C ratio (1.67) and a low H/C ratio (1.1). Approximately half of the total HOOA-1 signal was contributed from CO_2^+ ions, suggesting a large fraction of carboxylic acids in HOOA-1 [*Takegawa et al*., 2007; *Canagaratna et al*., 2015;]. The mass fraction of HOOA-1 in the marine aerosols (mean: 48%) was obviously higher than those in the urban (mean: 20%) and forest aerosols (mean: 9%), indicating that WSOM in marine aerosols was dominated by more processed oxygenated products.

The HOOA-2 factor contains abundant CS ions (16%), mainly including $CHSO^+$ (m/z 61), CH_2SO^+ (m/z 62), $CH_2SO_2^+$ (m/z 78), $CH_3SO_2^+$ (m/z 79) and $CH_4SO_3^+$ (m/z 96) ions (Figure 6.3). Among these ions, the most abundant CS ion in the mass spectrum of HOOA-2 is $CH_2SO_2^+$, which likely originated from methanesulfonic acid (CH_3SO_3H, MSA) [*Zorn et al*., 2008; *Huang et al*., 2015]. HOOA-2 contributes largely to the WSOM of marine aerosols (mean: 30%) and slightly to the WSOM of the urban (mean: 2%) and forest samples (mean: 5%). The relative abundance of HOOA-2 is particularly high in those marine samples collected over the eastern tropical Pacific Ocean in the Southern Hemisphere (mean: 46%), which is consistent with the high mass concentration ratios of MSA to WSOC [*Miyazaki et al*., 2016]. The above results suggest that HOOA-2 should be represented by the WSOM of marine aerosols. The characteristics of the low abundances of $C_xH_yO_z^+$ (10%) ions and high abundances of $C_xO_y^+$ (31%) and $C_xH_y^+$ (31%) ions in HOOA-2 are different from those of the PMF-derived marine organic aerosols in Paris, France ($C_xH_yO_z^+$, $C_xO_y^+$ and $C_xH_y^+$ were 41%, 17% and 32%, respectively) (URL: http://cires.colorado.edu/jimenez-group/HRAMSsd/) [*Crippa et al*., 2013].

This difference may be because marine aerosols were enriched in water-insoluble organic matter (WISOM), which may consist of hydrophobic sugar-like compounds [*Facchini et al*., 2008]. In fact, the WSOC/TC ratio was low (mean: 0.4), supporting the high abundance of WISOM in the marine aerosols [*Miyazaki et al*., 2016].

The LOOA-1 factor was dominated by $C_xH_y^+$ (38%) and $C_xH_yO_z^+$ (24%) ion groups. By contrast, CO_2^+ was very low in the LOOA-1 spectra, but abundant CO^+ (15%) was observed. This result suggests that LOOA-1 is associated with alcohols and ketones/aldehydes, and not with carboxylic acids and carboxylate esters [*Canagaratna et al*., 2015]. One of the remarkable characteristics of LOOA-1 in comparison with other factors is the higher mass fraction of the $C_xH_yN_q^+$ ion-group (6%), suggesting that nitrogen-containing compounds were abundant. The relative abundances of LOOA-1 in those urban aerosol samples, particularly in late winter and early spring samples (mean: 47%), were obviously higher than those in the forest and marine aerosol samples (Figure 6.2b). Hence, LOOA-1 is probably anthropogenic.

The mass spectrum of the LOOA-2 is largely contributed by the $C_xH_y^+$ (44%) and $C_xH_yO_z^+$ (31%) ion-groups and is characterized by the higher signal of $C_2H_3O^+$ (11%). The profile of the LOOA-2 factor was similar to that of the factor of semi-volatile oxygenated organic aerosols (SV-OOA), determined on the basis of the PMF analysis of the on-line HR-AMS data at the WFRS forest site, which was interpreted as locally formed BSOA [*Han et al*., 2014]. Furthermore, Figure 6.2b shows that LOOA-2 accounted for a large mass fraction of WSOM in forest aerosols (mean: 59%), which is higher than in the fractions of other aerosols. These results suggest that LOOA-2 should be represented by the water-soluble part of BSOA. The loadings of LOOA-2 in the urban aerosols were also high (mean: 39%), particularly in the case of summer aerosols (mean: 46%). Hence, BSOA must have also been abundant in Nagoya.

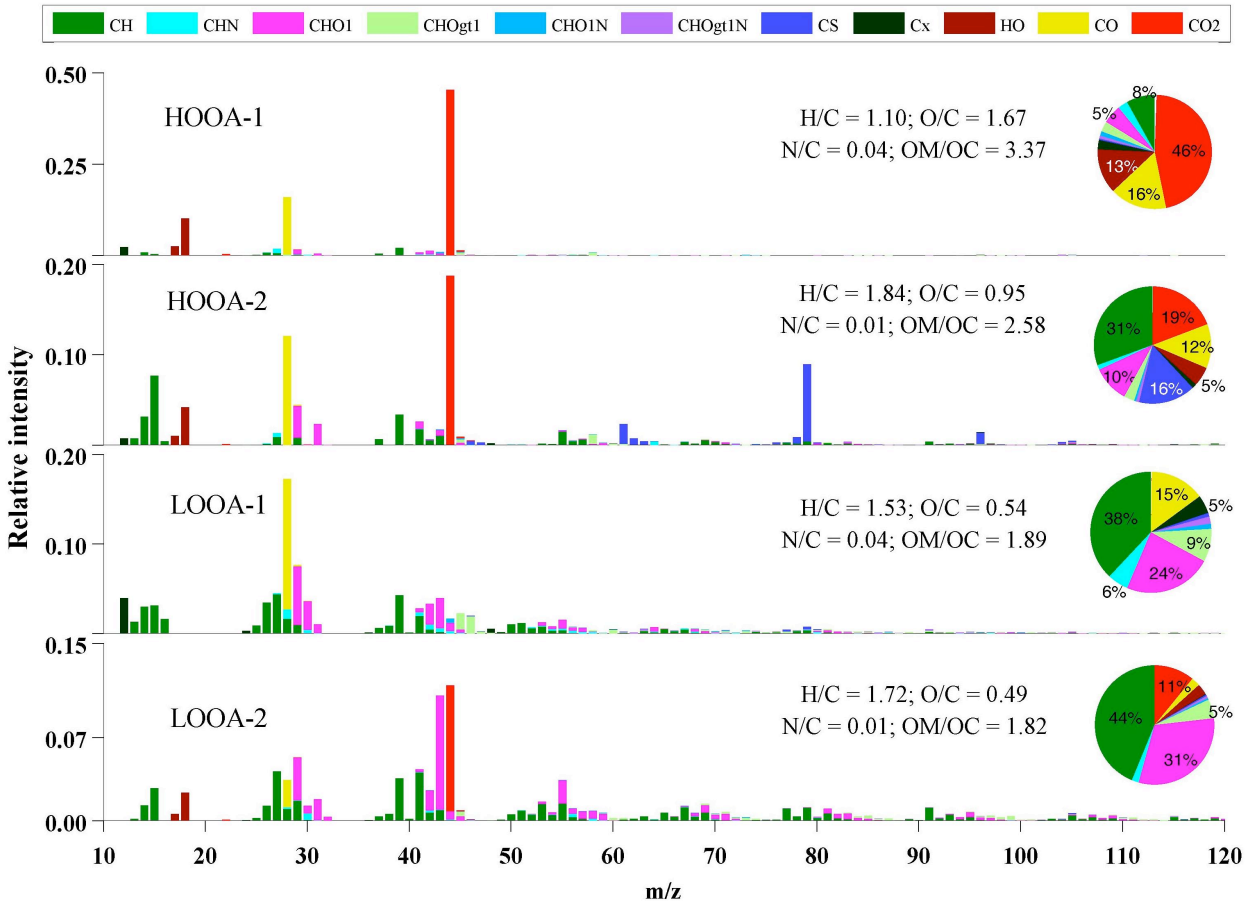

Figure 6.3. The mass spectra, elemental compositions, and relative intensities of ion-groups of the four components from the NMF analysis (HOOA-1, HOOA-2, LOOA-1 and LOOA-2) of the WSOM fractions.

6.3 Optical properties and chemical composition of WSOM versus the sample clusters

The optical properties and chemical composition of WSOM in aerosols varied from sample to sample. The forest and marine aerosols were unlikely rich in water-soluble chromophores. As Figure 6.2c presents, the values of MAE_{266} and NFV for the urban aerosols, particularly in late winter and early spring samples, were obviously higher than those for the forest and marine aerosols. This result is consistent with those reported in previous studies; the MAEs of WSOM in aerosols in the cities of Beijing and Los Angeles were obviously higher than the MAEs in

Atlanta and Kpuszta, where biogenic aerosols dominated [*Yang et al*., 2009; *Cheng et al*., 2011; *Zhang et al*., 2011; *Utry et al*., 2013;]. The MAE_{266} and NFV values were positively correlated with $C_2H_4O_2^+$ (Figure 6.4), an ion associated with organics from biomass burning organic aerosol (BBOA) [*Lee et al*., 2010]. This result indicates that the enhancement of the MAEs and NFVs in these urban aerosols is probably linked to biomass-burning sources. This result is consistent with the result suggested in section 4.4: the BrC in wintertime aerosols over Nagoya was suggested to be derived from biomass burning, and responsible for the increase of the MAEs and NFVs of both the water soluble- and insoluble organic matter. E_2/E_3 (the ratio of absorbance at 250 to that at 365 nm) in the UV-visible spectra generally relates to the total aromaticity of organics [*Heal and Hammonds*, 2014]. The E_2/E_3 values of the WSOM in late winter and early spring were on average 0.8 times that of the summer values, suggesting relatively high aromaticity in late winter and early spring.

The influences of aerosols from different origins on the optical properties and chemical composition were further analysed based on hierarchical cluster analysis of the samples (Figures 6.5 and 6.6) and backward trajectory analysis of the air masses (Figures 6.7 and 6.8). The results show that different cluster samples exhibit marked differences in terms of the relative abundances of fluorescent components and HR-AMS factors, as well as the trajectories. Clusters *a-f*, classified on the basis of the relative abundances of the HR-AMS factors, show that most of the urban aerosol samples are classified into clusters *a* and *b*. The remarkable difference of the two clusters from the others is that they have high mass fractions of LOOA-1 (mean: 42%). Air masses corresponding to cluster *b* were mainly from the Asian continent (red lines in Figure 6.8a), and have the higher MAE and NFV values. Most of the forest aerosol samples are classified into clusters *c* or *d*, which are characterized with a high mass fraction of LOOA-2 (mean: 60%). The marine aerosol samples are classified into clusters *e* and *f*. The remarkable

difference between cluster *f* and cluster *e* is that the air masses of the former were mainly from the southwest Pacific, and the relative abundance of HOOA-2 is high (mean: 46%).

The clusters of samples determined from the hierarchical cluster analysis on the basis of the relative abundances of the seven fluorescence components were similar to those from the HR-AMS factors. All urban aerosol samples are assigned to cluster *A* or cluster *B*. The difference of cluster *B* from cluster *A* is the relatively low abundance of HULIS-1 (mean: 37%) and high abundance of HULIS-2 (mean: 49%), and the higher MAE and NFV values. The air mass trajectories show that CWSOM in the cluster *B* samples was likely associated with air masses from the Asian continents (red line in Figure 6.8c). Marine aerosol samples are assigned to three clusters, i.e., *C*, *D* and *E*. The remarkable difference of cluster *E* from the others is that it has high abundance of PLOM (mean: 34%). Approximately half of the forest aerosol samples were classified to cluster *F*, which is characterized by the high abundance of HULIS-2 (mean: 52%).

The above results indicate that both the chemical composition and chromophore types are closely related to the origins of organic aerosol components. The correlation analysis between the relative abundances of fluorescence components and HR-AMS factors showed that HULIS-1, HULIS-2 and PLOM were positively correlated to the relative contents of HOOA-1 ($r = 0.66$, $p < 0.001$), LOOA-2 ($r = 0.62$, $p < 0.001$) and HOOA-2 ($r = 0.65$, $p < 0.001$), respectively. The retrieved origins of LOOA-2 and HOOA-2 suggest that HULIS-2 and PLOM were of terrestrial biological origin and marine origin, respectively. HULIS-2 was positively correlated with the signal intensity of $C_2H_4O_2^+$ ions ($r = 0.63$, $p < 0.001$), suggesting that HULIS-2 partly originated from biomass burning.

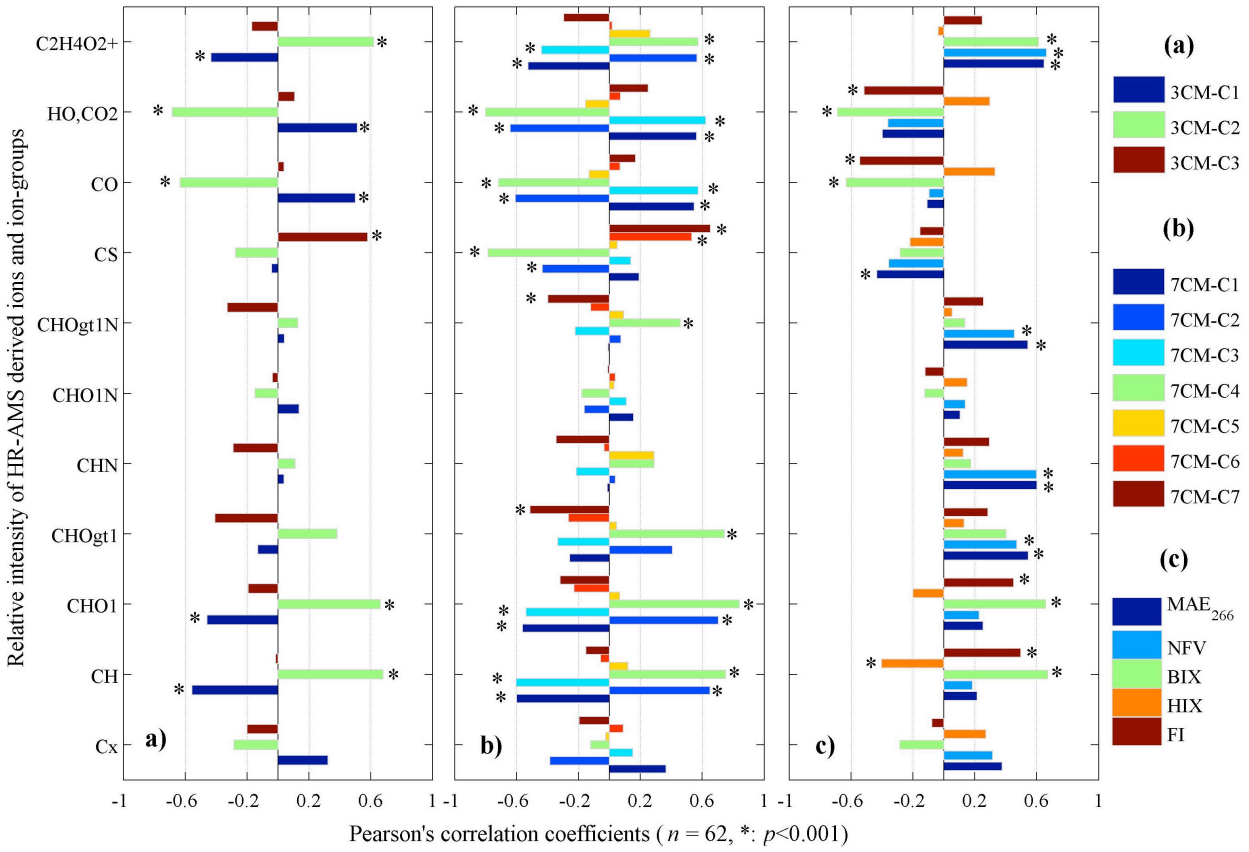

Figure 6.4. Pearson's correlation coefficients and significance levels (p, two-sided t-test) calculated through the correlation analysis of the relative intensities of ion groups in the HR-AMS spectra and relative contents of the (a) 3-component solution of PARAFAC (3CM-C1: HULIS-1; 3CM-C2: HULIS-2; 3CM-C3: PLOM) and (b) 7-component solution of PARAFAC (7CM-C1 and -C3 are associated with HULIS-1; 7CM-C2, -C4 and -C5 are associated with HULIS-2; 7CM-C6 and -C7 are associated with PLOM), and (c) MAE_{266}, NFV, and EEM-derived indices (fluorescence index (FI), biological index (BIX), and humification index (HIX)).

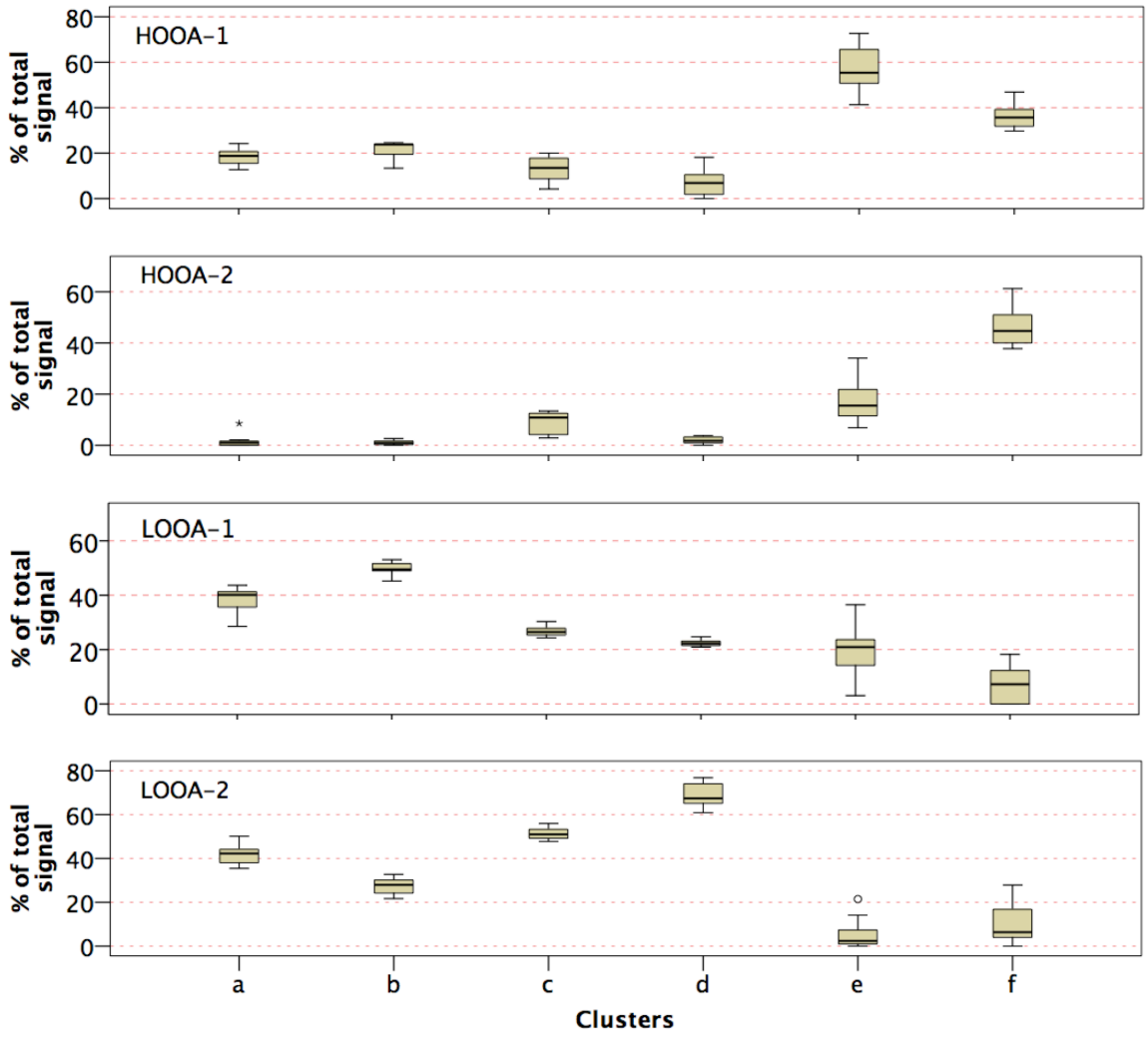

Figure 6.5. The boxplots of the relative contributions of four NMF factors to respective clusters. The boxes and whiskers show the 25th, 50th, and 75th percentiles and the ranges from minimum to maximum, respectively.

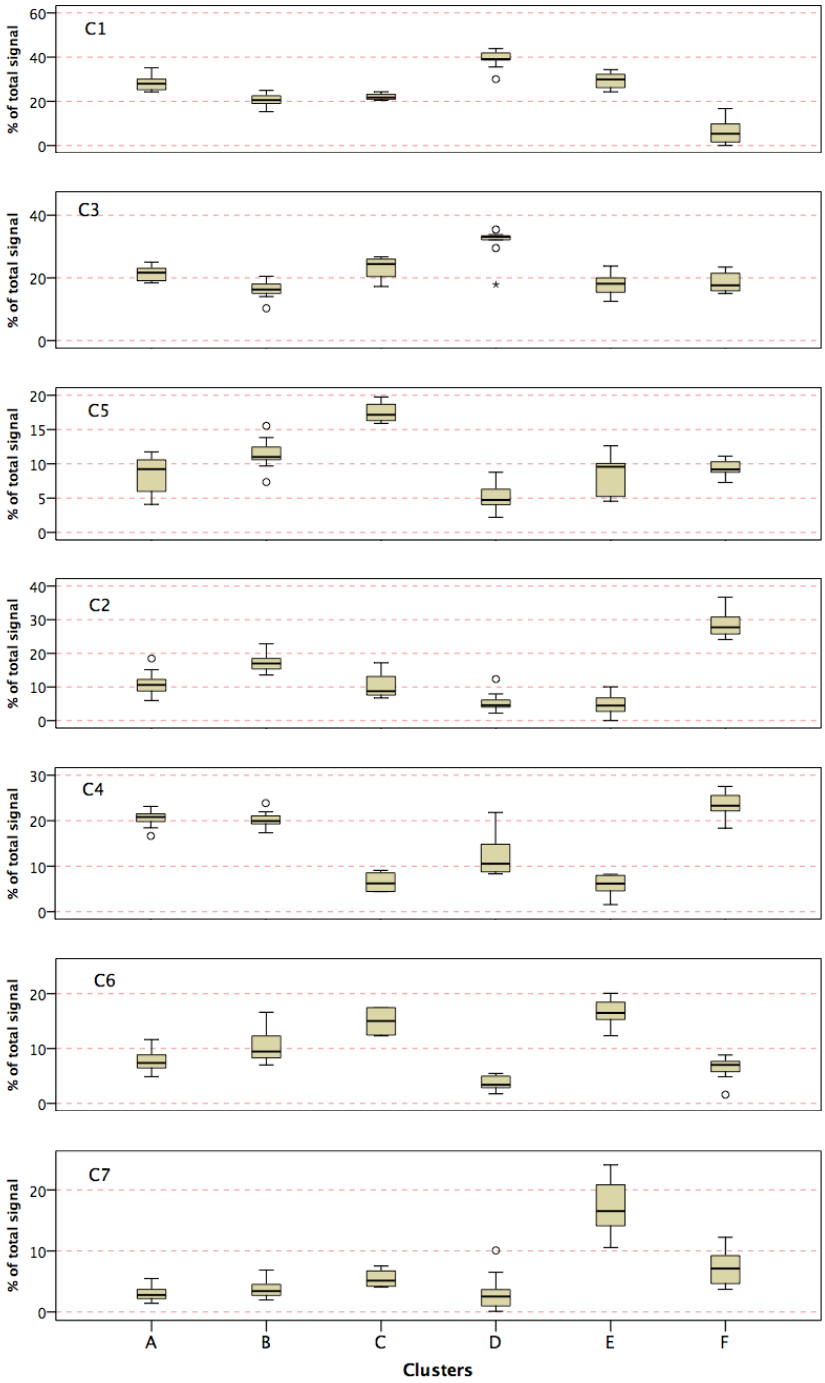

Figure 6.6. Boxplots of the relative contributions of seven PARAFAC components to respective clusters. The boxes and whiskers show the 25th, 50th, and 75th percentiles and the ranges from minimum to maximum, respectively.

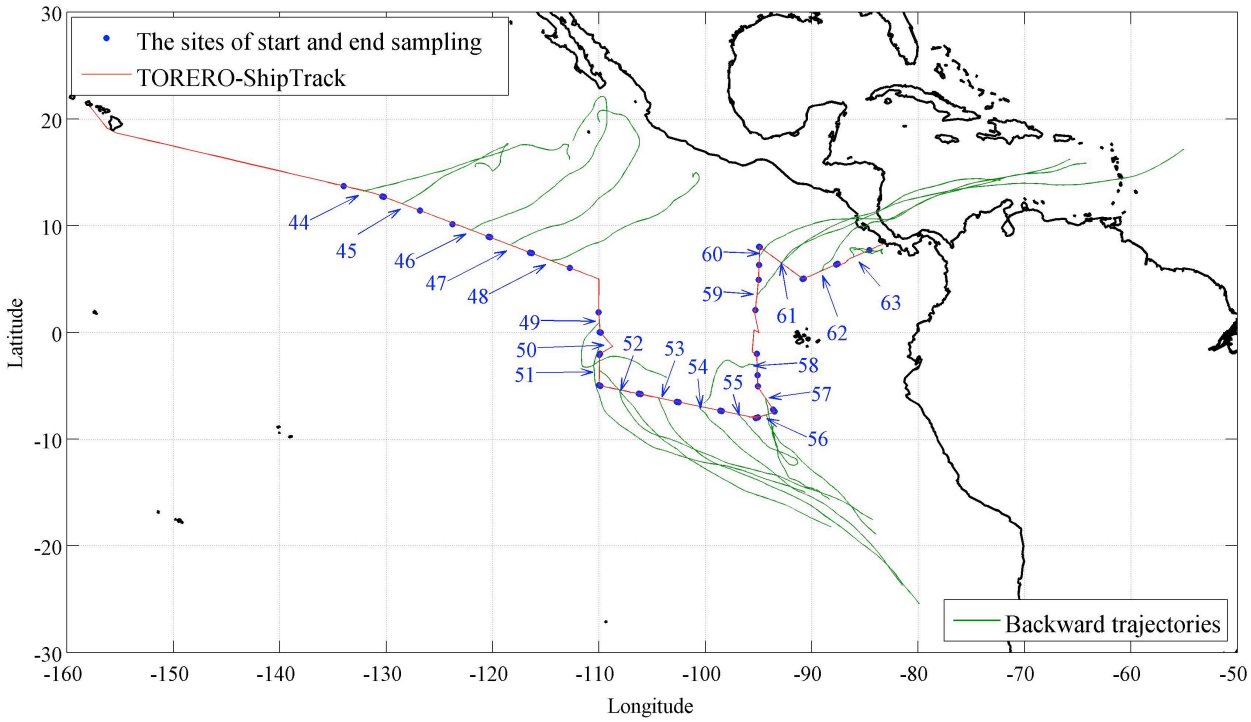

Figure 6.7. The ship tracks and the locations at the start and end of the collection of each sample during the TORERO/KA-12-01 cruise. Ten-day backward trajectories of air masses in the middle time of each sampling period were also plotted (start height: 500m above mean sea level). Analysis on air mass trajectories is also presented by *Coburn et al*. [2014].

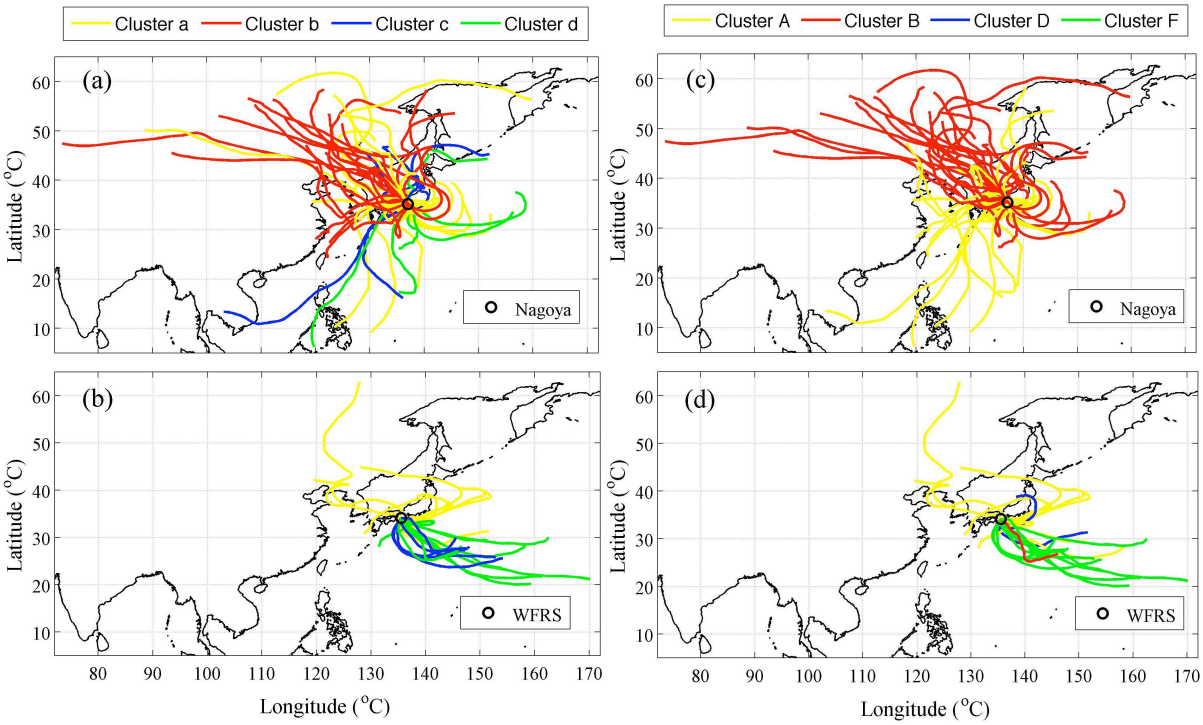

Figure 6.8. Ten-day backward trajectories of air masses for the (a and c) urban and (b and d) forest aerosol samples (start height: 500m above ground level). The colors of the trajectories represent the clusters of samples that correspond to respective trajectories of air masses in the middle time of each sampling period. The clusters are from the hierarchical cluster analysis based on (a and b) the relative contributions of NMF factors and (c and d) the PARAFAC components for different samples.

6.4 Chemical structures of chromophores

The possible chemical structures of water-soluble chromophores in aerosols were suggested from the HR-AMS spectra of water extracts from various samples. The relationship between HR-AMS ions, EEM components and optical indexes are presented in Figure 6.4. The MAE_{266} and NFV values were positively correlated with the relative signal intensity of $C_xH_yO_{>1}^+$, $C_xH_yN_p^+$ and $C_xH_yO_{>1}N_p^+$ ion-groups, suggesting that organic compounds with O and N atoms contributed largely to the total light absorption and fluorescence of water-soluble chromophores in the aerosols. This result is consistent with the result suggested in section 4.4: both the MAE and NFV values were positively correlated with the O- and N-containing ion-groups in the case of HULIS, i.e., the major water-soluble component in aerosols over Nagoya.

Figure 6.4 also shows that the fluorescence components of HULIS-1 and HULIS-2 were correlated positively with highly oxygenated ions (CO^+ and CO_2^+) and less oxygenated ions ($C_xH_y^+$ and $C_xH_yO_1^+$), respectively. The result suggests that the two components should relate to highly and less-oxygenated organic species, respectively. Although the PLOM component was usually assigned to biological proteins [*Yu et al*., 2015; *Fu et al*., 2015], it was not positively correlated with nitrogen-containing ions, i.e., $C_xH_yN_p^+$ and $C_xH_yO_zN_p^+$ ions, in the HR-AMS spectra, which is expected from nitrogen-containing compounds, e.g., amines and amino acids. This results suggest that non-nitrogen-containing species, e.g., naphthalene and phenol compounds, with similar fluorescence components as PLOM, may have also contributed to PLOM [*Mladenov et al*., 2011; *De Laurentiis et al*., 2013]. Particularly in the case of urban aerosols, naphthalene-like chromophores may have accounted for a major portion of the fluorescence of PLOM, given their presence in diesel-exhaust aerosols [*Mladenov et al*., 2011].

The indices of HIX, BIX and FI are possibly associated with the chemical structures of organics in atmospheric aerosols. Both the BIX and FI indices were positively correlated with

$C_xH_y^+$ and $C_xH_yO_1^+$, and negatively correlated with CO^+ and CO_2^+, respectively, implying their association with the oxidation degree of organics. Although HIX was not strongly correlated with any AMS ion-group, it was correlated with the ratios of fluorescence intensity of the HULIS to PLOM components in the log-log plot. This result confirms that HIX is suitable to represent the relative abundances of HULIS in the atmospheric organic aerosol component in the scale of fluorescence.

As presented in Figure 5, the HULIS-1 and HULIS-2 chromophores were associated with highly and less-oxygenated structures, respectively. This finding provides information on the bulk chemical structures of water-soluble chromophores, and may be useful to evaluate the reaction pathways for the formation/loss of organic chromophores in atmospheric aerosols. The fluorescence peak of rainwater samples is similar to band M of HULIS-2, which is suggested to shift to band A of HULIS-1 through the exposure of sunlight [*Kieber et al*., 2012]. This mechanism explains our results: The chromophores may have been degraded by sunlight exposure and converted to more oxygenated species. Furthermore, the chromophores corresponding to bands C and M can also be formed from photodegradation of the PLOM component, such as phenol and 4-phenoxyphenol [*De Laurentiis et al*., 2013; *Bianco et al*., 2014]. The chromophore group with the strongest fluorescence in WSOM was attributed to HULIS-1 for all samples, which may be due to photochemical reactions of the fluorescence compounds that have fluorescent properties similar to the chromophore groups of HULIS-2 and PLOM. We propose using these results in future studies to understand the chemical transformations, including both degradation and polymerization, of chromophores in the atmosphere.

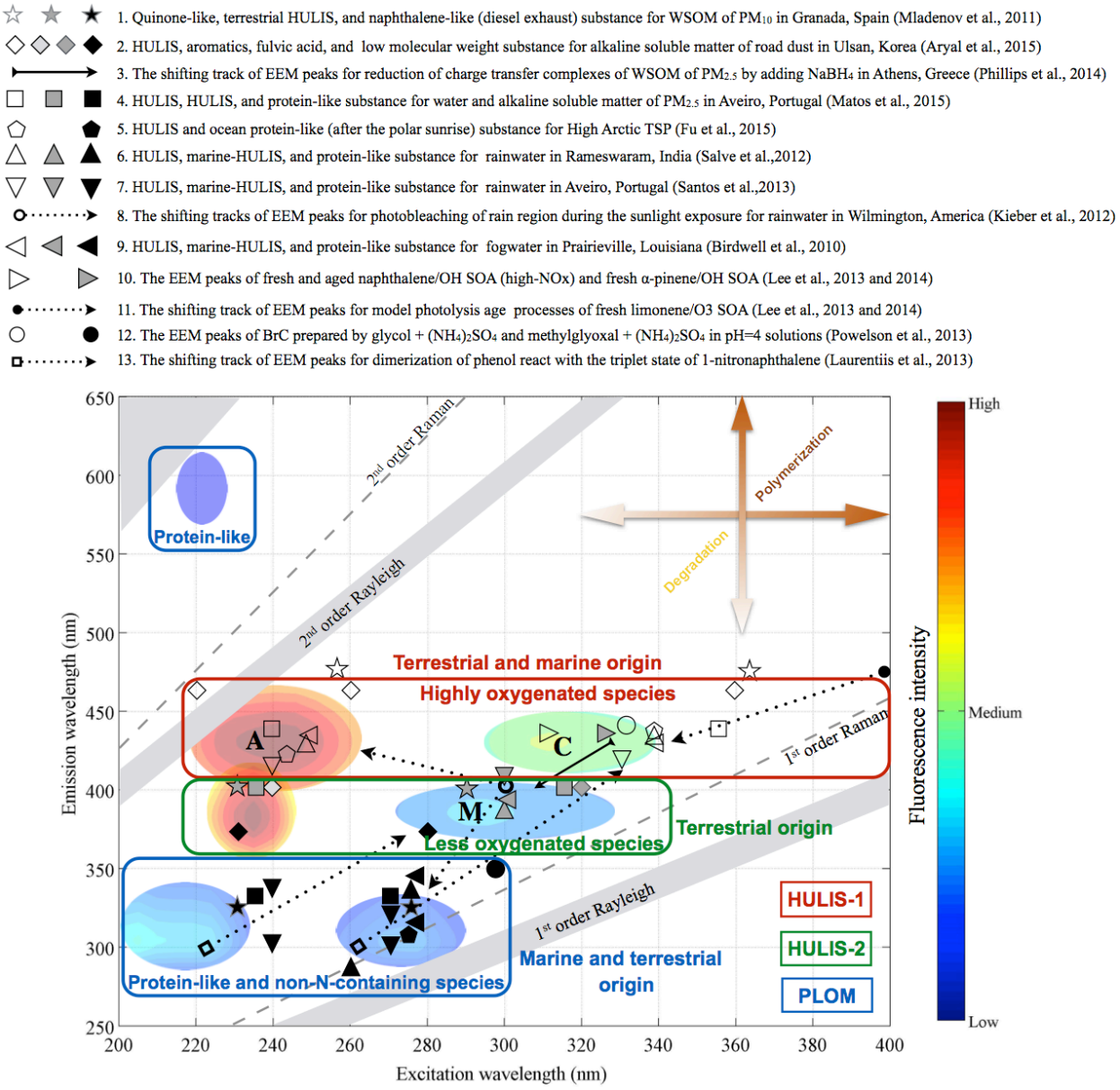

Figure 6.9. Diagram of the association of the EEM profiles with the possible chemical structures, sources, and atmospheric chemical processes of chromophoric water-soluble organics in atmospheric aerosols. The blue, green, and red boxes represent the fluorescence ranges of PLOM, HULIS-2, and HULIS-1, respectively. The colours of circles represent the relative fluorescence intensities around the peaks of EEM components. The designated peaks of A, C and M represent the UVC-excited, UVA-excited and marine humics that were defined for terrestrial and oceanic systems in previous studies.

7 Conclusions

7.1 Conclusions and potential implications

Figure 7.1 summerizes the original ideas, experimental methods, major results and potential implications of this study. This study presented an effective means to understand the concentrations, chemical structures and optical properties of atmospheric organic aerosol components from low- to high-polar compounds (including WIOSM and six sub-fractions of WISOM, and WSOM and three sub-fractions of WSOM, i.e., HULIS-n, -a and HP-WSOM). This approach is a combination of the separation of organic components using extraction techniques (solvent extraction and SPE separation) and their characterization with multiple analytical techniques, e.g., HR-AMS, FT-IR, ^{1}H-NMR, ESI/APCI-MS, OC/EC analyzer, UV-visible absorption and EEMs.

Nearly total aerosol organics, i.e., organics in fractions of WISOM, HULIS-n, -a and HP-WSOM were recovered from the urban TSP filter samples by the solvent extraction successively with water, MeOH and DCM/MeOH (2/1, v/v) and the SPE separation with an Oasis HLB column. The concentrations of total aerosol organics and their structural and optical characteristics were obtained. This approach may also be suitable for the extraction of total aerosol organics from other types of aerosols in different environments, and provide further insights into the concentrations, structural and optical characteristics, and sources and formation processes of organic aerosols.

The fractionated organic components were obviously different in view of the chemical structural characteristics i.e., mass fractions, elemental compositions, average molecular weights and the mass fractions of chemical functional groups. This result demonstrated that the presented methods is capable of separating total aerosol organics in several groups according to their

polarity and allow chemical characterization of organic matter at the level of overall chemical structures. Very complex aerosol organic mixtures were simplified to several groups by the separation methods, and different functional groups were identified and quantified. The knowledge on the overall chemical structures of organics is potentially useful for developing and validating the Quantitative Structure Activity Relationships (QSARs) models between the chemical structures of organic matter and their physicochemical properties that are frequently used in the community of atmospheric science, e.g., the density, viscosity, hygroscopicity parameter k, and phase distribution parameters of organics in aerosols.

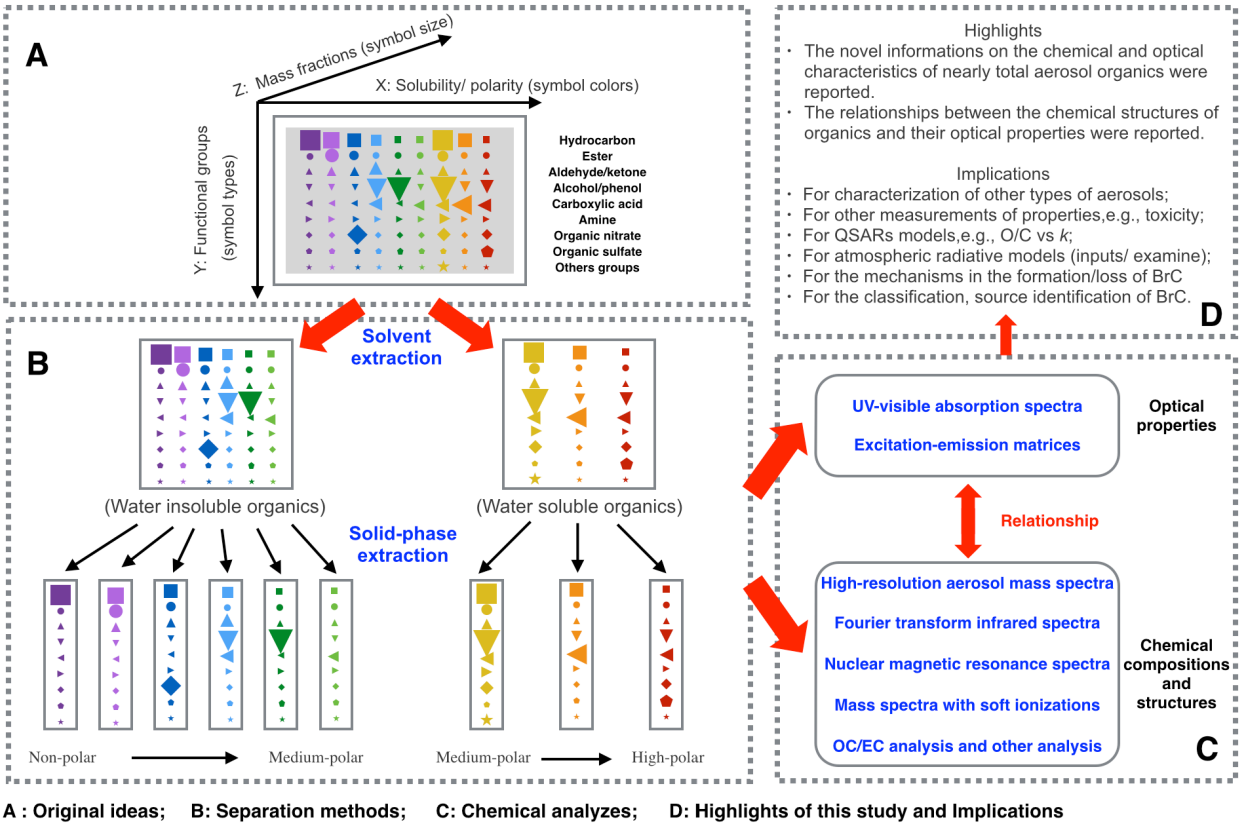

Figure 7.1. The overview of this study and potential implications of the results.

The fractionated organic components were also obviously different in view of the optical characteristics i.e., the MAE, *Å*, fluorescence efficiency and relative contribution of fluorescence components. This result demonstrated that the methods are also useful to explorer the relationship between the light absorption and fluorescence properties of organic aerosol matters and their overall chemical structural characteristics. The results indicate that organic compounds with oxygen and nitrogen atoms may contribute largely to the total light absorption and fluorescence of organic aerosol components. These findings provide insight into the composition and formation processes of complex aerosol BrC. Different fluorescence components in the EEMs of organic aerosols were also associated with their chemical structures. Two EEM components of HULIS-1 and HULIS-2 were associated with highly and less-oxygenated structures in all studied aerosols, respectively. These findings are useful for further studies regarding the classification, source identification, and evaluation of the reaction pathways in the formation/loss of chromophores in atmospheric aerosols.

This study shows that the light absorption of the organics in the visible region was unlikely important to the total light absorption by aerosols at least in the urban area of Nagoya. However, light absorption of the organics in the ultraviolet region was important because the MAEs increase sharply, which can account for approximately a quarter of the total light absorption by aerosols at approximately 300 nm. Thus, the effects of BrC on atmospheric photochemistry may be important in the atmosphere over the urban area. The major light-absorption organics have been found to be less polar (HULIS and polar parts of WISOM) and their MAEs have been found to be higher than the non- and more polar organic fractions. It highlights the potential importance of those organic fractions to aerosol photoreactions. The possible formation and loss of BrC by the conversions of non-polar organics to less polar organics and of less polar organics to more polar organics are processes to consider in future atmospheric radiative models. Our

results also show that the $\mathring{A}$ values increased with an increase of the wavelength and the polarity of the organics. This result illustrates the problems associated with the use of a single $\mathring{A}$ value for modeling aerosol BrC: the light absorption by organic aerosols in the near ultraviolet range may be overestimated, leading to an overestimation of the effect of BrC on atmospheric photochemistry. Therefore, different values of $\mathring{A}$ in different wavelength regions should be considered in future atmospheric radiative models.

7.2 Suggestions for future studies

Although the characterization of the chemical structures and optical properties of the different aerosol organic components was successful in this study, there remained several points to consider in future studies:

(1) Several fractions of aerosol organics were extracted and separated by the presented methods. However, the fractions are still complex, and contain a number of individual organic compounds. Further, the presented methods cannot identify compounds at molecular level or nearly molecular level. I suggest two methods to improve the knowledge on the chemical composition of the extracts: One is the application of ultrahigh-resolution mass spectrometer with soft ionization sources to the chemical characterization of organic compounds in different components to obtain the chemical composition of organic aerosols in molecular level. The other is a combination of chromatographic separation system (e.g., High-performance liquid chromatography and size exclusion chromatography etc.) with HR-AMS measurement to improve the ability of separation.

(2) The FT-IR analysis used in this study is to obtain semi-quantitative information on chemical functional groups, as well as the relative abundances of different chemical groups in fractionated organics. Further calibration of the absorptivity of different chemical groups using

standards (e.g., humic acid) with known concentrations makes it possible to quantify the absolute mass concentrations of organics in aerosol extracts by the FT-IR.

(3) Whereas the solvent-extractable aerosol matter was characterized, the chemical structural characteristics of aerosol carbons resided after the extraction with water, MeOH, DCM and n-hexane was not studied. I believe that the major component of the resided carbons in the case of urban aerosols is EC, but they may also contain small fraction of organic carbon. Chemical characterization of ambient EC is important to explain how chemical structures of EC change after the primary emissions and how the properties of primary aerosols such as the MAE and toxicity change. If organics are also present in the resided fractions, the analysis should help understand the influences of the unextractable organics on aerosol properties, which was not addressed sufficiently to date.

References

Aiken, A. C.; DeCarlo, P. F.; Kroll, J. H.; Worsnop, D. R.; Huffman, J. A.; Docherty, K.; Ulbrich, I. M.; Mohr, C.; Kimmel, J. R.; Sueper, D.; et al. O/C and OM/OC ratios of primary, secondary, and ambient organic aerosols with a high resolution time-of-flight aerosol mass spectrometer. *Environ. Sci. Technol.* **2008**, *42*(12), 4478–4485.

Alama, M. S.; Westb, C. E.; Scarlettb, A. G.; Rowlandb, S. J.; Harrison, R.M. Application of 2D-GCMS reveals many industrial chemicals in airborne particulate matter. *Atmos. Environ.* **2013**, *65*, 101–111.

Alexander, D.T.L.; Crozier, P.A.; Anderson, J.R. Brown carbon spheres in east asian outflow and their optical properties. *Science* **2008**, *321*, 833–836.

Allen, D. T.; Palen, E. J.; Haimov, M. I.; Hering, S. V.; Young, J. R. Fourier-Transform Infrared-Spectroscopy of Aerosol Collected In A Low-pressure Impactor (lpi/ftir)—Method Development and Field Calibration. *Aerosol Sci. Technol.* **1994**, *21* (4), 325–342.

Andreae, M. O.; Gelencsér, A. Black carbon or brown carbon? The nature of light-absorbing carbonaceous aerosols. *Atmos. Chem. Phys.* **2006**, *6*, 3131–3148.

Aryal, R.; Lee, B. K.; Beecham, S.; Kandasamy, J.; Aryal, N.; Parajuli, K. Characterisation of Road Dust Organic Matter as a Function of Particle Size: A PARAFAC Approach. *Water Air & Soil Pollut.* **2015**, *226*:24, DOI: 10.1007/s11270-014-2289-y.

Banfi, D.; Patiny, L. www.nmrdb.org: Resurrecting and Processing NMR Spectra On-line. *CHIMIA International Journal for Chemistry* **2008**, *62*, 280–281.

Barnard, J. C.; Volkamer, R.; Kassianov, E. I. Estimation of the mass absorption cross section of the organic carbon component of aerosols in the Mexico City Metropolitan Area. *Atmos. Chem. Phys.* **2008**, *8*, 6665-6679.

Bekircan, O.; Küxük, M.; Kahveci, B.; Kolayl, S. Convenient Synthesis of Fused Heterocyclic 1,3,5-Triazines from Some N-Acyl Imidates and Heterocyclic Amines as Anticancer and Antioxidant Agents. *Arch. Pharm. Chem. Life Sci.* **2005**, *338*, 365–372.

Bergstrom, R.W.; Pilewskie, P.; Russell, P.B.; Redemann, J.; Bond, T.C.; Quinn, P.K.; Sierau, B. Spectral absorption properties of atmospheric aerosols. *Atmos. Chem. Phys.* **2007**, *7*, 5937–5943.

Bianco, A.; Minella, M.; Laurentiis, E. D.; Maurino, V.; Minero, C.; Vione, D. Photochemical generation of photoactive compounds with fulvic-like and humic-like fluorescence in aqueous solution. *Chemosphere* **2014**, *111*, 529–536.

Birdwell, J. E.; Engel, A. S. Characterization of dissolved organic matter in caveand spring waters using UV-Vis absorbance and fluorescence spectroscopy. *Org. Geochem.* **2010**, *41* (3), 270–280.

Birdwell, J. E.; Valsaraj, K. T. Characterization of dissolved organic matter in fogwater by excitation–emission matrix fluorescence spectroscopy. *Atmos. Environ.* **2010**, *44* (27), 3246–3253.

Bond, T.C.; Bergstrom, R.W. Light absorption by carbonaceous particles: An investigative review. *Aerosol Science and Technology* **2006**, *40*, 27–67.

Bruns, E. A.; Perraud, V.; Zelenyuk, A.; Ezell, M. J.; Johnson, S. N.; Yu, Y.; Imre, D.; Finlayson-Pitts, B. J.; Alexander, M. L. Comparison of FTIR and Particle Mass Spectrometry for the Measurement of Particulate Organic Nitrates. *Environ. Sci. Technol.* **2010**, *44* (3), 1056–1061.

Canagaratna, M. R.; Jimenez, J. L.; Kroll, J. H.; Chen, Q.; Kessler, S. H.; Massoli, P.; Hildebrandt Ruiz, L.; Fortner, E.; Williams, L. R.; Wilson, K. R.; Surratt, J. D.; Donahue, N. M.; Jayne, J. T.; Worsnop, D. R. Elemental ratio measurements of organic compounds using

aerosol mass spectrometry: characterization, improved calibration, and implications. *Atmos. Chem. Phys.* **2015**, *15*, 253–272.

Chalbot, M. C. G.; Kavouras, I. G. Nuclear magnetic resonance spectroscopy for determining the functional content of organic aerosols: A review. *Environmental Pollution* **2014**, *191*, 232–249.

Chan, A. W. H.; Isaacman, G.; Wilson, K. R.; Worton, D. R.; Ruehl, C. R.; Nah, T.; Gentner, D. R.; Dallman, T. R.; Kirchstetter, T. W.; Harley, R. A.; Gilman, J. B.; de Gouw, J. A.; Offenberg, J. H.; Kleindienst, T. E.; Lin, Y. H.; Rubitschun, C. L.; Surratt, J. D.; Goldstein, A. H. Detailed chemical characterization of unresolved complex mixtures (UCM) in atmospheric organics: Insights into emission sources and atmospheric processing. *J. Geophys. Res.* **2013**, *118*, 2169–8996.

Chang, J. L.; Thompson, J. E. Characterization of colored products formed during irradiation of aqueous solutions containing H_2O_2 and phenolic compounds. *Atmos. Environ.* **2010**, *44*, 541–551.

Chen, W.; Westerhoff, P.; Leenheer, J.A.; Booksh, K. Fluorescence excitation–emission matrix regional integration to quantify spectra for dissolved organic matter. *Environ. Sci. Technol.* **2003**, *37*, 5701–5710.

Chen, Y.; Bond, T.C. Light absorption by organic carbon from wood combustion. *Atmos. Chem. Phys.* **2010**, *10*, 1773–1787.

Cheng, Y.; He, K.; Duan,F.; Du, Z.; Zheng, M.; Ma, Y. Characterization of carbonaceous aerosol by the stepwise-extraction thermal–optical-transmittance (SE-TOT) method. *Atmospheric Environment* **2012**, 59, 551–558.

Cheng, Y.; He, K.B.; Zheng, M.; Duan, F.K.; Du, Z.Y.; Ma, Y.L.; Tan, J.H.; Yang, F.M.; Liu, J.M.; Zhang, X.L.; Weber, R. J.; Bergin, M. H.; Russell, A.G. Mass absorption efficiency of

elemental carbon and water-soluble organic carbon in Beijing, China. *Atmos. Chem. Phys.* **2011**, *11* (22), 11497–11510.

Coburn, S.; Ortega, I.; Thalman, R.; Blomquist, B.; Fairall, C. W.; Volkamer, R. Measurements of diurnal variations and eddy covariance (EC) fluxes of glyoxal in the tropical marine boundary layer: description of the Fast LED-CE-DOAS instrument. *Atmos. Meas. Tech.* **2014**, *7*, 3579–3595.

Cory, R. M.; McKnight, D. M. Fluorescence spectroscopy reveals ubiquitous presence of oxidized and reduced quinones in dissolved organic matter. *Environ. Sci. Technol.* **2005**, *39* (21), 8142–8149.

Crippa, M.; El Haddad, I.; Slowik, J. G.; DeCarlo, P. F.; Mohr, C.; Heringa, M.; Chirico, R.; Marchand, N.; Sciare, J.; Baltensperger, U. Identification of marine and continental aerosol sources in Paris using high resolution aerosol mass spectrometry. *J. Geophys. Res.* **2013**, *118*, 1950–1963.

Dallmann, T. R.; Onasch, T. B.; Kirchstetter, T. W.; Worton, D. R.; Fortner, E. C.; Herndon, S. C.; Wood, E. C.; Franklin, J.; Worsnop, D. R.; Goldstein, A. G.; Harley, R. A. Characterization of particulate matter emissions from on-road gasoline and diesel vehicles using a soot particle aerosol mass spectrometer. *Atmos. Chem. Phys.* **2014**, *14*, 7585-7599.

Das, M. R.; Mahiuddin, S. Kinetics and adsorption behaviour of benzoate and phthalate at the alpha-alumina–water interface: Influence of functionality. *Colloids and Surfaces A: Physicochem. Eng. Aspects* **2005**, *264*, 90–100.

Day, D. A.; Liu, S.; Russell, L. M.; Ziemann, P. J. Organonitrate group concentrations in submicron particles with high nitrate and organic fractions in coastal southern California. *Atmos. Environ.* **2010**, *44* (16), 1970–1979.

De Laurentiis, E.; Buoso, S.; Maurino, V.; Minero, C.; Vione, D. Optical and photochemical characterization of chromophoric dissolved organic matter from lakes in Terra Nova Bay, Antarctica. Evidence of considerable photoreactivity in an extreme environment. *Environ. Sci. Technol.* **2013**, *47* (24), 14089–14098.

De Laurentiis, E.; Sur, B.; Pazzi, M.; Maurino, V.; Minero, C.; Mailhot, G.; Brigante, M.; Vione, D. Phenol transformation and dimerisation, photosensitised by the triplet state of 1-nitronaphthalene: A possible pathway to humic-like substances (HULIS) in atmospheric waters. *Atmos. Environ.* **2013**, *70*, 318–327.

DeCarlo, P. F.; Kimmel, J. R.; Trimborn, A.; Northway, M. J.; Jayne, J. T.; Aiken, A. C.; Gonin, M.; Fuhrer, K.; Horvath, T.; Docherty, K. S.; Worsnop, D. R.; Jimenez, J. L. Field-deployable, high-resolution, time-of-flight aerosol mass spectrometer. *Anal. Chem.* **2006**, *78* (24), 8281–8289.

Deng, C.; Brooks, S. D.; Vidaurre, G.; Thornton, D. C. O. Using Raman Microspectroscopy to Determine Chemical Composition and Mixing State of Airborne Marine Aerosols over the Pacific Ocean. *Aerosol Sci. Technol.* **2014**, *48* (2), 193–206.

Desyaterik, Y.; Sun, Y.; Shen, X.; Lee, T.; Wang, X.; Wang, T.; Collett Jr, J.L. Speciation of "brown" carbon in cloud water impacted by agricultural biomass burning in eastern China. *J. Geophys. Res.* **2013**, *118*, 7389–7399.

Dinar, E.; Taraniuk, I.; Graber, E. R.; Katsman, S.; Moise, T.; Anttila, T.; Mentel, T. F.; Rudich, Y. Cloud condensation nuclei properties of model and atmospheric hulis. *Atmos. Chem. Phys.* **2006**, *6*, 2465–2481.

Duarte, R. M. B. O.; Duarte, A. C. Unraveling the structural features of organic aerosols by NMR spectroscopy: a review. *Magn. Reson Chem.* **2015**, *53* (9). 658–666.

Duarte, R. M. B. O.; Santos, E. B. H.; Pio, C. A.; Duarte, A. C. Comparison of structural features of water-soluble organic matter from atmospheric aerosols with those of aquatic humic substances. *Atmos. Environ.* **2007**, *41* (37), 8100–8113.

Duarte, R.M.B.O.; Pio, C.A.; Duarte, A.C. Spectroscopic study of the water-soluble organic matter isolated from atmospheric aerosols collected under different atmospheric conditions. *Analytica Chimica Acta* **2005**, *530*, 7–14.

Dubnick, A.; Barker, J.; Sharp, M.; Wadham, J.; Lis, G.; Telling, J.; Fitzsimons, S.; Jackson, M. Characterization of dissolved organic matter (DOM) from glacial environments using total fluorescence spectroscopy and parallel factor analysis, *Annals of Glaciology* **2010**, *51*, 111–122.

Dzepina, K.; Arey, J.; Marr, L. C.; Worsnop, D. R.; Salcedo, D.; Zhang, Q.; Onasch, T. B.; Molina, L. T.; Molina, M. J.; Jimenez, J. L. Detection of particle-phase polycyclic aromatic hydrocarbons in Mexico City using an aerosol mass spectrometer. *Int. J. Mass Spectrom.* **2007**, *263*, 152–170.

El-Zanan, H. S.; Lowenthal, D. H.; Zielinska, B.; Chow, J. C.; Kumar, N. Determination of the organic aerosol mass to organic carbon ratio in improve samples. *Chemosphere* **2005**, 60 (4) 485–496.

Facchini, M. C.; Rinaldi, M.; Decesari, S.; Carbone, C.; Finessi, E.; Mircea, M.; Fuzzi, S.; Ceburnis, D.; Flanagan, R.; Nilsson, E. D.; de Leeuw, G.; Martino, M.; Woeltjen, J.; O'Dowd, C. D. Primary submicron marine aerosol dominated by insoluble organic colloids and aggregates. *Geophys. Res. Lett.* **2008**, *35*, L17814.

Fan, X.; Song, J.; Peng, P.Comparative study for separation of atmospheric humic-like substance (HULIS) by ENVI-18, HLB, XAD-8 and DEAE sorbents: Elemental composition, FT-IR, 1H

NMR and off-line thermochemolysis with tetramethylammonium hydroxide (TMAH) *Chemosphere* **2013**, 93, 1710–1719.

Farmer, D. K.; Matsunaga, A.; Docherty, K. S.; Surratt, J. D.; Seinfeld, J. H.; Ziemann, P. J.; Jimenez, J. L. Response of an aerosol mass spectrometer to organonitrates and organosulfates and implications for atmospheric chemistry. *Proc. Natl. Acad. Sci.* **2010**, *107*, 6670–6675.

Feng, Y.; Ramanathan, V.; Kotamarthi, V. R. Brown carbon: a significant atmospheric absorber of solar radiation? *Atmos. Chem. Phys.* **2013**, *13*, 8607–8621.

Fu, P.; Kawamura, K.; Chen, J.; Qin, M.; Ren, L.; Sun, Y.; Wang, Z.; Barrie, L. A.; Tachibana, E.; Ding, A.; Yamashita, Y. Fluorescent water-soluble organic aerosols in the High Arctic atmosphere. *Sci. Rep.* **2015**, *5*: 9845, DOI: 10.1038/srep09845

Galloway, M. M.; Chhabra, P. S.; Chan, A. W. H.; Surratt, J. D.; Flagan, R. C.; Seinfeld, J. H.; Keutsch, F. N. Glyoxal uptake on ammonium sulphate seed aerosol: reaction products and reversibility of uptake under dark and irradiated conditions. *Atmos. Chem. Phys.* **2009**, *9* (10), 3331–3345.

Gilardoni, S.; Liu, S.; Takahama, S.; Russell, L. M.; Allan, J. D.; Steinbrecher, R.; Jimenez, J. L.; Carlo, P. F. D.; Dunlea, E. J.; Baumgardner, D. Characterization of organic ambient aerosol during MIRAGE 2006 on three platforms. *Atmos. Chem. Phys.* **2009**, *9*, 5417–5432.

Gilardoni, S.; Russell, L. M.; Sorooshian, A.; Flagan, R. C.; Seinfeld, J. H.; Bates, T. S.; Quinn, P. K.; Allan, J. D.; Williams, B.; Goldstein, A. H.; Onasch, T. B.; Worsnop, D. R. Regional variation of organic functional groups in aerosol particles on four U.S. east coast platforms during the International Consortium for Atmospheric Research on Transport and Transformation 2004 campaign. *J. Geophys. Res.* **2007**, *112* (D10), 1–11.

Graber, E. R.; Rudich, Y. Atmospheric HULIS: how humic-like are they? A comprehensive and critical review. *Atmos. Chem. Phys.* **2006**, *6*, 729–753.

Gu, Q.; Kenny, J.E. Improvement of Inner Filter Effect Correction Based on Determination of Effective Geometric Parameters Using a Conventional Fluorimeter. *Anal. Chem.* **2009**, *81*, 420–426.

Guzman-Morales, J.; Frossard, A. A.; Corrigan, A. L.; Russell, L. M.; Liu, S.; Takahama, S.; Taylor, J. W.; Allan, J.; Coe, H.; Zhao, Y.; Goldstein, A. H. Estimated contributions of primary and secondary organic aerosol from fossil fuel combustion during the CalNex and Cal-Mex campaigns. *Atmos. Environ.* **2014,** *88*, 330–340.

Gysel, M.; Weingartner, E.; Nyeki, S.; Paulsen, D.; Baltensperger, U.; Galambos, I.; Kiss, G. Hygroscopic properties of water-soluble matter and humic-like organics in atmospheric fine aerosol. *Atmos. Chem. Phys.* **2004**, *4*, 35–50.

Hallquist, M.; Wenger, J. C.; Baltensperger, U.; Rudich, Y.; Simpson, D.; Claeys, M.; Dommen, J.; Donahue, N. M.; George, C.; Goldstein, A. H.; Hamilton, J. F.; Herrmann, H.; Hoffmann, T.; Iinuma, Y.; Jang, M.; Jenkin, M. E.; Jimenez, J. L.; Kiendler-Scharr, A.; Maenhaut, W.; McFiggans, G.; Mentel, T. F.; Monod, A.; Prevot, A. S. H.; Seinfeld, J. H.; Surratt, J. D.; Szmigielski, R.; Wildt, J. The formation, properties and impact of secondary organic aerosol: current and emerging issues *Atmos. Chem. Phys.* **2009**, 9, 5155–5236.

Han, Y.; Iwamoto, Y.; Nakayama, T.; Kawamura, K.; Mochida, M. Formation and evolution of biogenic secondary organic aerosol over a forest site in Japan. *J. Geophys. Res.* **2014**, *119*, 259–273.

Han, Y.; Kawamura, K.; Chen, Q.; Mochida, M. Formation of high-molecular-weight compounds via the heterogeneous reactions of gaseous C8-C10 n-aldehydes in the presence of atmospheric aerosol components. *Atmos. Environ.* **2016**, *126*, 290–297.

Hao, L.; Romakkaniemi, S.; Kortelainen, A.; Jaatinen, A.; Portin, H.; Miettinen, P.; Komppula, M.; Leskinen, A.; Virtanen, A.; Smith, J. N.; Sueper, D.; Worsnop, D. R.; Lehtinen, K. E. J.;

Laaksonen, A. Aerosol chemical composition in cloud events by high resolution time-of-flight aerosol mass spectrometry. *Environ. Sci. Technol.* **2013**, *47* (6), 2645–2653.

Hawkins, L. N.; Russell, L. M.; Covert, D. S.; Quinn, P. K.; Bates, T. S. Carboxylic acids, sulfates, and organosulfates in processed continental organic aerosol over the southeast Pacific Ocean during VOCALS-REx 2008. *J. Geophys. Res.* **2010**, *115* (D13), 1–16.

Heal, M.R.; Hammonds, M.D. Insights into the composition and sources of rural, urban and roadside carbonaceous PM_{10}. *Environ. Sci. Technol.* **2014**, *48* (16), 8995–9003.

Hoffer, A.; Gelencsér, A.; Guyon, P.; Kiss, G.; Schmid, O.; Frank, G.; Artaxo, P.; Andreae, M. O. Optical properties of humic-like substances (HULIS) in biomass-burning aerosols. *Atmos. Chem. Phys.* **2006**, *6*, 3563–3570.

Hoffer, A.; Tóth, A.; Nyirő-Kósa, I.; Pósfai, M.; Gelencsér, A. Light absorption properties of laboratory-generated tar ball particles. *Atmos. Chem. Phys.* **2016**, *16*, 239–246.

Huang, D.; Li, Y.; Lee, B. P.; Chan, C. K. Analysis of Organic Sulfur Compounds in Atmospheric Aerosols at the HKUST Supersite in Hong Kong Using HR-ToF-AMS. *Environ. Sci. Technol.* **2015**, *49* (6), 3672–3679.

Huang, R.-J.; Zhang, Y.; Bozzetti, C.High secondary aerosol contribution to particulate pollution during haze events in China. *Nature* **2014**, 514, 218–222.

Huguet, A.; Vacher, L.; Relexans, S.; Saubusse, S.; Froidefond, J.M.; Parlanti, E. Properties of fluorescent dissolved organic matter in the Gironde Estuary. *Organic Geochemistry* **2009**, *40*, 706–719.

Hunt, J.F.; Ohno, T. Characterization of fresh and decomposed dissolved organic matter using excitation–emission matrix fluorescence spectroscopy and multiway analysis. *Journal of Agricultural and Food Chemistry* **2007**, *55*, 2121–2128.

Jiang, B.; Liang, Y. M.; Xu, C. M.; Zhang, J. Y.; Hu, M.; Shi, Q. Polycyclic Aromatic Hydrocarbons (PAHs) in Ambient Aerosols from Beijing: Characterization of Low Volatile PAHs by Positive-Ion Atmospheric Pressure Photoionization (APPI) Coupled with Fourier Transform Ion Cyclotron Resonance. *Environ. Sci. Technol.* **2014**, *48* (9), 4716–4723.

Jimenez, J. L.; Canagaratna, M. R.; Donahue, N. M.; Prevot, A. S. H.; Zhang, Q.; Kroll, J. H.; DeCarlo, P. F.; Allan, J. D.; Coe, H.; Ng, N. L. Evolution of organic aerosols in the atmosphere. *Science* **2009**, *326*, 1525–1529.

Jo, D. S.; Park, R. J.; Lee, S.; Kim, S. W.; Zhang, X. A global simulation of brown carbon: implications for photochemistry and direct radiative effect. *Atmos. Chem. Phys. Discuss.* **2015**, *15*, 27805–27852.

Kameel, F.R.; Lee, S.H.; Hoffmann, M.R.; Colussi, A.J. Polarity and oxidation level of visible absorbers in model organic aerosol. *Chem. Phys. Lett.* **2014**, *603*, 57–61.

Kampf, C. J.; Jakob, R.; Hoffmann, T. Identification and characterization of aging products in the glyoxal/ammonium sulfate system-implications for light-absorbing material in atmospheric aerosols. *Atmos. Chem. Phys.* **2012**, *12*(14), 6323–6333.

Kaul, D.S.; Gupta, T.; Tripathi, S.N. Source Apportionment for Water Soluble Organic Matter of Submicron Aerosol: A Comparison between Foggy and Nonfoggy Episodes. *Aerosol and Air Quality Research* **2014**, *14*, 1527–1533.

Ki, J.; Jung, D.; Park, Y.; Kim, Y.; Moon, D. W.; Lee, T. G. Quantitative analysis of surface amine groups on plasma-polymerized ethylenediamine films using UV–visible spectroscopy compared to chemical derivatization with FT-IR spectroscopy, XPS and TOF-SIMS. *Applied Surface Science* **2007**, *253* (8), 4112–4118.

Kieber, R. J.; Adams, M. B.; Willey, J. D.; Whitehead, R. F.; Avery Jr, G. B.; Mullaugh, K. M.; Mead, R. N. Short term temporal variability in the photochemically mediated alteration of

chromophoric dissolved organic matter (CDOM) in rainwater. *Atmos. Environ.* **2012,** *50*, 112–119.

Kieber, R. J; Willey, J.D.; Whitehead, R.F.; Reid, S.N. Photobleaching of chromophoric dissolved organic matter (CDOM) in rainwater. *J. Atmos. Chem.* **2007**, *58,* 219–235.

Kieber, R.J.; Adams, M.B.; Willey, J.D.; Whitehead, R.F.; Avery Jr., G.B.; Mullaugh, K.M.; Mead, R.N. Short term temporal variability in the photochemically mediated alteration of chromophoric dissolved organic matter (CDOM) in rainwater. *Atmos. Environ.* **2012**, *50*, 112–119.

Kirchner, U.; Scheer, V.; Vogt, R. FTIR Spectroscopic Investigation of the Mechanism and Kinetics of the Heterogeneous Reactions of NO_2 and HNO_3 with Soot. *J. Phys. Chem. A.* **2000**, *104* (39), 8908–8915.

Kiss, G.; Tombácz, E.; Varga, B.; Alsberg, T.; Persson, L. Estimation of the average molecular weight of humic-like substances isolated from fine atmospheric aerosol. *Atmos. Environ.* **2003**, *37* (27), 3783–3794.

Kiss, G.; Varga, B.; Galambos, I.; Ganszky, I. Characterization of water-soluble organic matter isolated from atmospheric fine aerosol. *J. Geophys. Res. Atmos.* **2002**, *107*, ICC 1-1–ICC 1-8.

Kondo, Y.; Miyazaki, Y.; Takegawa, N.; Miyakawa, T.; Weber, R. J.; Jimenez, J. L.; Zhang, Q.; Worsnop, D. R. Oxygenated and water-soluble organic aerosols in Tokyo. *J. Geophys. Res.* **2007**, *112* (D1), 1–11.

Krivácsy, Z.; Kiss, G.; Ceburnis, D.; Jennings, G.; Maenhaut, W.; Salma, I.; Shooter, D. Study of water-soluble atmospheric humic matter in urban and marine environments. *Atmos. Res.* **2008**, *87* (1), 1–2.

Kuwata, M.; Zorn, S. R.; Martin, S. T. Using Elemental Ratios to Predict the Density of Organic Material Composed of Carbon, Hydrogen, and Oxygen. *Environ. Sci. Technol.* **2012**, *46* (2), 787–794.

Kweon, C.B.; Okada, S.; Foster, D.E.; Bae, M.S.; Schauer, J.J. Effect of engine operating conditions on particle-phase organic compounds in engine exhaust of a heavy-duty, direct-injection (D.I.) diesel engine. *In: SAE Technical Paper Series* **2003**, *01-0342*, 73–89.

Lack, D.A.; Bahreni, R.; Langridge, J.M.; Gilman, J.B.; Middlebrook, A.M. Brown carbon absorption linked to organic mass tracers in biomass burning particles. *Atmos. Chem. Phys.* **2013**, *13*, 2415–2422.

Lack, D.A.; Cappa, C.D.; Covert, D.S.; Baynard, T.; Massoli, P.; Sierau, B.; Bates, T.S.; Quinn, P.K.; Lovejoy, E.R.; Ravishankara, A.L. Bias in filter-based aerosol light absorption measurements due to organic aerosol loading: Evidence from ambient measurements. *Aerosol Science and Technology* **2008**, *42*, 1033–1041.

Lambe, A.T.; Cappa, C.D.; Massoli, P.; Onasch, T.B.; Forestieri, S.D.; Martin, A.T.; Cummings, M.J.; Croasdale, D.R.; Brune, W.H.; Worsnop, D.R.; Davidovits, P. Relationship between oxidation level and optical properties of secondary organic aerosol. *Environ. Sci. Technol.* **2013**, *47*, 6349–6357.

Laskin, A.; Laskin, J.; Nizkorodov, S. A.Chemistry of atmospheric brown carbon. *Chem. Rev.* **2015**, *115* (10), 4335–4382.

Laurentiis, E.D.; Sur, B.; Pazzi, M.; Maurino, V.; Minero, C.; Mailhot, G.; Brigante, M.; Vione, D. Phenol transformation and dimerisation, photosensitised by the triplet state of 1-nitronaphthalene: A possible pathway to humic-like substances (HULIS) in atmospheric waters. *Atmos. Environ.* **2013**, *70*, 318–327.

Lawaetz, A.J.; Stedmon, C.A. Fluorescence intensity calibration using the Raman scatter peak of water. *Appl. Spectrosc.* **2009**, *63*, 936–940.

Lee, H. J. J.; Aiona, P.; Laskin, A.; Laskin, J.; Nizkorodov, S. A. Effect of solar radiation on the optical properties and molecular composition of laboratory proxies of atmospheric brown carbon. *Environ. Sci. Technol.* **2014**, *48* (17), 10217–10226.

Lee, H.J.; Laskin, A.; Laskin, J.; Nizkorodov, S.A. Excitation–emission spectra and fluorescence quantum yields for fresh and aged biogenic secondary organic aerosols. *Environ. Sci. Technol.* **2013**, *47*, 5763–5770.

Lee, T.; Sullivan, A.P.; Mack, L.; Jimenez, J. L.; Kreidenweis, S.M.; Onasch, T. B.; Worsnop, D. R.; Malm, W.; Wold, C. E.; Hao, W. M.; Collett, J. L. Chemical smoke marker emissions during flaming and smoldering phases of laboratory open burning of wildland fuels. *Aerosol. Sci & Tech.* **2010**, *44* (9), i–v, DOI: 10.1080/02786826.2010.499884

Li, Y.; Ngom, A. The non-negative matrix factorization toolbox for biological data mining. *Source Code for Biology and Medicine* **2013**, *8*:10.

Lim, Y. B.; Turpin, B. J. Organic peroxide and OH formation in aerosol and cloud water. *Atmos. Chem. Phys. Discuss.* **2015**, *15*, 17367–17396.

Lin, P.; Laskin, J.; Nizkorodov, S. A.; Laskin, A. Revealing Brown Carbon Chromophores Produced in Reactions of Methylglyoxal with Ammonium Sulfate. *Environ. Sci. Technol.* **2015b**, *49* (24), 14257-14266.

Lin, P.; Liu, J.; Shilling, J. E.; Kathmann, S. M.; Laskin, J.; Laskin, A. Molecular characterization of brown carbon (BrC) chromophores in secondary organic aerosol generated from photo-oxidation of toluene. *Phys. Chem. Chem. Phys.* **2015a**, *17*, 23312-23325.

Liu, J.; Scheuer, E.; Dibb, J.; Ziemba, L. D. Brown carbon in the continental troposphere. Geophys. *Res. Lett.* **2014**, *41*, 2191–2195.

Liu, S.; Shilling, J. E.; Song, C.; Hiranuma, N.; Zaveri, R. A.; Russell, L. M. Hydrolysis of organonitrate functional groups in aerosol particles. *Aerosol Sci. Technol.* **2012**, *46* (12), 1359–1369.

Liu, Y.; Sklorz, M.; Schnelle-Kreis, J.; Orasche, J.; Ferge, T.; Kettrup, A.; Zimmermann, R. Oxidant denuder sampling for analysis of polycyclic aromatic hydrocarbons and their oxygenated derivates in ambient aerosol: Evaluation of sampling artifact. *Chemosphere* **2006**, *62*, 1889–1898.

Mané, C.; Sommerer, N.; Yalcin, T.; Cheynier, V.; Cole, R. B.; Fulcrand, H. Assessment of the Molecular Weight Distribution of Tannin Fractions through MALDI-TOF MS Analysis of Protein-Tannin Complexes. *Anal. Chem.* **2007**, *79* (6), 2239–2248.

Maria, S. F.; Russell, L. M.; Turpin, B. J.; Porcja, R. J. FTIR measurements of functional groups and organic mass in aerosol samples over the Caribbean. *Atmos. Environ.* **2002**, *36* (33), 5185–5196.

Maria, S. F.; Russell, L. M.; Turpin, B. J.; Porcja, R. J.; Campos, T. L.; Weber, R. J.; Huebert, B. J. Source signatures of carbon monoxide and organic functional groups in Asian Pacific Regional Aerosol Characterization Experiment (ACE-Asia) submicron aerosol types. *J. Geophys. Res.* **2003**, *108* (D23), 1–5.

Matos, J. T. V.; Freire, S. M. S. C.; Duarte, R. M. B. O.; Duarte, A. C. Natural organic matter in urban aerosols: Comparison between water and alkaline soluble components using excitation-emission matrix fluorescence spectroscopy and multiway data analysis. *Atmos. Environ.* **2015**, *102*, 1–10.

Matsumoto, K.; Ishii, Y.; Kim, S.; Kaneyasu, N.; Kobayashi, H. Volatility of water-soluble organic carbon in ambient aerosols. *Journal of Aerosol Science* **2014**, *67*, 38–47.

Mendoza, W.G.; Zika, R.G. On the temporal variation of DOM fluorescence on the southwest Florida continental shelf. *Progress in Oceanography* **2014**, *120*, 189–204.

Mihara, T.; Mochida, M. Characterization of solvent-extractable organics in urban aerosols based on mass spectrum analysis and hygroscopic growth measurement. *Environ. Sci. Technol.* **2011**, *45* (21), 9168–9174.

Miyazaki, Y., Coburn, S., Ono, K., Ho, D. T., Pierce, R. B., Kawamura, K., and Volkamer, R.: Contribution of dissolved organic matter to submicron water-soluble organic aerosols in the marine boundary layer over the eastern equatorial Pacific. *Atmos. Chem. Phys. Discuss.* **2016**, DOI: 10.5194/acp-2016-164

Mladenov, N.; Alados-Arboledas, L.; Olmo, F. J.; Lyamani, H.; Delgado, A.; Molina, A.; Reche, I. Applications of optical spectroscopy and stable isotope analyses to organic aerosol source discrimination in an urban area. *Atmos. Environ.* **2011**, *45*, 1960–1969.

Mohr, C.; Decarlo, P. F.; Heringa, M. F.; Chirico, R.; Slowik, J. G.; Richter, R.; Reche, C.; Alastuey, A.; Querol, X.; Seco, R.; Peñuelas, J.; Jiménez, J. L.; Crippa, M.; Zimmermann, R.; Baltensperger, U.; Prévôt, A. S. H. Identification and quantification of organic aerosol from cooking and other sources in Barcelona using aerosol mass spectrometer data. *Atmos. Chem. Phys.* **2012**, *12*, 1649–1665.

Moise, T.; Flores, J. M.; Rudich, Y. Optical properties of secondary organic aerosols and their changes by chemical processes. *Chem. Rev.* **2015**, *115* (10), 4400–4439.

Murphy, K. R.; Stedmon, C. A.; Graeber, D.; Bro, R. Fluorescence spectroscopy and multi-way techniques. PARAFAC. *Anal. Methods* **2013**, *5*, 6557–6566.

Murphy, K.R.; Butler, K.D.; Spencer, R.G.M.; Stedmon, C.A. Boehme, J.R.; Aiken, G.R. Measurement of Dissolved Organic Matter Fluorescence in Aquatic Environments: An Interlaboratory Comparison. *Environ. Sci. Technol.* **2010**, *44* (24), 9405–9412.

Murphy, K.R.; Stedmon, C.A.; Waite, T.D.; Ruiz G.M. Distinguishing between terrestrial and autochthonous organic matter sources in marine environments using fluorescence spectroscopy. *Marine Chemistry* **2008**, *108*, 40–58.

Musa Bandowe, B. A.; Meusel, H.; Huang, R.; Ho, K.; Cao, J.; Hoffmann, T.; Wilcke, W. $PM_{2.5}$-bound oxygenated PAHs, nitro-PAHs and parent-PAHs from the atmosphere of a Chinese megacity: Seasonal variation, sources and cancer risk assessment. *Science of the Total Environment* **2014**, *473–474*, 77–87.

Net, S.; Sempere, R.; Delmont, A.; Paluselli, A.; Ouddane, B. Occurrence, fate, behavior and ecotoxicological state of phthalates in different environmental matrices. *Environ. Sci. Technol.* **2015**, *49* (7), 4019–4035.

Ng, N. L.; Canagaratna, M. R.; Zhang, Q.; Jimenez, J. L.; Tian, J.; Ulbrich, I. M.; Kroll, J. H.; Docherty, K. S.; Chhabra, P. S.; Bahreini, R.; Murphy, S. M.; Seinfeld, J. H.; Hildebrandt, L.; Donahue, N. M.; DeCarlo, P. F.; Lanz, V. A.; Prevot, A. S. H.; Dinar, E.; Rudich, Y. & Worsnop, D. R. Organic aerosol components observed in Northern Hemispheric datasets from Aerosol Mass Spectrometry. *Atmos. Chem. Phys.* **2010**, *10*, 4625–4641.

Nocun, M. S.; Schantz, M. M. Determination of selected oxygenated polycyclic aromatic hydrocarbons (oxy-PAHs) in diesel and air particulate matter standard reference materials (SRMs). *Anal Bioanal Chem.* **2013**, *405* (16), 5583–5593.

Nozière, B.; Dziedzic, P.; Córdova, A. Products and Kinetics of the Liquid-Phase Reaction of Glyoxal Catalyzed by Ammonium Ions (NH_4^+). *J. Phys. Chem. A* **2009**, *113* (1), 231–237.

Okuda, T.; Naoi, D.; Tenmoku, M.; Tanaka, S.; He, K. B.; Ma, Y. L.; Yang, F. M.; Lei, Y.; Jia, Y. T.; Zhang, D. H. Polycyclic aromatic hydrocarbons (PAHs) in the aerosol in Beijing, China, measured by aminopropylsilane chemically-bonded stationary-phase column chromatography and HPLC/fluorescence detection. *Chemosphere* **2006**, *35*, 427–435.

Paglione, M.; Kiendler-Scharr, A.; Mensah, A. A.; Finessi, E.; Giulianelli, L.; Sandrini, S.; Facchini, M. C.; Fuzzi, S.; Schlag, P.; Piazzalunga, A.; Tagliavini, E.; Henzing, J. S.; Decesari, S. Identification of humic-like substances (HULIS) in oxygenated organic aerosols using NMR and AMS factor analyses and liquid chromatographic techniques. *Atmos. Chem. Phys.* **2014**, *14*, 25–45.

Park, S. S.; Schauer, J. J.; Cho, S. Y. Sources and their contribution to two water-soluble organic carbon fractions at a roadway site. *Atmos. Environ.* **2013**, *77*, 348-357.

Peuravuori, J.; Pihlaja, K. Molecular size distribution and spectroscopic properties of aquatic humic substances. *Anal. Chim. Acta.* **1997**, *337*, 133–149.

Phillips, S. M. Smith, G. D. Further evidence for charge transfer complexes in brown carbon aerosols from excitation–emission matrix fluorescence spectroscopy. *J. Phys. Chem. A* **2015**, *119*, 4545–4551.

Phillips, S. M.; Smith, G. D. Light absorption by charge transfer complexes in brown carbon aerosols. *Environ. Sci. Technol. Lett.* **2014**, *1* (10), 382–386.

Polidori, A.; Turpin, B. J.; Davidson, C. I.; Rodenburg, L. A.; Maimone, F. Organic $PM_{2.5}$: Fractionation by Polarity, FTIR Spectroscopy, and OM/OC Ratio for the Pittsburgh Aerosol. *Aerosol Science and Technology* **2008**, *42* (3), 233–246.

Popovicheva, O.; Kistler, M.; Kireeva, E.; Persiantseva, N.; Timofeev, M.; Kopeikin, V.; Kasper-Giebl, A. Physicochemical characterization of smoke aerosol during large-scale wildfires: Extreme event of August 2010 in Moscow. *Atmos. Environ.* **2014**, *96*, 405–414.

Pöschl, U. Atmospheric Aerosols: Composition, Transformation, Climate and Health Effects. *Angewandte Chemie International Edition* **2005**, *44* (46), 7520–7540.

Powelson, M. H.; Espelien, B. M.; Hawkins, L. N.; Galloway, M. M.; De Haan, D. O. Brown Carbon Formation by Aqueous-Phase Carbonyl Compound Reactions with Amines and Ammonium Sulfate. *Environ. Sci. Technol.* **2013**, *48* (2), 985–993.

Psichoudaki, M. and Pandis, S. N. Atmospheric Aerosol Water-Soluble Organic Carbon Measurement: A Theoretical Analysis. *Environ. Sci. Technol.* **2013**, *47* (17), 9791–9798.

Ramesh, P.; Sampath, S. Electrochemical and spectroscopic characterization of quinone functionalized exfoliated graphite. *Analyst* **2001**, *126*, 1872–1877.

Russell, L. M. Aerosol Organic-Mass-to-Organic-Carbon Ratio Measurements. *Environ. Sci. Technol.* **2003**, *37* (13), 2982–2987.

Russell, L. M.; Takahama, S.; Liu, S.; Hawkins, L. N.; Covert, D. S.; Quinn, P. K.; Bates, T. S. Oxygenated Fraction and Mass of Organic Aerosol from Direct Emission and Atmospheric Processing Measured on the R/V Ronald Brown During TEXAQS/GoMACCS 2006. *J. Geophys. Res.* **2009**, *114* (D7), 1–15.

Sakurai, H.; Tobias, H. J.; Park, K.; Zarling, D.; Docherty, S.; Kittelson, D. B.; McMurry, P. H.; Ziemann, P. J. On-line measurements of diesel nanoparticle composition and volatility. *Atmos. Environ.* **2003**, *37* (9-10), 1199–1210.

Salim, C. J.; Liu, H.; Kennedy, J. F. Comparative study of the adsorption on chitosan beads of phthalate esters and their degradation products. *Carbohydrate Polymers* **2010**, *81*, 640–644.

Salma, I.; Mészáros, T.; Maenhaut, W. Mass size distribution of carbon in atmospheric humic-like substances and water soluble organic carbon for an urban environment. *Journal of Aerosol Science* **2013**, *56*, 53–60.

Salma, I.; Ocskay, R.; Chi, X.G.; Maenhaut, W. Sampling artefacts, concentration and chemical composition of fine water-soluble organic carbon and humic-like substances in a continental urban atmospheric environment. *Atmos. Environ.* **2007**, *41*, 4106–4118.

Samburova, V.; Szidat, S.; Hueglin, C.; Fisseha, R.; Baltensperger, U.; Zenobi, R.; Kalberer, M. Seasonal variation of high molecular weight compounds in the water-soluble organic fraction of urban aerosols. *J. Geophys. Res.* **2005**, *110* (D23), 1–9.

Santos, P. S. M.; Santos, E. B. H.; Duarte, A. C. Seasonal and air mass trajectory effects on dissolved organic matter of bulk deposition at a coastal town in south-western Europe. *Environ Sci Pollut Res.* **2013**, *20*, 227–237.

Sax, M.; Zenobi, R.; Baltensperger, U.; Kalberer, M. Time Resolved Infrared Spectroscopic Analysis of Aerosol Formed by Photo-Oxidation of 1,3,5-Trimethylbenzene and α-Pinene. *Aerosol Science and Technology* **2005**, *39* (9), 822–830.

Seaton, P. J.; Kieber, R. J.; Willey, J. D.; Brooks Avery Jr., G.; Dixon, J. L. Seasonal and temporal characterization of dissolved organic matter in rainwater by proton nuclear magnetic resonance spectroscopy. *Atmos. Environ.* **2013**, *65*, 52–60.

Shapiro, E. L.; Szprengiel, J.; Sareen, N.; Jen, C. N.; Giordano, M. R.; McNeill, V. F. Light-absorbing secondary organic material formed by glyoxal in aqueous aerosol mimics. *Atmos. Chem. Phys.* **2009**, *9*(7), 2289–2300.

Sierra, M.M.D.; Giovanela, M.; Parlanti, E.; Soriano-Sierra, E.J. Fluorescence fingerprint of fulvic and humic acids from varied origins as viewed by single-scan and excitation/emission matrix techniques. *Chemosphere* **2005**, *58*, 715–733.

Simoneit, B. R. T. Bi, X.; Oros, D. R.; Medeiros, P. M.; Sheng, G.; Fu, J. Phenols and hydroxy-PAHs (Arylphenols) as tracers for coal smoke particulate matter: source tests and ambient aerosol assessments. *Environ. Sci. Technol.* **2007**, *41* (21), 7294–7302.

Simoneit, B. R. T.; Kobayashi, M.; Mochida, M.; Kawamura, K.; Huebert, B. J. Aerosol particles collected on aircraft flights over the northwestern Pacific region during the ACE-Asia

campaign: Composition and major sources of the organic compounds. *J. Geophys. Res.* **2004**, *109* (D19S10), D19S10; doi: 10.1029/2004JD004565.

Sirita, J.; Phanichphant, S.; Meunier, F. C. Quantitative Analysis of Adsorbate Concentrations by Diffuse Reflectance FT-IR. *Anal. Chem.* **2007**, *79* (10), 3912–3918.

Song, J.; He, L.; Peng, P.; Zhao, J.; Ma, S. Chemical and Isotopic Composition of Humic-Like Substances (HULIS) in Ambient Aerosols in Guangzhou, South China. *Aerosol Science and Technology* **2012**, *46* (5), 533–546.

Staudt, S.; Kundu, S.; Lehmler, H.J.; He, X.; Cui, T.; Lin, Y.H.; Kristensen, K.; Glasius, M.; Zhang, X.; Weber, R.J.; Surratt, J.D.; Stone, E.A. Aromatic organosulfates in atmospheric aerosols: Synthesis, characterization, and abundance. *Atmos. Environ.* **2014**, *94*, 366–373.

Stocker, T. F., Qin, D., Plattner, G. K., Tignor, M., Allen, S. K., Boschung, J., Nauels, A., Xia, Y., Bex, V., and Midgley, P. M. Climate Change 2013: The Physical Science Basis. Intergovernmental Panel on Climate Change, Working Group I Contribution to the IPCC Fifth Assessment Report (AR5); Cambridge Univ. Press: New York, **2013**.

Sun, Y.; Zhang, Q.; Zheng, M.; Ding, X.; Edgerton, E. S.; Wang, X. Characterization and source apportionment of water-soluble organic matter in atmospheric fine particles ($PM_{2.5}$) with high-resolution aerosol mass spectrometry and GC–MS. *Environ. Sci. Technol.* **2011**, *45* (11), 4854–4861.

Sundaraganesan, N.; Ilakiamani, S.; Dominic Joshua, B. FT-Raman and FT-IR spectra, abinitio and density functional studies of 2-amino-4,5-difluorobenzoic acid. *Spectrochimica Acta Part A: Molecular and Biomolecular Spectroscopy* **2007**, *67* (2), 287–297.

Takahama, S.; Johnson, A.; Russell, L. M. Quantification of Carboxylic and Carbonyl Functional Groups in Organic Aerosol Infrared Absorbance Spectra. *Aerosol Science and Technology* **2013**, *47* (3), 310–325.

Takegawa, N.; Miyakawa, T.; Kawamura, K.; Kondo, Y. Contribution of selected dicarboxylic and oxocarboxylic acids in ambient aerosol to the m/z 44 signal of an Aerodyne aerosol mass spectrometer. *Aerosol Sci. Tech.* **2007**, *41*, 418–437.

Toja, F.; Saviello, D.; Nevin, A.; Comelli, D.; Lazzari, M.; Levi, M.; Toniolo, L.; The degradation of poly(vinyl acetate) as a material for design objects: A multi-analytical study of the effect of dibutyl phthalate plasticizer. Part 1. *Polymer Degradation and Stability* **2012**, *97*, 2441–2448.

Utrya, N.; Ajtaia, T.; Filepa, Á.; Pintéra, M. D.; Hofferb, A.; Bozokia, Z.; Szabó, G. Mass specific optical absorption coefficient of HULIS aerosol measured by a four-wavelength photoacoustic spectrometer at NIR, VIS and UV wavelengths. *Atmos. Environ.* **2013**, *69*, 321–324.

Varga, B.; Kiss, G.; Ganszky, I.; Gelencser, A.; Krivacsy, Z. Isolation of water-soluble organic matter from atmospheric aerosol. *Talanta* **2001**, *55* (3), 561–572.

Verma, V.; Rico-Martinez, R.; Kotra, N.; King, L.; Liu, J.; Snell, T. W.; Weber, R. J. Contribution of water-soluble and insoluble components and their hydrophobic/hydrophilic subfractions to the reactive oxygen species-generating potential of fine ambient aerosols. *Environ. Sci. Technol.* **2012**, *46* (20), 11384–11392.

Verma, V.; Rico-Martinez, R.; Kotra, N.; Rennolds, C.; Liu, J.; Snell, T.W.; Weber, R. J. Estimating the toxicity of ambient fine aerosols using freshwater rotifer *Brachionus calyciflorus* (Rotifera: Monogononta). *Environ. Pollut.* **2013**, *182*, 379–384.

Willoughby, A. S.; Wozniak, A. S.; Hatcher, P. G.A molecular-level approach for characterizing water-insoluble components of ambient organic aerosol particulates using ultrahigh-resolution mass spectrometry. *Atmos. Chem. Phys.* **2014**, 14, 10299–10314.

Worton, D. R.; Isaacman, G.; Gentner, D. R.; Dallmann, T. R.; Chan, A. W. H.; Ruehl, C.; Kirchstetter, T. W.; Wilson, K. R.; Harley, R. A.; Goldstein, A. H. Lubricating oil dominates primary organic aerosol emissions from motor vehicles. *Environ. Sci. Technol.* **2014**, *48* (7), 3698–3706.

Wozniak, A. S.; Bauer, J. E.; Dickhut, R. M. Characteristics of water-soluble organic carbon associated with aerosol particles in the eastern United States. *Atmos. Environ.* **2012**, *46*,181–188.

Wozniak, A. S.; Bauer, J. E.; Sleighter, R. L.; Dickhut, R. M.; Hatcher, P. G. Technical note: Molecular characterization of aerosol-derived water soluble organic carbon using ultrahigh resolution electrospray ionization fourier transform ion cyclotron resonance mass spectrometry. *Atmos. Chem. Phys.* **2008**, *8* (17), 5099–5111.

Wu, P. G.; Yang, D. J.; Zhang, L. Q.; Shen, X. H.; Pan, X. D.; Wang, L. Y.; Zhang, J.; Tan, Y.; Feng, L.; Ying, Y. Simultaneous determination of 17 phthalates esters in edible vegetable oils by GC-MS with silica/PSA-mixed solid-phase extraction. *J. Sep. Sci.* **2012**, *35*, 2932– 2939.

Yan, C.; Zheng, M.; Sullivan, A. P.; Bosch, C.; Desyaterik, Y.; Andersson, A.; Li, X.; Guo, X.; Zhou, T.; Gustafsson, Ö.; Collett Jr, J. L. Chemical characteristics and light-absorbing property of water-soluble organic carbon in Beijing: Biomass burning contributions. *Atmos. Environ.* **2015**, *121*, 4–12.

Yang, M.; Howell, S. G.; Zhuang, J.; Huebert, B. J. Attribution of aerosol light absorption to black carbon, brown carbon, and dust in China – interpretations of atmospheric measurements during EAST-AIRE. *Atmos. Chem. Phys.* **2009**, *9*, 2035–2050.9

Yu, H.; Liang, H.; Qu, F.; Han, Z.H.; Shao, S.; Chang, H.; Li, G. Impact of dataset diversity on accuracy and sensitivity of parallel factor analysis model of dissolved organic matter fluorescence excitation-emission matrix. *Sci. Rep.* **2015**, *5*, 10207, doi: 10.1038/srep10207

Zhan, Q.; Zenobi, R.; Buseck, P.R.; Teerman, S. Analysis of Polycyclic Aromatic Hydrocarbons in Kerogens Using Two-Step Laser Mass Spectrometry. *Energy & Fuels* **1997**, *11*, 144-149.

Zhang, Q.; Jimenez, J. L.; Canagaratna, M. R.; Allan, J. D.; Coe, H.; Ulbrich, I. M.; Alfarra, M. R.; Takami, A.; Middlebrook, A. M; Sun, Y. L.; Dzepina, K.; Dunlea, E.; Docherty, K.; DeCarlo, P. F.; Salcedo, D.; Onasch, T. B.; Jayne, J. T.; Miyoshi, T.; Shimono, A.; Hatakeyama, S.; Takegawa, N.; Kondo, Y.; Schneider, J.; Drewnick, F.; Borrmann, S. L.; Weimer, S.; Demerjian, K.; Williams, P.; Bower, K. N.; Behreini, R.; Cottrell, L.; Griffin, R. J.; Rautiainen, J.; Sun, J. Y.; Zhang, Y. M.; Worsnop, D. R. Ubiquity and dominance of oxygenated species in organic aerosols in anthropogenically-influenced northern hemisphere midlatitudes. *Geophys. Res. Lett.* **2007**, *34* (13), 1–12.

Zhang, X.; Lin, Y,-H.; Surratt, J. D.; Zotter, P.; Prévôt, A. H. S.; Weber, R. J. Light-absorbing soluble organic aerosol in Los Angeles and Atlanta: A contrast in secondary organic aerosol *Geophys. Res. Lett.* **2011**, *38*, L21810, DOI: 10.1029/2011GL049385

Zhang, X.; Lin, Y.H.; Surratt, J.D.; Weber, R.J. Sources, composition and absorption Ångström exponent of light-absorbing organic components in aerosol extracts from the Los Angeles Basin. *Environ. Sci. Technol.* **2013**, *47*, 3685–3693.

Zhang, X.; Lin, Y.H.; Surratt, J.D.; Zotter, P.; Prévot, A.S.H.; Weber, R.J. Light-absorbing soluble organic aerosol in Los Angeles and Atlanta: A contrast in secondary organic aerosol. *Geophys. Res. Lett.* **2011**, *38*, L21810, doi:10.1029/2011GL049385

Zhang, X.; Liu, Z.; Hecobian, A.; Zheng, M.; Frank, N. H.; Edgerton, E. S.; Weber, R. J. Spatial and seasonal variations of fine particle water-soluble organic carbon (WSOC) over the Southeastern United States: Implications for secondary organic aerosol formation. *Atmos. Chem. Phys. Discuss.* **2012**, *12*, 9621–9664.

Zhao, R.; Lee, A. K. Y.; Huang, L.; Li, X.; Yang, F.; Abbatt, J. P. D. Photochemical processing of aqueous atmospheric brown carbon. *Atmos. Chem. Phys.* **2015**, *15*, 6087–6100.

Zorn, S. R.; Drewnick, F.; Schott, M.; Hoffmann, T.; Borrmann, S. Characterization of the South Atlantic marine boundary layer aerosol using an aerodyne aerosol mass spectrometer. *Atmos. Chem. Phys.* **2008**, *8* (16), 4711–4728.

Acknowledgments

I would like to thank many people who have contributed to my Ph.D. study.

I am very grateful to my Ph.D. advisor, Prof. Michihiro Mochida. His constructive suggestions have greatly promoted the Ph.D. study. I have learned so many things, e.g., science rigorousness and logicality through discussions with him, which have directly and indirectly contributed to my study.

I thank Dr. Fumikazu Ikemori and Prof. Yuzo Miyazaki for the provision of filter samples, chemical analyses and many valuable suggestions on this study, and Prof. Kimitaka Kawamura and Prof. Kiyoshi Matsumoto and Mr. Hayato Higo and Dr. Daichi Asakawa for chemical analyses. I also thank Dr. Sean Coburn and Dr. Rainer Volkamer and Dr. Yoko Iwamoto for provide the filter samples and many comments, and Mr. Sathiyamurthi Ramasamy and Prof. Shungo Kato and Dr. Akira Ida and Prof. Yoshizumi Kajii for the provision of VOC data.

I thank Dr. Yuemei Han and Dr. Kaori Kawana for the technical support to use the AMS, and Mr. Shuhei Ogawa and Ms. Sara Kagami and Ms. Yange Deng for many comments. I also thank Research Center for Materials Science, Nagoya University for the use of their fluorescence spectrometers, UV-vis spectrometers, FT-IR, NMR and ESI/APCI-MS, and Drs. K. Oyama and Y. Maeda for the technical support to the use of the instruments, Prof. Lynn M. Russell and Prof. Satoshi Takahama for providing FT-IR peak pattern data for carboxylic COH. I acknowledge NOAA's Air Resources Laboratory (ARL) for providing the HYSPLIT model (http://ready.arl.noaa.gov/HYSPLIT.php).

Conference presentation

陳慶彩, 池盛文数, 持田陸宏. 都市エアロゾルに含まれる非水溶性有機物の化学構造および光吸収の特徴.第 21 回大気化学討論会, 2015 年 10 月 19 日~10 月 21 日, 東京,日本. (口頭)

Qingcai Chen, Fumikazu Ikemori, Hayato Higo, Daichi Asakawa, Michihiro Mochida. Characterization of organic matter isolated from total suspended particulates in the atmosphere over Nagoya, Japan. 2014 International Aerosol Conference, Aug. 28–Sep. 2, 2014, BEXCO, Busan, Korea. (Poster)

陳慶彩, 池盛文数, 肥後隼人, 持田陸宏. 名古屋の大気エアロゾルに含まれる有機物の紫外可視光吸収およびその化学構造的特徴との関係. 第 20 回大気化学討論会, 2014 年 10 月 27 日~10 月 29 日, 府中 (東京),日本. (口頭)

陳慶彩, 池盛文数, 肥後隼人, 持田陸宏. 名古屋の大気エアロゾルに含まれる有機物の抽出とその化学的特徴の解析. 第 19 回大気化学討論会, 2013 年 11 月 6 日~11 月 8 日, 七尾, 日本. (口頭)

List of publication

Qingcai Chen, Fumikazu Ikemori, Hayato Higo, Daichi Asakawa, Michihiro Mochida*. Chemical structural characteristics of HULIS and other fractionated organic matter in urban aerosols: Results from mass spectral and FT-IR analysis. ***Environ. Sci. Technol.*** 2016, 50, 1721−1730.

Papers submitted and in preparation

Qingcai Chen, Fumikazu Ikemori, Michihiro Mochida*. Insight into structural and optical characteristics of water-insoluble organic complex mixtures in submicron aerosols over Nagoya, Japan. (In preparation for resubmission to *Environ. Sci. Technol.*)

Qingcai Chen, Yuzo Miyazaki, Kimitaka Kawamura, Kiyoshi Matsumoto, Sean Coburn, Rainer Volkamer, Yoko Iwamoto, Sara Kagami, Yange Deng, Shuhei Ogawa, Sathiyamurthi Ramasamy, Shungo Kato, Akira Ida, Yoshizumi Kajii, Michihiro Mochida*. Characterization of chromophoric water-soluble organics in an urban, a forest, and the eastern equatorial Pacific aerosols using EEM and HR-ToF-AMS spectroscopy. (Submitted to *Environ. Sci. Technol.*)

Qingcai Chen, Fumikazu Ikemori, Michihiro Mochida*. Light absorption and excitation-emission fluorescence of urban organic aerosol components and their connection to the chemical structures. (Submitted to *Environ. Sci. Technol.*)

Note

As of August 15, 2016, a part of the study in this dissertation is published in the following papers.

(1) Qingcai Chen, Fumikazu Ikemori, Hayato Higo, Daichi Asakawa, Michihiro Mochida*. Chemical structural characteristics of HULIS and other fractionated organic matter in urban aerosols: Results from mass spectral and FT-IR analysis. *Environ. Sci. Technol.* 2016, 50, 1721−1730.

(2) Qingcai Chen, Yuzo Miyazaki, Kimitaka Kawamura, Kiyoshi Matsumoto, Sean Coburn, Rainer Volkamer, Yoko Iwamoto, Sara Kagami, Yange Deng, Shuhei Ogawa, Sathiyamurthi Ramasamy, Shungo Kato, Akira Ida, Yoshizumi Kajii, Michihiro Mochida*. Characterization of chromophoric water-soluble organic matter in an urban, a forest, and the eastern equatorial Pacific aerosols using EEM and HR-ToF-AMS spectroscopy. (Accepted for publication in *Environ. Sci. Technol.,* DOI: 10.1021/acs.est.6b01643)